Landscape evolution and Cenozoic sea-levels of the Geographe Bay hinterland, southwestern Australia

R DENNIS GEE

Busselton, Western Australia

✉ *dennis.gee@bigpond.com*

Abstract

The Busselton area in southwestern Australia is characterised by three distinct coastal plains along the foot of Whicher Range that formed mainly by marine attrition during progressive sea-level falls through the Cenozoic and, to a lesser extent, erosion by long-lived rivers. None of the geological and geomorphic units, all of which overlie the Lower Cretaceous Leederville Formation, show evidence of tectonic tilting so, in the absence of masking dune systems, this area offers a reference for Cenozoic global sea levels.

The oldest landform, a marine erosional surface at 112–166 m ASL on Whicher Range, is a remnant of the Blackwood Plateau capped by in situ laterite of likely Eocene age. The Whicher Scarp, with relief of about 120 m, formed by marine erosion removing much of the Leederville Formation during a progressive Eocene–Miocene sea-level fall (~43–13 Ma). At 72–83 m ASL, the Yelverton Bench represents a probable Miocene stillstand during this fall. The scarp below this bench is characterised by a piedmont laterite lithologically and spatially distinct from the older plateau laterite on Whicher Range. The toe-line at 41 m ASL marks the base of the Whicher Scarp and the beginning of the coastal plains—it represents the geomorphic expression of a buried Pliocene (~2.8 Ma) erosional surface at 29 m ASL.

At 21–41 m ASL, the Ambergate Plain is a terrestrially re-sedimented marine erosion surface covered by continuous strand facies of the upper Pliocene Yoganup Formation, which in turn is overlain by lateritized clay that may correlate with the Pliocene–Pleistocene Guildford Formation. The main heavy-mineral strands formed as ancestral shorelines and are embedded within the Yoganup Formation across the entire Ambergate Plain. The Cemetery Scarp, with a relief of 11 m and associated erosion surface at 5 m ASL, cuts into the Ambergate Plain and probably formed during an early Pleistocene interglacial highstand, possibly MIS 11 (~400 ka).

The Ludlow Plain at 3–5 m ASL is covered by low eolian swales and ridges of shelly calcareous sand up to 6 m thick containing coral fragments of possible MIS 5e (~124 ka) age attributed to the Tamala Limestone, which marks the beginning of marine platform carbonate production. The Busselton Wetland Plain was formed during a gentle recession after the Holocene highstand at 7.5 ka following the last glacial maximum and is recognised from a low scarp on the seaward edge of the Ludlow Plain. Although the Capel River has a history spanning the last 30–40 Ma, most rivers draining the scarp postdate the Pliocene. The build-up of barrier beach dunes during the last 7500 years next to the present coast has diverted rivers on the Wetland Plain and forced outlets to Geographe Bay to migrate laterally. Lateritization was episodic, principally in the Eocene, Miocene and Pliocene, but after the deposition of the Guildford Formation, did not extend through the Pleistocene or Holocene.

KEYWORDS: ancestral shorelines, Holocene highstand, laterite, Yoganup Formation, Guildford Formation, heavy-mineral strands, Tamala Limestone, Whicher Scarp, river diversion

Manuscript received 30 July 2021; accepted 20 December 2021

INTRODUCTION

The coastal plains and hinterland adjacent to Geographe Bay have long been known for their arcuate geomorphic features that mimic the present shape of the bay and are related to Cenozoic strandlines. However, their sedimentology and geospatial relationships have previously only been documented and interpreted in a perfunctory manner. This paper examines the evolution of these landforms between the Capel River and the western granitic shoreline beyond Dunsborough in relation to changing sea level, erosion, sedimentation, lateritization and drainage development based on new detailed geological mapping. The study area (Fig. 1) extends across the southern extension of the Swan Coastal Plain and over the Whicher Scarp to include remnants of the Blackwood Plateau. The southern boundary is the drainage divide between north-flowing rivers (Capel, Ludlow, Sabina, Abba, Vasse, Buayannup) and the south and west draining Blackwood and Margaret systems.

Although some high-latitude coastal areas around the globe show signs of uplift due to isostatic compensations

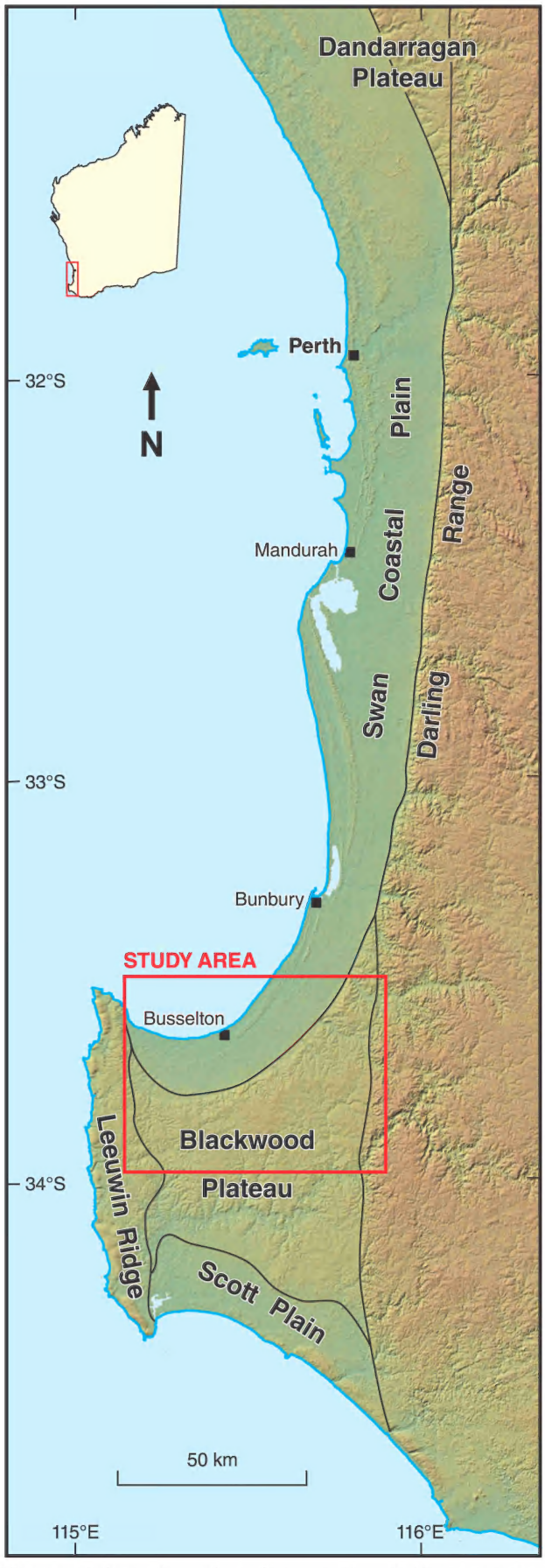

Figure 1. Location of study area in relation to major geomorphic elements of southwest Western Australia.

from Pleistocene ice sheets, the southwest of Western Australia has been relatively tectonically stable. Measurements of Whitney & Hengesh (2015) indicate this stability extends north along the coast for about 1000 km to Cape Cuvier and Cape Range where there is evidence of Cenozoic tectonism and uplift (Mylroie *et al*. 2017). This regional stability allows the southern onshore geomorphic features to be dated from global sea level curves, especially as these have become increasingly precise in terms of age and elevation over the last two decades, and forms the basis of the chronostratigraphic framework of this study (Fig. 2). These factors make the Geographe Bay hinterland, with its minimal dissection and absence of extensive inland dune systems, an ideal area to study Cenozoic geomorphic systems.

Some of the ancestral strandline deposits contain economic accumulations of heavy-mineral sands, predominantly ilmenite, which have been exploited for over 60 years. Although these buried deposits have minimal surface expression, they and other geomorphic features in the area have been related to Cenozoic sea levels (e.g. Fairbridge 1961; Baxter 1977, fig. 6). Such strands have colloquially been referred to as 'shorelines'. However, these geomorphic features are not simply residual surficial accumulations abandoned on a progressively receding marine erosional surface, and do not necessarily represent the true sea level at the time of deposition. It is therefore necessary to distinguish between the geomorphic expressions of ancestral shoreline features and erosional surfaces formed by sea-level changes.

Interpreting the landscape evolution of the region incorporated: a) detailed mapping compiled into MapInfo-Discover GIS with b) elevation information from a 30 m-pixel Shuttle Radar Topography Mission digital surface model (DSM), and c) voluminous open-file mineral exploration drilling data available via WAMEX (https://dmp.wa.gov.au/WAMEX-Minerals-Exploration-1476.aspx) of the Geological Survey of Western Australia. The revised geological map of the study area is shown in Figure 3.

REGIONAL GEOLOGICAL SETTING

The hinterland of Geographe Bay extends from the Archean Yilgarn Craton along the Darling Range, across the Darling Fault and its associated scarp, and westwards over Cretaceous strata of the southern Perth Basin to the Proterozoic granitic complex of the Leeuwin Ridge. The Cenozoic features of this study largely overlie the Lower Cretaceous Leederville Formation of the Perth Basin between the Proterozoic and Archean basement highs.

Throughout most of the Phanerozoic, Western Australia was a passive continental margin with rifting events in the Permian to Early Cretaceous. Following the final separation of Greater India from Australia in the Valanginian, siliciclastic and carbonate shelfs prograded across the erosional breakup unconformities to form the present continental shelf, whereas onshore the western part of the continent was largely subjected to fluvial and associated chemical processes apart from near the present coast.

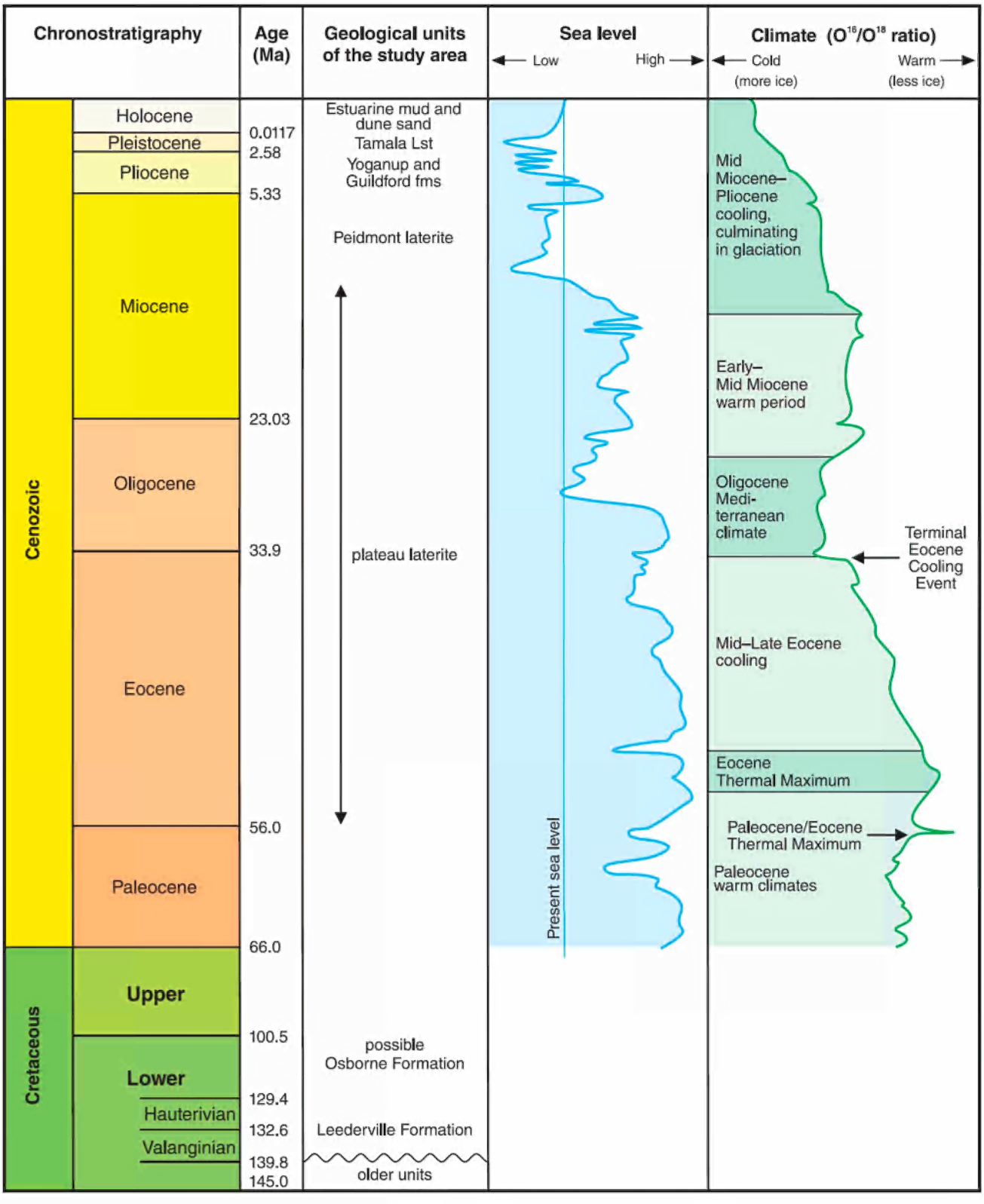

Figure 2. Chronostratigraphic framework for the study area; sea-level curve and climate intervals adapted from Słodkowski *et al*. (2013) and Miller *et al*. (2020).

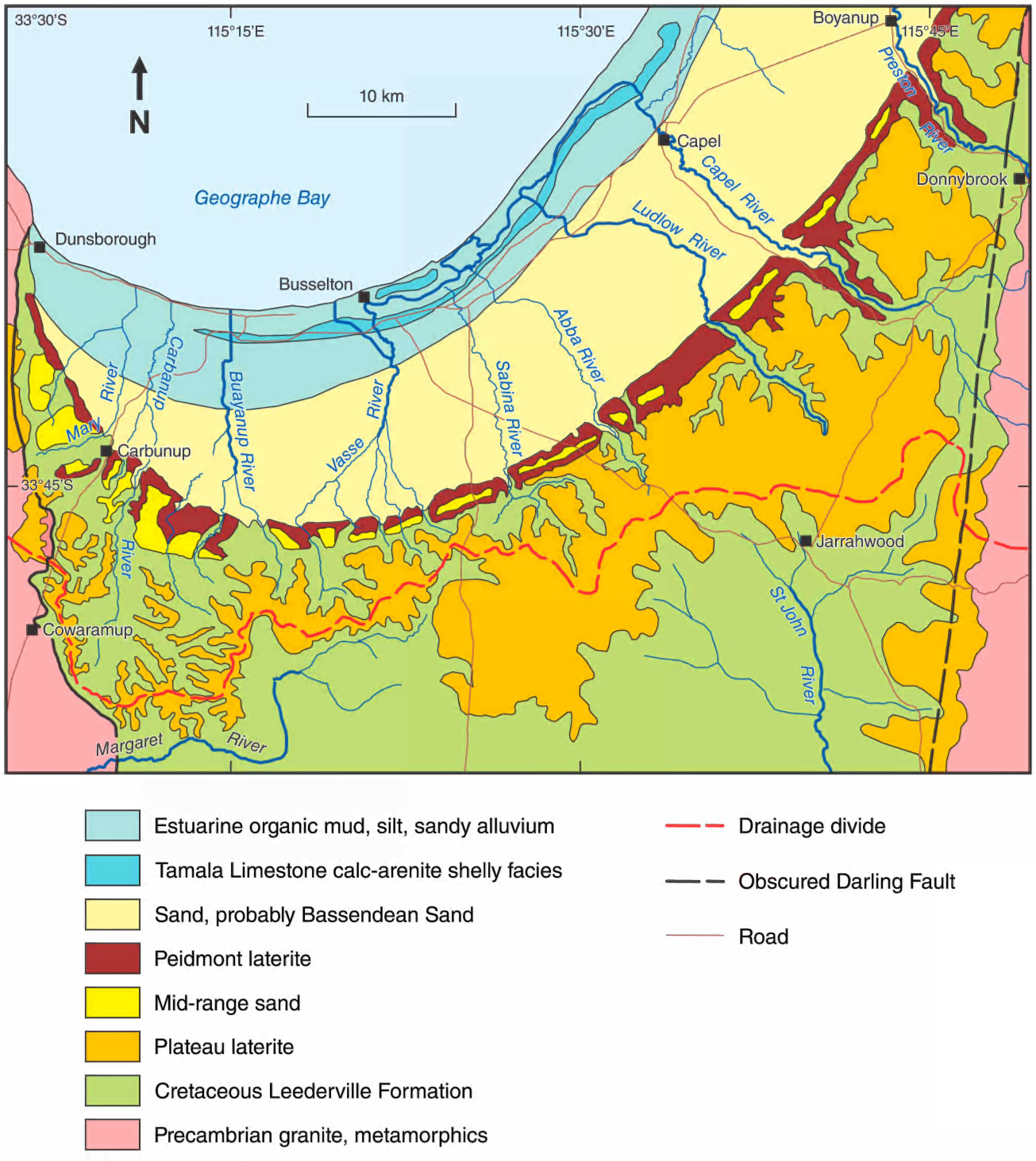

Figure 3. Revised geological map of the study area.

Leederville Formation

The Leederville Formation (Cockbain & Playford 1973) directly underlies all contemporary landforms from Geographe Bay to Whicher Range. This extensive sandstone-dominated unit is about 140 m thick (Thomas 2018), of Early Cretaceous (Hauterivian–Aptian; ~132–113 Ma) age and together with the overlying Osborne Formation, records the final fill of the southern Perth Basin. It was deposited in a shallow marine-to-fluvial environment, and unconformably onlaps Precambrian basement rocks along the Darling Scarp to the east and the Leeuwin Ridge to the west (Lowry 1967).

The base of the Leederville Formation onlaps the Valanginian (136 Ma) breakup unconformity at the onset of sag-phase tectonics followed by the separation of Australia from Antarctica along the western and southern margins of the continent (Norvick 2004; White *et al*. 2013). Mild post-breakup tilting due to uplift along the southern

margin of the continent (Sandiford 2007; Dicaprio *et al*. 2009; Cockbain 2014) probably was the last significant tectonic event to affect the area and initiated the Cenozoic geomorphic evolution of the study area. Tilting can be measured from the relative levels of internal stratigraphic markers within the Leederville Formation. The Upper Mowen Member of the Leederville Formation (Schaffer *et al*. 2008, fig. 5) indicates a regional dip of 0.13° to the north. This interpretation is consistent with glauconitic siltstone at shallow depths in water bores in the Busselton area (Passmore 1962; Hirschberg 1989)—this likely to be the Osborne Formation, which lies stratigraphically above the Leederville Formation.

Despite being extensive, outcrop of the Leederville Formation is rare and typically consists of saprolitic grey clayey sand. In the subsurface the unit is a medium-grained sub-arkose with subangular to subrounded monocrystalline quartz grains, up to 40% of angular K-feldspar grains and up to 2% pyrite (Descourvieres *et al*. 2011). There is no quartz or carbonate cement and compaction is minimal. In a 5 m-thick section in the walls of a 'refuge' dug into the lower part of the Whicher Scarp off Palmer Road (115.5070°E 33.7257°S) the unit is thickly bedded, with internal gritty lenses and rip-up shale clasts between cross beds (Fig. 4).

The lithological features make it susceptible to weathering, lateritization and erosion, thus becoming a prime source of sand for post-Cretaceous sedimentation. It is the likely source of the ilmenite strands on the coastal plains (Collins & Baxter 1984), a proposition supported by ore-grade concentrations in the Leederville Formation in the Carbunup area (Johnson 2004).

GEOMORPHIC UNITS

Geomorphic elements of the study area (Fig. 5) are underpinned by the revised geology, and include several newly defined elements in this paper. As yet, there are few precise Cenozoic age determinations within the study area. Attribution of age depends on regional correlation with global sea-level curves and established climatic events through the Cenozoic based on chronometric benthic $\delta^{18}O$ temperature data, ice-volume calculations, adjustments for glacial isostatic uplift, back-stripping of paralic sediments and ocean-basin dynamic changes (Dutton *et al.* 2015, Miller *et al*. 2020). The Pleistocene glacial and interglacial events and associated sea-level models are increasingly tied to accurate elevations and precise age dating at well-studied geological sites (Rovere *et al*. 2014, Dutton *et al*. 2015, Miller *et al*. 2020). The traditional Exxon curve still has chronological value, albeit imprecise, for sea levels in older geological epochs, although amplitudes relative to present sea level may be overstated (Miller *et al*. 2020).

Figure 4. Leederville Formation exposed at Palmer Road 'refuge' (115.5070°E, 33.7257°S) showing diffuse coarse cross bedding, granule lenses and shale intraclasts.

Blackwood Plateau

The term Blackwood Plateau was invoked by Playford *et al*. (1976) for the uplands between indurated Archaean rocks of the Darling Plateau at 230 m above sea level (ASL) on the east and similarly resistant metamorphic rocks of the Leeuwin Ridge at 150 m ASL to the west. As the Blackwood Plateau is dissected by current drainage systems only remnants remain across Whicher Range, which now forms a major drainage divide. The DSM shows a gently sloping planar surface (gradient 0.02°) falling from 166 m ASL on the eastern plateau remnant to 142 m ASL where it abuts the Leeuwin Ridge. This may be a remnant of an old marine erosional surface, but there is no direct evidence for its age. It may be analogous to the Dandaragan Plateau 300 km to the north—an erosional surface capped by the Poison Hill Greensand, which is dated as latest Cretaceous (83–66 Ma) by Mory *et al.* (2005).

PLATEAU LATERITE

The Blackwood Plateau across Whicher Range is capped by a typical plateau lateritic duricrust akin to, and continuous with, that described by Anand & Paine (2002) across the Yilgarn Craton. The weathering profile consists of 3–5 m of duricrust which is topped by loose goethite and maghemite pisolites, and underlain by a mottled zone above a pallid saprolite of leached sandstone. The duricrust contains concentrically zoned goethite–hematite nodules, plus angular fragments of highly-ferruginized hematitic sandstone with goethite cutans and abundant small pellets of maghemite.

Morphologically, the laterite is a remnant of a once-extensive blanket on the pre-dissected Blackwood Plateau. It therefore preserves part of a flat erosion surface pre-dating regional lateritization. As described for the Darling Range by Wilde & Walker (1982), in situ lateritic duricrust extends part-way down spurs of contemporary valleys within the Whicher Range. This is especially so for the Preston and Capel rivers, which are the largest to cross the Whicher Scarp. This indicates plateau lateritization continued once dissection of the plateau commenced.

The regional geochronological framework of plateau laterite in southwest Western Australia is provided by paleomagnetic dating (Pillans 2005), which records the position of the pole of remnant magnetism on the trace of the Australian apparent polar wander path (Schmidt & Clark 2000). The phase change from goethite to hematite records the remnant magnetism. Pillans (2005) documents

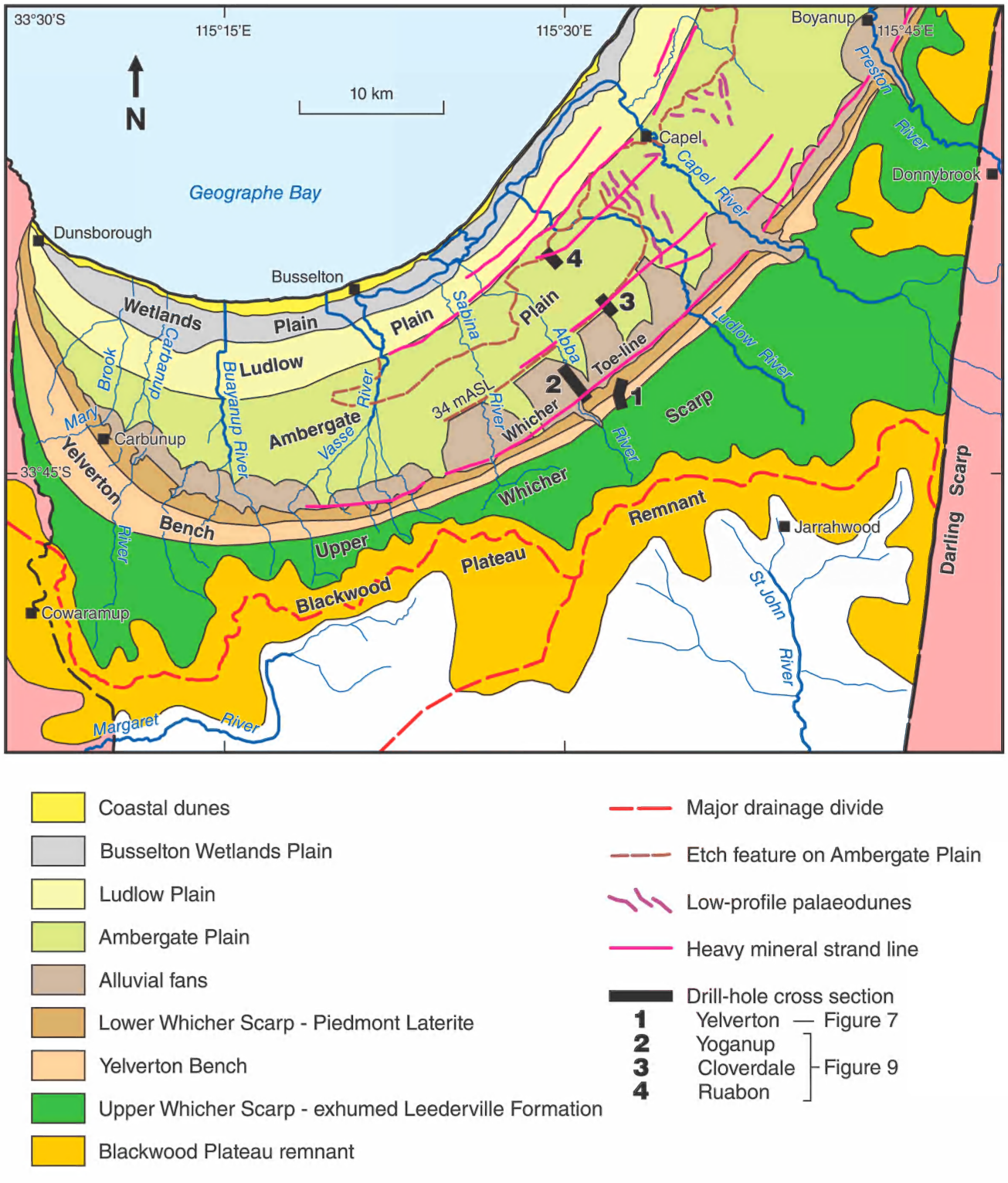

Figure 5. Geomorphic elements of the study area.

paleomagnetic determinations from many sites in the Yilgarn Craton, showing distinctly bi-modal distribution of ages in the Cenozoic with a major event at ~50–60 Ma (late Paleocene – early Eocene) and a younger one at ~10 Ma (late Miocene).

Also of relevance are ribbons of silcreted quartz sandstone, grit and conglomerate on some of the older drainages of the southwestern margin of the Yilgarn Craton (Wilde & Walker 1982) which are subject to lateritic duricrust. These include sediments at Kirup, Kojanup and Muradup—the latter contain Eocene plant fossils (Wilde & Backhouse 1976). Cockbain (2014) correlates these occurrences with the Plantagenet Group on the south coast which falls within the Eocene Climatic Optimum (~50–40 Ma; Miller *et al.* 2020), when there

were ideal conditions for deep chemical weathering and laterite development.

Duricrust possibly forms during continuous alternations between desiccation and saturation near the top of the water table, whereby goethite transforms to hematite, and under some conditions of sub-aerial exposure reduces partially to maghemite (Anand & Gilkes 1987). Attempts to radiometrically date laterite using U/Th suggest that the process takes tens of millions of years. Thus, the relatively young ages in Darling Range laterite of 10.0 – 7.5 Ma determined by Pidgeon *et al.* (2004) and 5.7 – 3.9 Ma by Wells *et al.* (2018), may record the lock-in of daughter products and helium into maghemite during a prolonged period of maturation. Alternatively, these ages may be due to a separate episode of duricrust formation in accordance with the younger event at 10 Ma of Pillans (2005).

Whicher Scarp

The Whicher Scarp (Lowry 1967; Finkl 1971) rises to a maximum of 125 m above the coastal plain in the east. Where not affected by watercourses it is expressed as smooth slopes, preserving close to the original 2.9° erosional gradient. In the west near Yelverton and Yallingup, it is only 100 m above the plain, and forms rolling dissected hills and marshy creeks, with an overall gradient of less than 0.6°.

The scarp formed by marine erosion into soft sandstone of the Leederville Formation after the main period of Eocene plateau lateritization. As with the Gingin Scarp 300 km to the north (Harrison 1990), marine erosion could not have commenced until after the deposition of the Upper Cretaceous glauconite sands, chalk and marls at ~72 Ma (Ingram & Cockbain 1979). The initiation of this scarp seemingly coincides with global sea-level falls that commenced about 43 Ma after the Eocene Climatic Optimum (Miller *et al.* 2020).

YELVERTON BENCH

A distinctive feature within the Whicher Scarp is a bench, which corresponds to the 'mid-range sand' in Figure 3. Welch (1964) previously called this the 'Middle-Escarpment Shoreline' and indicated an altitude of about 76 m ASL. Wilde & Walker (1982, p. 27) recognised it as the 'Happy Valley Shoreline' at 'about 80 m above sea level' where the Capel River cuts the Whicher Scarp. South of Dunsborough in the far west of the study area, Marnham *et al.* (2000) identified a regolith-landform

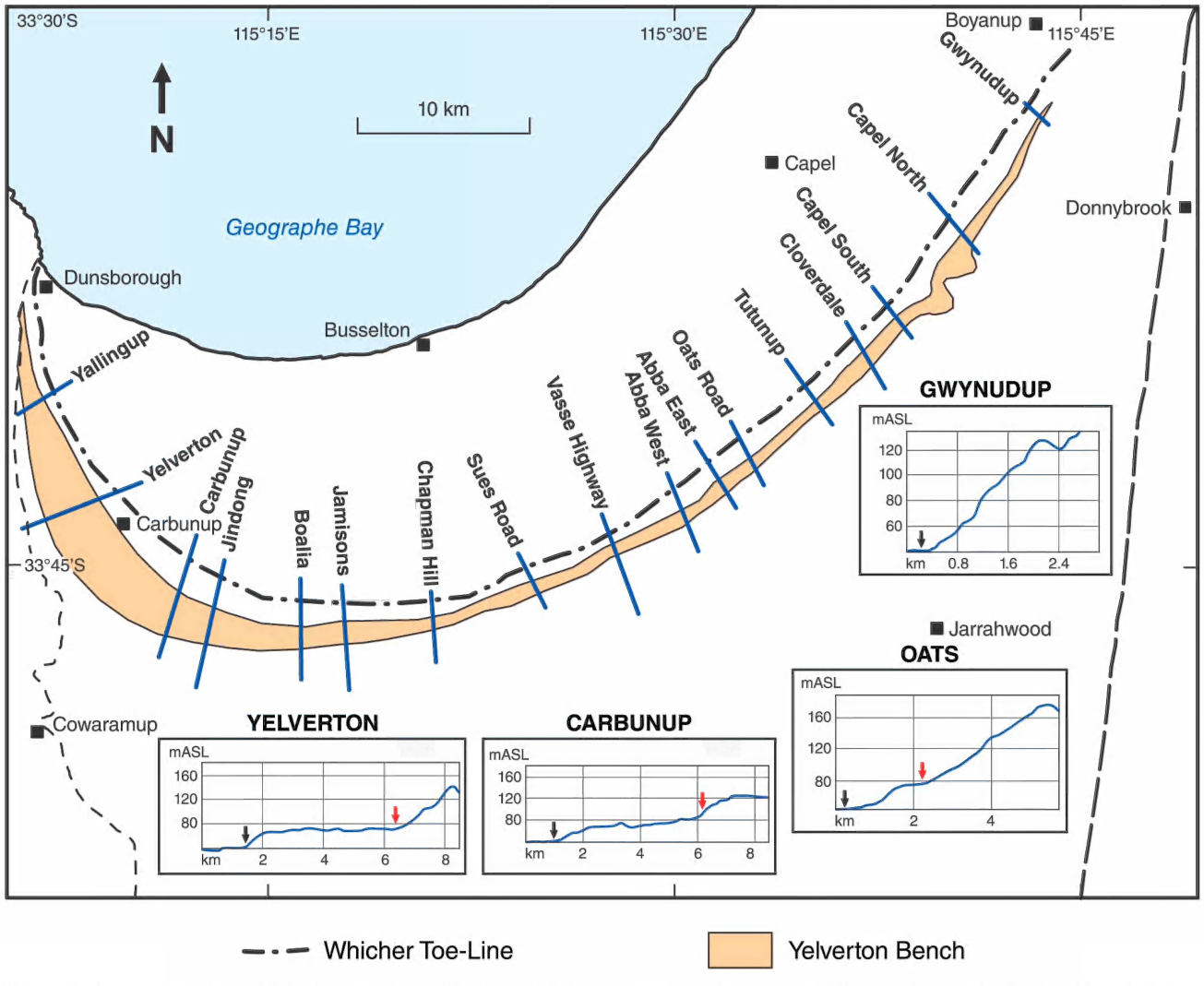

Figure 6. Transects of the Whicher Scarp and representative profiles; red arrows indicate head of Yelverton Bench, black arrows indicate base of Whicher Scarp.

of subdued rolling hills at some 60–90 m ASL which they called the 'Yelverton System'. Gozzard (2010, fig. 23) subsequently renamed it as the 'Yelverton Shelf'; however, the geomorphic term Yelverton Bench is preferred here.

Lowry (1965) relates this mid-scarp bench to the Ridge Hill Shelf along the Darling Scarp in the Perth hinterland, which Prider (1948) noted has 10 m of ferruginous cemented sandstone and detrital laterite, at 67–91 m ASL. Baxter (1977) gave a more precise elevation of 82 m, but it is not clear if this is the geomorphic expression of the bench, or erosional notch cut into the basement. Its age has not been determined by paleontology or radiometric dating.

The Yelverton Bench has not previously been documented in detail along the entire length of the Whicher Scarp. For this study, 17 regularly spaced profiles along its full extent, in transects avoiding watercourses, were constructed from the DSM using the raster functions in MapInfo. Parameters such as bench width, slope and height were then measured and assessed for regional tilting (Table 1) from sub-surface information to define the shoreline elevation. Representative topographic profiles (Fig. 6) show preservation of the flat bench and the talus wedge at the notch. The toe of the talus wedge is taken as the morphological elevation of the bench (Table 1). Because of the layer of stranded shoreline sediment on the bench, the morphological elevation is markedly higher than the marine erosional surface.

The Yelverton Bench is not developed north of Preston River whereas it is 390 m across on the Gwynudup Transect on the southern valley wall of the Preston River. It progressively widens westward to 4 km in the Carbunup and Yelverton localities, before abruptly terminating at the Leeuwin Ridge. In profile the bench has gentle seaward gradients. A linear regression line of the geomorphic elevation of the 17 transects indicates a fall from 83 m at Gwynudup to 72 m at Yallingup, giving a drop of 11 m over 60 km. Cloverdale at 90 m is the only transect that is anomalously high, being 5 m above the regression line. This is interpreted to represent thicker preserved sediment on the bench. Furthermore, information from heavy-mineral exploration indicates the apparent fall in elevation results from progressive loss of sediment from the western tracts of the bench.

Diagnostic information on the internal construction of the Yelverton Bench comes from exploration drilling by Cable Sands at the Whicher heavy-mineral deposit (Heptinstall 2003) which underlies the Oats Transect of this study. Available data includes drill-hole collar coordinates, RL (effectively metres ASL), lithology, heavy mineral layers and position of the erosional unconformity with the Leederville Formation. The cross section in Figure 7 is derived from that exploration report. The clastic wedge at the notch is 250 m wide and 18 m thick at its maximum point, and directly overlies Leederville Formation. The wedge consists of up to 9 m of reddish-brown, medium- to coarse-grained sand with abundant (3.5%) heavy mineral, overlain by 9 m of brownish-grey clayey sand, in turn capped by 2 m of lateritic duricrust. Two steps are evident in the erosional surface in the notch position. The principal erosional surface under the main part of the bench is 6 m below the geomorphic expression, indicating an erosional surface on the Oats transect at 68 m ASL.

Exploration drilling by Cable Sands near Jamieson Transect 25 km to the west, (Heptinstall 2003) indicates

Table 1. Bench widths, slopes and elevations of the Yelverton Bench on selected transects from east to west, showing Whicher Toe-line elevations for reference. See Figure 6 for locations.

Transect	Yelverton Bench			Whicher Toe-line elevation (m ASL)
	Bench width (m)	Seaward slope (°)	Elevation	
Gwynudup	390	0.99	83	41.2
Capel River N	940	0.70	80.1	41.5
Capel River S	1260	0.13	83.3	39.1
Cloverdale	1360	0.23	90	39.6
Tutunup	1540	0.53	77.4	42
Oats Road	1560	0.10	74	42
Abba E	1490	0.07	76	42.8
Abba W	1320	0.07	79.2	39
Vasse Hwy	1020	0.69	82	40.9
Sues Road	790	1.10	79.5	40
Chapman Hill	1140	0.46	72.8	39
Jamison Road	1450	0.28	64.3	42
Boalia Road	1240	0.25	66.5	42
Jindong	3610	0.34	75	42.4
Carbunup	4510	0.20	80.2	41.4
Yelverton	2720	0.10	75.6	39.8
Yallingup	1420	0.10	75.6	38.7

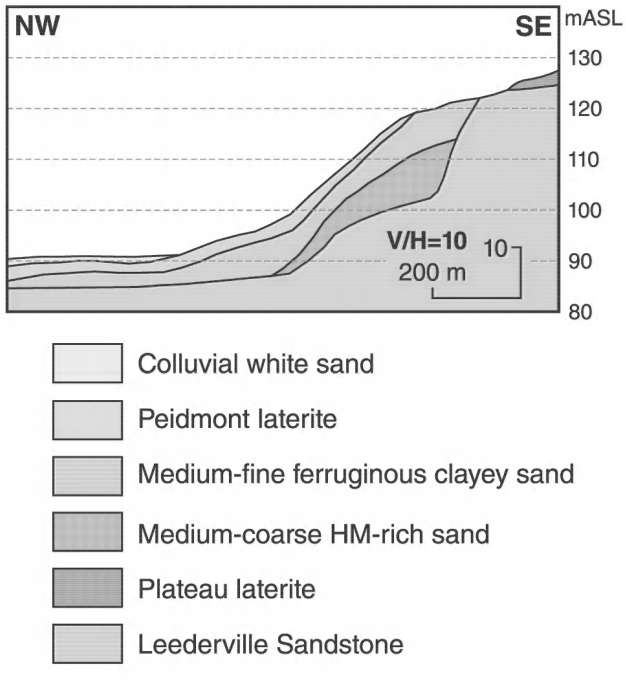

Figure 7. Geological cross-section of the Yelverton Bench based on Cable Sands drilling data in Heptinstall (2003); centre of section is at 115.5443°E, 33.7215°S and its location is shown on Figure 5.

only 4–6 m of residual sand on the bench and an erosion surface at 70 m ASL. Near the Metricup Transect, 18 km farther west, exploration drilling by Iluka, (Johnston 2004b) indicates 3 m of sediment overlies the Leederville Formation erosion surface at 72 m ASL. Thus, the apparent westward fall of the Yelverton Bench is due to the removal of sediment from the erosional bench rather than tectonic tilting.

PIEDMONT LATERITE

Piedmont laterite is younger than the plateau laterite and forms a thin apron of duricrust on and below the Yelverton Bench. It does not physically join with the plateau laterite higher up the scarp. Except where eroded it extends continuously to the base of the Whicher Scarp, where it characteristically exhibits convex morphological profiles (Fig. 8a).

The duricrust is platy, 1–2 m thick on the slopes, thickening to 2–3 m at the base of the Whicher Scarp. It is heterogeneous and contains 0.5 – 5 cm angular fragments of reddish-brown hematite-cemented sandstone, and composite clasts with thin goethite cutans, together with small pellets of detrital maghemite (Fig. 8b). The matrix is goethite-cemented quartz grit showing varying degrees of angularity. It is devoid of concentric pisolites and the clay (gibbsite) matrix characteristic of the plateau laterite. Patches of matrix form potholes in irregular surfaces on fragmental duricrust. The duricrust is underlain by a mottled zone 2–3 m of loose nodular gravels in clay matrix, (Fig. 8c), indicating mostly in situ development. These gravels have been scraped extensively along the lower scarp for use as road base and land fill.

The piedmont laterite is intact in the eastern tracts of the Whicher Scarp, between Preston River and Vasse Highway, where Wilde & Walker (1982) and Belford (1987) mapped it as lower-level laterite. In these eastern tracts it abuts and overlaps the plateau laterite where it traverses down paleovalley slopes. Mapping in the present study shows kilometre-scale re-entrants of piedmont laterite into the valleys of the two older rivers (viz. the Preston and Capel rivers). In a cutting of the Capel–Donnybrook Road (115.6601°E, 33.6266°S),

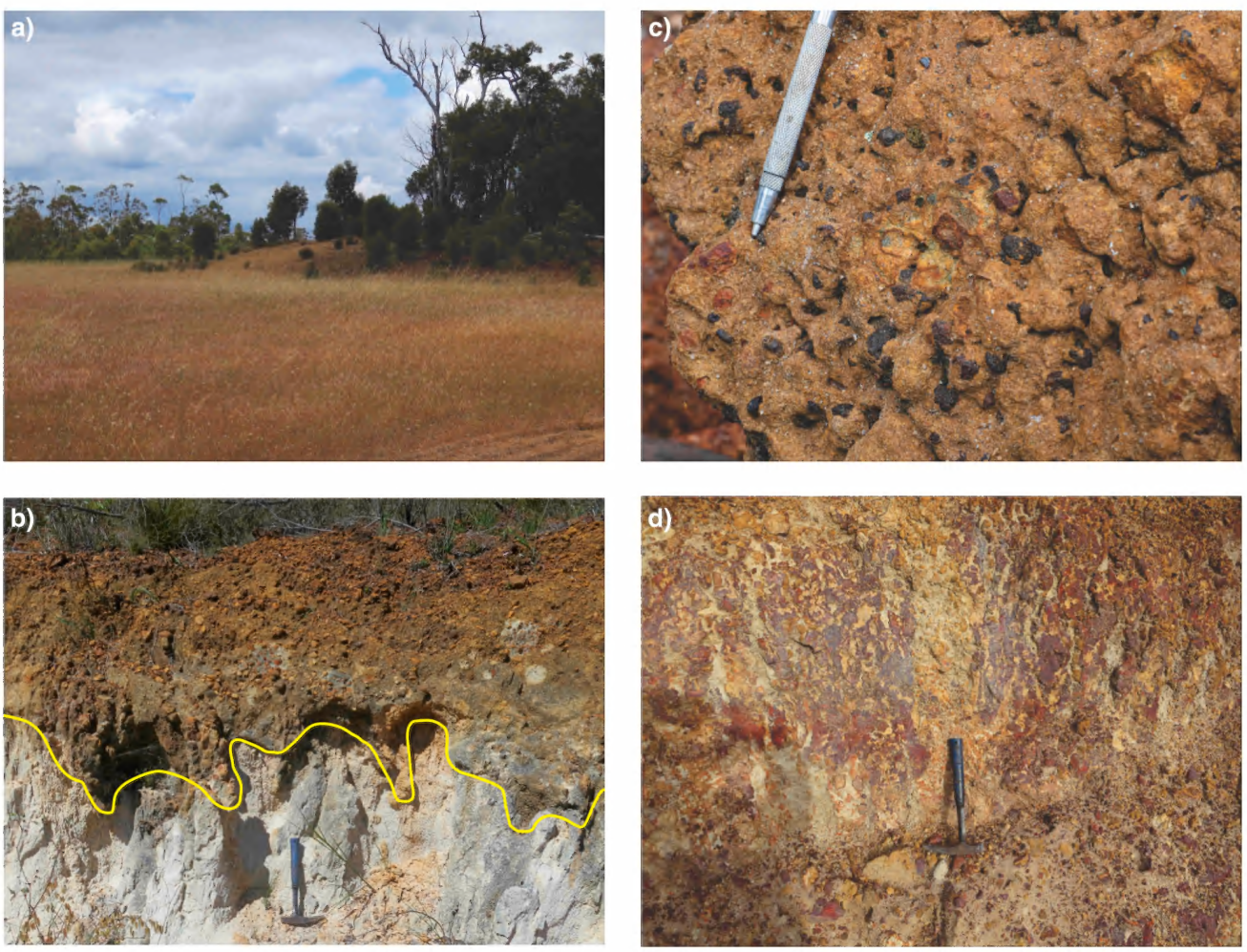

Figure 8. Piedmont laterite: **a)** convex apron of duricrust of piedmont laterite descending under alluvial fan at base of Whicher Scarp, southern end of Jamison Road (115.2929°E, 33.7889°S); **b)** piedmont laterite unconformably overlying Leederville Formation, Capel–Donnybrook Road cutting (115.6601°E, 33.6266°S); **c)** piedmont laterite showing angular clasts of ferruginized sandstone, maghemite pellets and quartz-limonite matrix. Palmer Road (115.5085°E, 33.7256°S); and **d)** mottled zone below duricrust indicating insitu development of piedmont laterite, Leeuwin Civil quarry, Price Road (115.2318°E, 33.7969°S).

2 km into the Capel River valley, the laterite is crudely bedded with internal potholes and neptunian dykes. It unconformably overlies the Leederville Formation (Fig. 8d) and at this lower level is interpreted as lateritized talus.

Westward around the arc of the Whicher Scarp, the piedmont laterite becomes increasingly dissected and is expressed as a line of isolated aprons of duricrust shelving down to the base of the scarp. These remnants are surrounded by sand shed from the underlying Leederville Formation and the exhumed clastic wedge of the Yelverton Bench. In these western tracts the piedmont laterite is always separated from the plateau laterite by exposed Leederville Formation.

Whicher Toe-line

Baxter (1977) initially used 'Yoganup Shore Line' for the conspicuous geomorphic feature at the toe of the Whicher Scarp, a term well embedded in subsequent geological literature. The precise position or elevation of this ancestral shoreline is uncertain. Moreover, not all of the superimposed stacked sedimentary successions on this line can be attributed to the Yoganup Formation. To avoid confusion the term Whicher Toe-line is applied to just the geomorphic feature.

The Whicher Toe-line forms a 100 km arc extending from Boyanup (Fig. 2) to Dunsborough. It has been intensely investigated because of associated rich ilmenite sands, of which the Yoganup deposit is the archetype. Baxter (1977) noted a clay unit, buried laterite and superimposed alluvial fans overlying the shore-facies sands. Such alluvial fans are evident on DSM images along the entire Whicher Toe-line (Figs 2 and 5). Elevations of the Whicher Toe-line derived from the 17 transects averages 40.7 m ASL with a standard deviation of only 1.4 m. There is no regional variation in elevation over the entire arc, demonstrating no tilting since its formation. This is at variance with Cope (1975) who suggested northward tilting based on his placing the shoreline at 47 m ASL at Yoganup and 37 m ASL at Dardanup.

Ambergate Plain

The term Ambergate Plain is introduced for the coastal plain between the Whicher Toe-Line at 41 m ASL and an erosional scarp at its seaward edge at 19 m ASL (Fig. 5). This flat featureless plain extends through the Busselton rural localities of Ruabon, Yalyalup, Ambergate (after which it is named) and Yoongarillup. It is 10 km across with a gentle seaward slope of 0.06°, is covered by a veneer of loose sand and, except for some low sand hills northeast of Capel, is largely devoid of recognisable dunes. This sand layer has been ascribed to the Bassendean Dunes (McArthur & Bettenay 1960) and the Bassendean Sand (Playford & Low 1972, Bufurale *et al.* 2019). Despite its seemingly featureless aspect, Ambergate Plain had a complex evolution.

Alluvial fans on the Whicher Toe-Line are up to 8 m thick and extend onto the Ambergate Plain for up to 4 km (Fig. 5). They are not lateritized. Smaller fans relate to the young watercourses that arise within the scarp. Larger fans relate to outflows of the Capel, Ludlow, Abba and Sabina rivers, and have distal fronts terminated by a subtle feature at 34 m ASL that forms a median trace on the Ambergate Plain (Fig. 5). This 34 m ASL feature swings in a broad arc to the Ludlow area to meet the seaward edge of the Ambergate Plain (Fig. 5). It may reflect an underlying paleo-embayment caused by a buried paleo-headland of Bunbury Basalt. An equally subtle embayment, etched into the seaward edge of the Ambergate Plain, occurs in the tract between Ludlow and Vasse rivers (Fig. 5. This area is characterised by swamps and a 'pock-marked' pattern on the DSM at an elevation 1.5 – 2.5 m lower than the plain. This etch-like feature unearthed the underlying Capel ilmenite-rich strands thereby facilitating the discovery and initial development of eolian heavy-mineral sands on the Ambergate Plain.

The Ambergate Plain equates to parts of the Pinjarra Plain (McArthur & Bettenay 1960). However, that geomorphic term, if applied to the Busselton area, would cover several diverse erosional and depositional features, and therefore is not used here. Internal features discussed below show the Ambergate Plain is a terrestrially re-sedimented marine planation surface.

YOGANUP FORMATION

The term 'Yoganup Formation' (Playford *et al.* 1976) was originally applied to the variably lateritized, mixed association of sand, conglomerate and clay along the 'Yoganup shoreline' at the base of the Whicher Scarp. This usage inappropriately groups the talus phase of the piedmont laterite, the 'Yoganup strands', lateritized clays and the overlying alluvial fans. Current industry practice is to use 'Yoganup Formation' for the beach-facies sand that extends continuously in the subsurface across the full width of the Ambergate Plain, rather than just under the Whicher Toe-Line. The Ambergate Plain has been probed by thousands of drillholes for mineral-sand mining. Full interrogation of these massive datasets is beyond the scope of this study; however, selective cross sections are presented to illustrate the subsurface strata.

Below the landward edge of the Ambergate Plain (i.e. under the Whicher Toe-Line), the eroded top of the Leederville Formation progressively steps down through a series of buried paleo-seacliffs and benches to reach a base level at 22 m ASL (Fig. 9a). These features are recognised in drill sections at Tutunup mine (Dixon 2008) and Yoganup Extended (Johnston 2004a). From this landward location, the unconformity between the underlying Leederville Formation and the overlying Yoganup Formation gently shelves through a series of small steps, to reach 11 m ASL at the seaward edge of the Ambergate Plain near Ruabon and Capel South mines (Dixon & Johnson 2007, Dixon 2008).

A series of stacked, partially overlapping seaward-dipping beach-facies strands, many with ilmenite enrichments, extend well beyond the Whicher Toe-Line, under the Ambergate Plain. For example, the Cloverdale Strand (Dixon & Johnston 2007) occurs 4 km seaward from the Whicher Toe-Line (Fig. 9b) whereas the Ruabon (Capel) Strands occur 9 km seaward of the Whicher Toe-Line (Fig. 9c).

The Yoganup Formation is correlated with the Ascot Formation near Perth (Baxter & Hamilton 1981), which

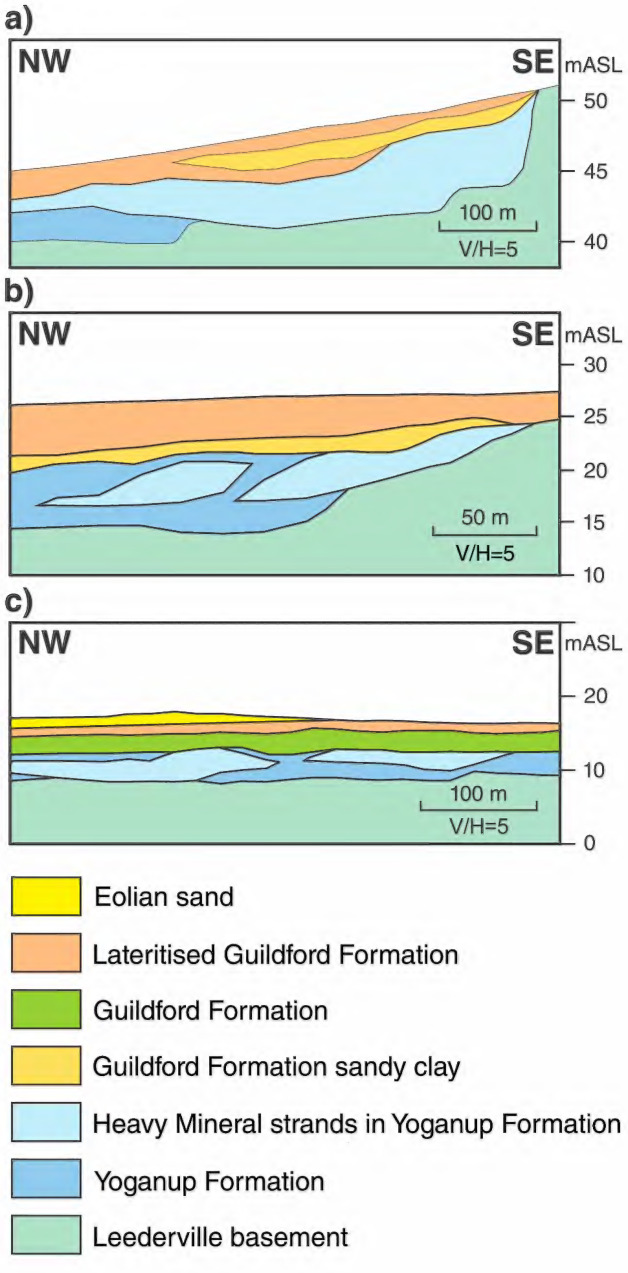

Figure 9. Geological cross sections of strands of the Yoganup Formation beneath Ambergate Plain from mineral exploration drilling: **a)** Yoganup deposit, eastern margin of Ambergate Plain (Dixon 2008); and **b)** Cloverdale deposit, central Ambergate Plain, (Dixon & Johnston 2007); and **c)** Ruabon (South Capel) deposit, western margin of Ambergate Plain (Dixon & Johnston 2007); locations shown on Figure 5.

contains diagnostic mollusc and bivalve fossils indicating late Pliocene age (Kendrick 1981, Kendrick *et al.* 1991). The Yoganup Formation is generally devoid of fossils. However, a sandy shell bed was encountered in an Iluka drill hole at 115.6001°E, 33.5264°S, 4.5 km northeast of Capel town at a depth of 16–19 m below the Ambergate Plain, equating to 3–6 m ASL (Johnston 2005). George Kendrick (in Appendix 2 of the Iluka report by Johnston (2005) confirmed correlation with Ascot Beds and the late Pliocene age.

Floaters of fossiliferous limestone have been reported on the Ambergate Plain at a locality 11 km southwest of Busselton (115.2698°E, 33.7321°S), at 28 m ASL—this locality was examined by Edgell (1967), reported by Lowry (1965) and discussed in Playford *et al.* (1976). The material was re-examined by Kendrick *et al.* (1991) who considered it middle–late Pleistocene rather than Pliocene, which is consistent with the interpretations in this paper. Field examination of this locality indicates the limestone floaters lie within surficial quartz sand and are probably introduced 'Tamala-type' limestone. This locality can no longer be used to claim that lateritisation continued through the Pleistocene.

GUILDFORD FORMATION

Below the Ambergate Plain the Guildford Formation forms a continuous unit up to 12 m thick of estuarine and alluvial sandy clay, which always overlies the Yoganup Formation. The Guildford Formation extends 250 km to the north along the plains adjacent to the Darling Scarp and marks the terrestrial advance of sediment across this plain during a marine regression. The age of the formation is not well constrained (Playford *et al.* 1976), and the name is commonly applied to any clay of Pleistocene and Holocene age. Gozzard (2007) considers the term should be restricted to strata directly below paleochannel sediments of the ancestral Swan River. This is consistent with the present sedimentological model for the Ambergate Plain and points to a late Pliocene to early Pleistocene age (~2.6 Ma).

The Guildford Formation is extensively lateritized, with exposures typically found in excavations and streambeds, a situation which has led some commentators to use 'valley ferricrete'. However, mineral-sand drilling indicates the lateritized clays extend continuously beneath surficial sands of the Ambergate Plain. When exposed it is seen to be crudely stratified goethite-cemented gritty sand and limonitic ironstone with a platy biscuit-like texture (Figs 10a, b). It is typically vermiform with dense ironstone linings of tubes and voids, which may be after tree rootlets. Pisolites and nodules are absent. It is distinct from the older forms of laterite and represents a period of lateritization that post-dates the cutting of the marine erosional surface at the base of the Yoganup and Guildford formations, and pre-dates the development of alluvial fans on the Ambergate Plain.

Cemetery Scarp

The 'Cemetery Scarp is introduced here for the geomorphic feature that forms the seaward edge of the Ambergate Plain and marks its separation from the lower coastal plains closer to the present coast. It is an erosional scarp cut into the Ambergate Plain. It is well expressed by the incline on the Vasse Highway at the Busselton Cemetery (115.3858°E, 33.6825°S—otherwise known as Four-Mile Hill. Here the Ambergate Plain drops sharply from 22 m ASL to 11 m ASL. Elsewhere the scarp is subject to varying degrees of erosional degradation, but it can be mapped on the DSM from Capel to Dunsborough as an arc mimicking the shape of other ancestral shorelines. There is no measurable regional variation in its level.

Figure 10. Lateritized clay of the Guildford Formation: **a)** crudely stratified quartz-rich gritty laterite developed on sandy clay, Willmott Farm (115.3802°E, 33.6990°S); and **b)** claystone showing disrupted platy fabric, Coolilup Road crossing of Ludlow River (115.5236°E, 33.6061°S).

The scarp is draped by yellow-brown windblown sand, such that the underlying strata are not exposed. However, 'Yoganup-type' strands and lateritized clays akin to those of the Guildford Formation are present in exploration drill holes under much of the Ambergate Plain adjacent to the Cemetery Scarp (Hill 2014; Carruthers 1998a). In the far western tracts Lowry (1965) recognised it as a sandy rise which he called the Carbunup Dunes. Here the scarp is degraded to the extent that the Yoganup and Guildford formations have been removed and only 3–4 m of eolian sand directly overlies Leederville Formation (Stewart 2007).

The Cemetery Scarp marks the seaward limit of the Yoganup and Guildford formations, and the beginning of marine carbonate deposition. It also coincides with the last lateritic duricrusts. The postulations of late Pleistocene and Recent laterite by Lowry (1965), leading to the often-repeated statement that laterite is forming today (Johnstone *et al*. 1973, Playford *et al*. 1976), cannot be substantiated in the study area. Geological observations indicate lateritization was episodic with principal events in the Eocene, Miocene and Pliocene.

Ludlow Plain

The Ludlow Plain extends around the full arc of Geographe Bay between the Ambergate Plain and the Busselton Wetland Plain. It is 3–4 km wide, with an altitude of ~11 m ASL at the base of the Cemetery Scarp, and ~8 m ASL at its seaward edge, where it shelves perceptibly into the Busselton Wetlands Plain (Fig. 5). In undisturbed areas it is covered with a mixture of eolian quartz and calcareous sand 2–3 m thick, through which limestone caprock protrudes. The map of Belford (1987) depicted this feature as a thin strip of Tamala Limestone.

Exploration drilling indicates the Ludlow Plain is underlain by 5–6 m of 'Tamala-type' limestone across its full width (Carruthers 1998b). Heavy-mineral concentrations occur in the surficial eolian sands above the limestone such as at the old Ludlow mine pits (Harewood 2001) where the buried top of the limestone at 2 m ASL is an irregular karstic surface with low pinnacles and hardcap formed by paleo-subaerial weathering. Exploration drilling in the Tuart Forest along the line of the degraded Cemetery Scarp indicates a wedge of poorly sorted sand, grit and gravel (McGoldrick 1990) which probably represents the paleo-shoreline against which the limestone sheet was deposited.

The limestone is mostly underlain by Leederville Formation sandstone, but in places multi-coloured (red, purple, green, black) sandy clay with patches of ferruginous 'coffee rock' are noted in drill holes. Passmore (1962) ascribes this latter material to the glauconitic Osborne Formation above the Leederville Formation. Hirschberg (1989) records glauconite below limestone in water bore BN4 drilled through the Ludlow Plain in the Tuart Forest, which supports this correlation. A cored geotechnical hole drilled by WML Consulting Engineers (Gorczynska 2020) through the limestone at the pedestrian bridge (115.3281°E, 33.5146°S) as part of the Vasse Diversion Drain upgrade, gave incomplete recovery through a calcarenite with shell fragments throughout and coral rubble in the lowermost 20 cm. At 1 m below sea level this hole passed into Leederville Formation with thin coaly intercalations.

SIGNIFICANCE OF 'TAMALA-TYPE' LIMESTONE

Traditionally, the thick calcareous eolianite deposits, together with the thinner marine and estuarine shelly beds, which extend for over 700 km along the west coast of Western Australia, are grouped into the Tamala Limestone (Playford *et al*. 1976). Recent research discussed below on the morphology, stratigraphy and age of this unit has shown that it is a composite entity with separate episodes of carbonate production, deposition and re-working, that can be related to glacial–interglacial cycles and associated sea level changes through the late Pleistocene. For this paper it is convenient to use 'Tamal-type", as it does not imply lithostratigraphic correlation.

In the Perth–Rottnest area an extensive eolianite ridge close to the present coast has yielded optically stimulated luminescence (OSL) ages from 120–103 ka (with appropriate uncertainty errors), indicating various sub-stages in Marine Isotope Stage (MIS) 5 (Brooke *et al.* 2014). Geological features indicate sea level at 2 m ASL. They also record eolian ridges well inland from the coastal ridge with OSL ages of 415 ka (MIS 11) and

310 ka (MIS 9). Farther north on the mid-west coast, including the Pinnacles Desert, Lipar & Webb (2014) and Lipar *et al.* (2017) identify five morphostratigraphic 'members' of the Tamala Limestone, each consisting of a cycle of eolian calcarenite and calcrete microbiolite with a karstic paleosol. Dating of the paleosol by OSL and U/Th methods shows a progressive seaward younging of the eolianite members which can be related to the major interglacial highstands of MIS 13 (landward) through MIS 11, 9, 7 and late 5 (seaward). Still farther north at Cape Cuvier a cluster of ~125 ka ages indicative of MIS 5e are recorded from corals in eolianite and related strand deposits near the coast at ~3.5 m ASL (Hearty *et al.* 2007, Stirling *et al.* 1995). The regional chronologic framework for much of the Tamala Limestone along the west coast facilitates correlation of limestone members from their morphostratigraphy. Central to this is the recurrence of the MIS 5e member along the present coast only a few metres above present sea level.

In contrast to the extended west coast, there is no build-up of the signature eolian facies of the Tamala Limestone around Geographe Bay. Eolian dunes on the rocky coast of the Leeuwin Ridge reappear on the plains north of Capel River. It is likely the Leeuwin Ridge protected the hinterland from strong onshore winds that built these facies. In its place is a 6 m-thick shelly limestone that accumulated on a shallow sub-tidal marine terrace, and which underlies the Ludlow and Busselton Plains.

Bunting (2014) describes a shelly conglomeratic limestone below eolian facies limestone at Shelley Beach 12 km east of Dunsborough (115.0298°E, 33.5379°S) a few metres above sea level. This is probably a talus deposit peripheral to the shelly limestone on the Ludlow Plain. McCulloch and Mortimer (2008) dated corals in a similar limestone at 2.5 m ASL on the ocean-side of the Leeuwin Ridge at 128–125 Ka. This age is the last interglacial equating to MIS 5e. It is likely that the shelly facies of the Tamala Limestone around Geographe Bay is of this age.

On the tectonically stable southern coasts of Australia the highstand of the last inter-glacial at 125 ka was 2–4 m ASL (Lewis *et al.* 2012, Murray-Wallace *et al.* 2016) and preceded the staged fall into the last glacial maximum, believed to be 23–17 ka in Australia. At this time sea level was about 130 m below its present level, exposing an extensive wind plain to the west. Thus, the shelly facies limestone under Ludlow Plain was sub-aerially exposed for over 100 000 years, during which time the hard cap and karstic surface formed.

Busselton Wetland Plain

This feature is expressed by silt-covered marshy flats that contain estuarine and lagoonal tracts of the Busselton, Broadwater and Wonnerup wetlands. It forms the lowermost coastal plain, extending laterally from Ludlow Plain at 4 m ASL to the modern coastal dunes at 1 m ASL. Low ridges of poorly sorted, medium-grained, quartz–carbonate sand occur on the seaward margin of the Ludlow Plain in the Tuart Forest. These are evident as gentle undulations on Layman Road at 115.4300°E, 33.6304°S, and mark the Holocene interglacial highstand.

The Busselton Wetlands Plain is underlain primarily by multi-coloured green–purple–reddish sandy clays of likely Osborne Formation, as well as underlying Leederville Formation. However, there are some tracts of shelly facies 'Tamala-type' limestone, similar to that under the Ludlow Plain, as indicated in water bores around Busselton (Passmore 1962; Wharton 1982; Hirschberg 1989) and in the partially excavated canals at Port Geographe. The limestone is 6–7 m thick with a recrystallized hardcap at 0 m ASL.

Geotechnical drilling and penetrometer probing associated with the Port Geographe development suggests the limestone forms ribbons or bars, rather than a continuous sheet as under the Ludlow Plain. This may indicate either multiple bars of buried limestone, or eroded remnants of a larger single sheet.

Quindalup Dunes

The present coast is characterised by the Quindalup Dunes (McArthur & Bettenay 1960; Semeniuk *et al.* 1989). This back-beach system consists of twin ridges, the anatomy of which has been studied by Hamilton & Collins (1997). The landward ridge is the higher of the two at up to 18 m ASL and encroaches onto the sandy muds of the Busselton Wetlands Plain. It is composed of quartz-calcarenite sand with landward dipping eolian fore-sets. Radiocarbon dates indicate the landward (older) dune commenced building at 6850±130 years before present (y BP) and continued till at least 5650±90 y BP. The seaward (younger) dune extends up to 10 m ASL and developed on an organic layer of seagrass peat giving carbon ages of 3770±60 y BP. It is likely that the older dune ridge was a barrier system with marine lagoons on the landward side, which were the precursors of the current wetlands.

DISCUSSION

Sea Levels

Because of the paucity of datable material, assigning ages to the erosional surfaces that underpin the landscape features is best done by relating them to global sea-level curves. The germinal Exxon curve (Haq *et al.* 1987) denotes a Late Cretaceous erosion surface 220 m ASL, descending to a Paleocene–Eocene surface at 110 m. These levels accord with the erosional plateau of the adjacent Yilgarn Craton and the Blackwood Plateau respectively. Modern curves (Miller *et al.* 2020) denote the Eocene Climatic Optimum as a global ice-free period with its true sea level 90 m ASL.

The Whicher Scarp formed by marine erosion and removal offshore of a large volume of sediment during an extended period when sea level fell slowly falling by some 115 m. If the Whicher and Gingin scarps are related, the volume of sediment removed between these two features during the Eocene to Miocene was at least 1000 km^3. The sea-level curve of Miller *et al.* (2020) depicts a progressive fall through the Oligocene–Miocene transition to ephemeral non-global ice caps, an interval of some 40 million years.

The age of the Yelverton Bench remains uncertain and correlation with sea-level curves is equivocal. The bench could represent either a stillstand during the progressive fall in sea level through the Oligocene and Miocene, or an oscillatory rise related to the Middle Miocene Climatic Optimum of Miller *et al.* (2020).

The Whicher Toe-line at 41 m ASL marks the sharp boundary between the Whicher Scarp and the marine-cut coastal pediments. In this respect it is analogous to the Roe Plain at 19–31 m ASL on the south coast of Western Australia. Rovere *et al*. (2014) relate this feature to the Mid Pliocene warm period of 3.3 – 2.9 Ma. At that time the stillstand was 30 m ASL, which is close to the observed erosional surface under the Whicher Toe-line.

The Mid Pliocene warm period preceded the global cooling trend that descended into the cyclic bi-polar Pleistocene ice ages and the commensurate oscillatory falls in sea level. These trends are now well documented by global $\delta^{18}O$ data (Lisiecki & Raymo 2005; Spratt & Lisiecki 2016). It is here proposed the erosional surface below the Ambergate Plain, which steps down from 29 m to 8 m ASL, relates to the early Pleistocene stage of this trend.

The Cemetery Scarp marks the seaward limits of Yoganup and Guildford formations, and the cessation of lateritic regimes. It also coincides with the onset of widespread carbonate production on marine terraces, a phenomenon tentatively attributed to the commencement of the warm Leeuwin Current (Collins *et al.* 1991).

The Ludlow Plain is substantially built from shallow-marine shelly limestone, provisionally assigned to the last interglacial MIS 5e (~125 ka). The limestone accumulated on a pre-cut erosional surface 3–5 m ASL, cut into sandstone of the Leederville Formation and abutting the Cemetery Scarp. It is unlikely that the sedimentary processes that deposited the limestone were responsible for the cutting of the scarp, inferring that the scarp is older than MIS 5.

If the Ludlow Plain limestone is MIS 5 in age, the morphological expressions and sedimentary products of previous interglacials (MIS 7, 9, 11 and 13) are to be expected, but are not obviously evident. The warmest and most long-lived interglacial of the ~100 ka cyclic phase of global Pleistocene glaciations is MIS 11 (~400 ka), which induced highstands of up to 13 m ASL for a period of some 30 000 years (Dutton *et al*. 2015). As such, it is possible that the Cemetery Scarp formed at this time, as may the shelly unit within the Ambergate Plain in the Elgin area just northeast of Capel, but the latter requires further investigation. Alternatively, the 'Tamala-type' limestone under the Ludlow Plain may represent a condensed sequence of several interglacial stages. The author is unaware of any continuous core through the limestone with complete recovery to test this possibility.

The highstand of the last inter-glacial at 125 ka was 6–9 m ASL (Dutton *et al*. 2015) and preceded the staged fall into the last glacial maximum. In Australia this maximum is believed to be 20 000 to 17 000 y BP (Barrows *et al*. 2002) when the sea level fell to about 130 m below its present level (Miller *et al.* 2020) exposing an extensive wind plain to the west. Thus, the shelly facies limestone was sub-aerially exposed for over 100 000 years, during which time the hard cap and pinnacles would have formed.

The sea level curve for the last 10 000 years of Twiggs & Collins (2010) is the key to interpreting near-shore processes in Geographe Bay. From this curve it is inferred that the post-glacial marine transgression passed the current position of the coast at 7500 y BP to reach a highstand of 2–3 m ASL at 7000 y BP. A mini scarp with low sand ridges near Wonnerup House marks this highstand. Subsequently the sea level slowly receded to its present position. This last recession exposed the Busselton Wetlands Plain, upon which coastal barrier dunes developed, creating wetlands and river diversions.

River Evolution

River activity has played a significant, but secondary role to sea-level changes, in shaping the scarps and plains. The Preston and Capel rivers, which form the larger drainages of the area, have catchments on the adjacent Yilgarn Craton, and cut substantial valleys through the Whicher Scarp. They dissect the old lateritized surface of the Blackwood and Darling Plateaus and have remnants of plateau laterite that descend partially down the valley spurs, indicating initial valley development commences during the Eocene about 40 million years ago. Rivers experienced slow prolonged rejuvenation by sea-level fall, leading to deep incision into sandstone of the Leederville Formation during the major erosional event that formed the Whicher Scarp. The re-entrant of the Yelverton Bench into the Capel River valley indicates it was already a substantial gorge by the mid-Miocene (around 15 Ma). These rivers also have re-entrants of piedmont laterite into their range-front valleys at the Whicher Toe-line. The rejuvenation process that formed the Capel River therefore probably lasted more than 30 million years.

In contrast, the smaller rivers (viz. the Ludlow, Abba, Sabina, Vasse, Carbunup and Buayanup) drain only the Whicher Scarp, and probably were initiated during the Pliocene (around 3 Ma) when sea-level retreat became more rapid and the coastal plains developed over a much shorter period. After disgorging from their range-front valleys, all rivers build alluvial fans at the Whicher Toe-line and incise the coastal plains as they flow down the gentle topographic gradient. Depth of incision is up to 11 m in the upper tracts of the Ambergate Plain and 7 m at its western edge. Submarine paleo-valleys evident on bathymetric light-detection-and-ranging (LIDAR) images align with some of the present rivers, indicating they were extant during the Pleistocene glacial maxima when sea levels were markedly lower than at present and the shore extended some 80 km to the west.

RIVER DIVERSION ON THE WETLAND PLAIN

In the present interglacial, all rivers were subject to obstruction and diversion by the build-up of the post-glacial Quindalup dune barrier. The Vasse River at the present site of Busselton City deflects orthogonally onto the east-draining estuary. LIDAR bathymetry indicates it previously continued across the wind plain during the glacial maximum. The barrier at Busselton appeared soon after 7500 y BP, when the coast assumed its present position and coastal dunes started to build. All vestiges of the ancestral outlet of the Vasse River at Busselton have disappeared but is projected to have been directly west of the Busselton Jetty.

After gathering flows from the Abba and Sabina rivers, the re-directed Vasse River takes a major bend toward the present coast at Wonnerup and then turns again eastward to its present outlet (Fig. 11). The Capel River joined the Vasse at this S-bend prior to its engineering

Figure 11. River systems and geomorphic elements of Busselton – Port Geographe area showing distribution of 'Tamala-type' limestone (green barbed line) and position of ancestral Vasse–Capel outlet at Wonnerup.

diversion directly to the coast in the late 1880s. The two rivers discharged into the sea at the Wonnerup townsite. This explains the relatively low profile of the present-day barrier dunes at this point. Drillholes and geotechnical penetrometer probes put down during the Port Geographe development (Cocks 1990, 1995, 2000, 2005) show the position of the ancestral Wonnerup outlet. A sand-filled channel at least 18 m deep cuts through a bar of 'Tamala-type' limestone at the position of the eastern revetment of the Port Geographe development (Fig. 11). The present-day Vasse River outlet is 2 km east of the now-sealed Wonnerup outlet. Altogether, the Vasse River has deflected 7 km since the early outlet at Busselton Jetty was sealed some 7000 years ago. This amounts to a 1 km per millennium migration. On this metric, the ancestral Wonnerup outlet was operating 2000 years ago.

CONCLUSIONS

All principal geomorphic elements, and their elevations (Fig. 2, Table 2) can be interpreted in terms of marine erosion of the underlying Leederville Formation during progressively falling sea levels through the Cenozoic, rather than through tectonic uplift. The last possible uplift is recorded by the low northerly dip of internal stratigraphic markers within the Leederville Formation. Lateritization was episodic throughout the Cenozoic, principally in the Eocene, Miocene and Pliocene, but not thereafter.

The oldest landform is the top of the Whicher Range which is a remnant of the Blackwood Plateau. This pre-Eocene marine erosional surface lies at 166–112 m ASL and has been subjected to deep chemical weathering and plateau lateritization prior to dissection by rivers. The Whicher Scarp formed by coastal marine erosion during a progressive fall in sea level of 115 m over a period about 40 Ma between the Eocene and the Pliocene. A Miocene stillstand during the otherwise progressive development of the Whicher Scarp, formed the Yelverton Bench, with an erosional surface at 72 m ASL. An apparent westerly fall in elevation is attributed to loss of stranded sediment from the bench.

The Whicher Toe-line at the base of the Whicher Scarp

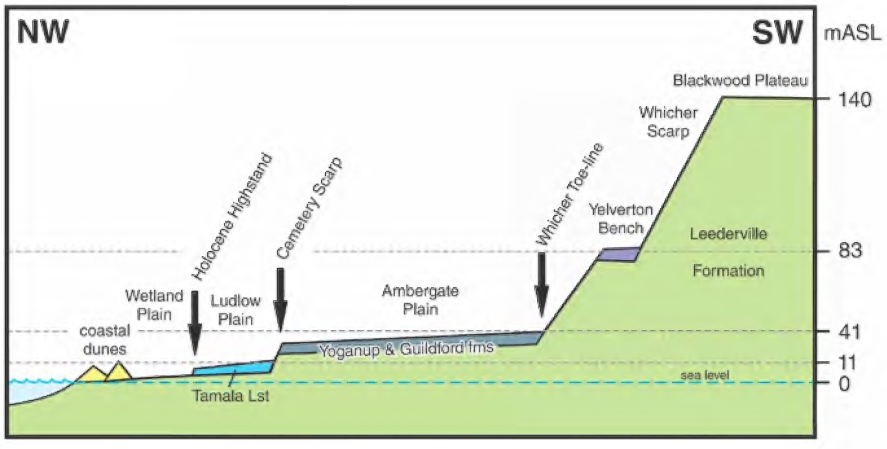

Figure 12. Schematic profile of geomorphic elements, showing key elevations (not to scale).

Table 2. Attributes of the key geomorphic elements in chronological order

Feature	Genesis	Altitude (m ASL) Geomorphic	Erosional	Age	Climatic Event
Blackwood Plateau	Marine erosion	166–112	166–112	Eocene (42–39	Eocene Climatic Optimum, subsequent progressive sea-level regression
Yelverton Bench	Marine erosion	83	72	Miocene (~15	Miocene Climatic Optimum high stand, subsequent progressive sea-level regression
Whicher Toe-line	Toe of scarp	41	n/a	Pliocene (3.3 – 2.9	Pliocene Climatic Optimum still stand
Ambergate Plain	Terrestrial re-sedimented marine erosion surface	41–21	29–8	Late Pliocene – early Pleistocene	Onset of oscillatory ice ages
Cemetery Scarp	Marine erosion	21	n/a	400 000 y BP (MIS 11)	MIS 11 stillstand
Ludlow Plain	Terrestrial & marine sedimented marine erosion surface	11–8	5–3	125 000 y BP (MIS 5E)	Onset cyclic Pleistocene ice ages. Beginning of carbonate production on marine terraces
Layman Ridges	Mini scarp	4	n/a	7000 y BP	Holocene highstand
Busselton Wetlands	Marine & terrestrial erosion	4–1	0 to -6	7000 y BP to present	Regression in current interglacial

marks the beginning of rapid post-Pliocene cyclic marine erosion that shaped the bounding surfaces of younger deposits across the coastal plains. The geomorphic level of the Whicher Toe-line is regionally consistent at 41 m ASL, whereas the marine erosional surface, which more precisely records the sea level, is at 29 m ASL.

The coastal plains of the Geographe Bay hinterland consist of three different coastal plains, (Ambergate, Ludlow and Busselton Wetlands) each with distinct geology, geomorphology, genesis and age pointing to a complex history for the commonly applied term 'Swan Coastal Plain'. The Ambergate Plain is a terrestrially re-sedimented, marine-cut surface upon which the Yoganup Formation strands were deposited during a late Pliocene marine regression. The erosion surface cut into the Leederville Formation shelves gently seaward from 22 m ASL through a series of erosional steps to 11 m ASL. The 'Yoganup strands' were subsequently covered by paralic lagoonal and fluvial mud and sand attributed to the Guildford Formation.

The distinctive Cemetery Scarp, which cuts the Ambergate Plain, marks the seaward extent of paralic sedimentation, the limit of lateritized terrains and the beginning of carbonate shelf sedimentation in the region. A thin layer of 'Tamala-type' limestone, of likely MIS 5e age (~124 ka) underlies the Ludlow Plain and was probably deposited against the pre-cut Cemetery Scarp that may be as old as MIS 11 (~400 ka).

The Busselton Wetlands Plain formed after sea level receded from the Holocene highstand at 2–3 m ASL in the current interglacial, after the last glacial maximum. It has been the site of significant river diversions caused by the build-up of the present coastal dunes.

With tectonic stability, and the absence of masking dune systems, this area offers a key reference for Cenozoic global sea levels; this will require further precise dating and the construction of a form surface of the erosion surface of the Leederville Formation from the voluminous open-file mineral exploration drilling. In extrapolating the sea-level indicators outside the Geographe Bay hinterland, it is essential that sub-surface data, particularly from mineral exploration, be taken into account. Meaningful correlation cannot be done on geomorphic levels alone.

ACKNOWLEDGEMENTS

I am indebted to David Haig and Arthur Mory who have provided encouragement, support and critical appraisals of the manuscript in various stages. I have benefited from field visits to the study area by David Haig, Peter Baillie and Eckhart Håkansson. Simon Maris of WML Consulting Engineers and Tim Malseed of JWI Contractors are thanked for facilitating access to technical reports, drill core and site examinations, associated with the Vasse Diversion Upgrade Project. I am grateful to Daniel Peyrot for palynological confirmation of Cretaceous sand in the Vasse Diversion Channel. Geoff Cox kindly gave information on the geotechnical aspects relating to the Port Geographe development, and facilitated the delivery of useful technical reports. Colin Murray-Wallace and an anonymous reviewer are thanked for their perspicacious comments and suggested improvements to the paper. Ron Jensen gave friendly assistance during the field work of the project. Art Hoffman is thanked for professionally re-creating my figures.

REFERENCES

Anand R R & Paine M 2002. Regolith geology of the Yilgarn Craton, Western Australia: implications for exploration. *Australian Journal Earth Sciences* **49**, 3–162.

Anand R R & Gilkes R J 1987. The association of maghemite and corundum in Darling Range laterites. *Australian Journal of Soil Research* **35**, 305–311.

Barrows T T, Stone J O, Fifield L K & Cresswell R G 2002. The timing of the Last Glacial Maximum in Australia. *Quaternary Science Reviews* **21**, 159–173.

Baxter J L 1977. Heavy mineral sand deposits of Western Australia. Geological Survey Western Australia Bulletin 10.

Baxter J L & Hamilton R 1981. The Yoganup Formation and Ascot Beds as possible facies equivalents. Geological Survey of Western Australia Annual Report for 1980, 42–43.

Belford S M 1987. Capel Environmental Geology 1:50 000 map series. Geological Survey of Western Australia.

Brooke B P, Olley J M, Pietsch T, Playford P E, Haines P W, Murray-Wallace C V & Woodroffe C D 2014. Chronology of Quaternary coastal aeolianite deposition and the drowned shorelines of southwestern Western Australia — a reappraisal. *Quaternary Science Reviews* **93**, 106–124.

Bufarale G, O'Leary M & Bourget J 2019. Sea level controls on the geomorphic evolution of Geographe Bay, south-west Australia. *Journal of the Royal Society of Western Australia* **101**, 83–97.

Bunting J A 2014. *A geological field guide to the Capes Region of Southwest WA*. Earth Science Western Australia, Kensington, Western Australia.

Carruthers S 1998a. Annual technical report for ML 70/785 for the period 26/3/97 to 25/3/98, Grice Project, RGC Mineral Sands, Geological Survey of Western Australia WAMEX A54738 (open file).

Carruthers S 1998b. Annual technical report 98/70 for MC 1002 and 1024L 70/785 for the period 26/3/97 to 25/3/98, Ludlow Pines Project, Westralian Sands Ltd, Geological Survey of Western Australia WAMEX A56532 (open file).

Cockbain A E & Playford P E 1973. Stratigraphic nomenclature of Cretaceous rocks in the Perth Basin. Geological Survey of Western Australia Annual Report for 1972, 26–31.

Cockbain A E 2014. Australia goes it alone — the emerging island continent 100 Ma to present. Geological Survey of Western Australia Unearthed Series, 63p.

Cocks G C 1990. Report to Sinclair Knight: Port Geographe Project Geotechnical Studies. Coffey Partners P361/1-AK (unpublished; held by the Western Australian Museum, copy no. UR1610).

Cocks G C 1995. Report to Cossil Webley: Port Geographe Eastern End, additional friction core penetrometer. Coffey Partners P709/3-AB, 33p (unpublished; held by the Western Australian Museum, copy no. UR1611).

Cocks G C 2000. Preliminary Report to Clarke Hawkins: Geotechnical studies resort housing site Lot 624 Port Geographe. Coffey Geosciences P2554-HAB, 50p (unpublished; held by the Western Australian Museum, copy no. UR1613).

Cocks G C 2005. Report to Seaport Pty Ltd: Port Geographe south of Layman Rd Phases 1 and 2 studies. Coffey Geosciences P2554, 240p (unpublished; held by the Western Australian Museum, copy no. UR1613).

Collins L B & Baxter J B 1984. Heavy mineral-bearing strandline deposits associated with high-energy beach environments, southern Perth Basin, Western Australia. *Australian Journal of Earth Sciences* **31**, 287–292.

Collins L B, Wyroll K-H & France R E 1991. The Abrolhos carbonate platforms: geological evolution and Leeuwin Current activity. *Journal of the Royal Society of Western Australia* **74**, 47–57.

Cope R N 1975. Tertiary epeirogeny in the southern part of Western Australia. Geological Survey of Western Australia Annual Report for 1974, 40–46.

Descourieres C, Douglas G, Leyland L, Hartog N & Prommer H 2011. Geochemical reconstruction of the provenance, weathering and deposition of detrital-dominated sediments in the Perth Basin: the Cretaceous Leederville Formation, Southwest Australia. *Sedimentary Geology* **236**, 62–76.

Dicaprio L, Gurnis M & Muller R D 2009. Long-wavelength tilting of the Australian continent since the Late Cretaceous. *Earth and Planetary Science Letters* **278**, 175–185.

Dixon K & Johnson T E 2007. Technical report T15240 on C105/2002 Capel Group for the period 1/5/2006 to 30/4/2007, Iluka Resource Ltd, Geological Survey of Western Australia WAMEX A75398 (open file).

Dixon K 2008. Technical report T15992, on C105/2002 tenements for the period 1/5/2007 to 30/4/2008, Iluka Resources Ltd, Geological Survey of Western Australia WAMEX A78758 (open file).

Dutton A, Carlson A E, Long A J, Milne G A, Clark P U, Deconto R, Horton B P, Rahmstorf S & Raymo M E 2015. Sea-level rise due to polar ice-sheet mass loss during past warm periods. *Science* **349**, doi: 10.1126/science.aaa4019

Edgell H S 1957. Pleistocene mollusca from the vicinity of Busselton. Geological Survey of Western Australia Palaeontology Report 8/1963.

Fairbridge R W 1961. Eustatic changes in sea level. *Physics and Chemistry of the Earth* **4**, 99–185.

Finkl C W 1971. Levels and laterites in southwestern Australia. *Search* **2**, 382–383.

Gorczynska A 2020. Geotechnical report 9502-G-R-001 Pedestrian Bridge – Vasse diversion drain upgrade. WML Consulting Engineers (unpublished; held by the Western Australian Museum, copy no. UR1614).

Gozzard J R 2007. The Guildford Formation re-evaluated. *Australian Geomechanics Journal* **42 (3)**, 59–79.

Gozzard J R 2010. Sea to scarp — geology, landscape, and land-use planning in the southern Swan Coastal Plain. Geological Survey of Western Australia, 72p.

Haq B U, Hardenbol J & Vail P R 1987. Chronology of fluctuating sea levels since the Triassic (250 million years ago to present). *Science* **235**, 1156–1167.

Hamilton N T M & Collins L B 1997. Morphostratigraphy and evolution of a Holocene composite barrier at Minninup,

southwestern Australia. *Australian Journal of Earth Sciences* **44**, 113–124.

Harewood G P 2001. Annual mineral exploration report on ML70/86 for the period 6/11/2000 to 5/11/2001, Ludlow Project, Cable Sands Pty Ltd, Geological Survey of Western Australia WAMEX A63745 (open file).

Harrison P H 1990. Mineral Sands. Pages 694–701 *in* Geology and Mineral Resources of Western Australia. Geological Survey of Western Australia Memoir 3.

Hearty P J, Hollin J T, Neumann A C, O'Leary M & McCulloch M J 2007. Global sea-level fluctuations during the Last Interglaciation (MIS 5e). *Quaternary Science Reviews* **26**, 2090–2112.

Heptinstall A 2003. Surrender report for the period 23/8/2000 to 22/8/2003, EL70/2238, Whicher Project, Cable Sands Pty Ltd, Geological Survey of Western Australia WAMEX A67787 (open file).

Hill A P 2014. Annual mineral exploration report C186/2012 Wonnerup Project. Cristal Mining (Cable Sands Pty Ltd) Geological Survey of Western Australia WAMEX A101978 (open file).

Hirschberg K-JB 1989. Busselton shallow drilling groundwater investigation. Geological Survey of Western Australia Professional Papers p17.

Ingram B S & Cockbain A E, 1979. Stratigraphy of Ginginup No 1, central Perth Basin. Geological Survey of Western Australia Annual Report for 1978, 49–50.

Johnstone M H, Lowry D C & Quilty P G 1973, The geology of southwestern Australia — a review. *Journal of the Royal Society of Western Australia* **56**, 5–15.

Johnston T E 2004a.Technical report T10628 on group C105/2002 tenements for the period 1/5/2003 to 30/4/2004, Iluka Resources Ltd, Geological Survey of Western Australia WAMEX A68753 (open file).

Johnston T E 2004b. Technical report TR10577 of E70/1052 and E70/1620 for the period 1/1/2003 to 31/12/2003 Metricup Project, Iluka Resources Ltd, Geological Survey of Western Australia WAMEX A68209 (open file).

Johnston T E 2005. Technical report TR12199 on group C105/2002 for the period 1/5/2004 to 30/4/2005 Capel Project, Iluka Resources Ltd, Geological Survey of Western Australia WAMEX A70912 (open file).

Kendrick G W 1981. Molluscs from the Ascot Beds from the Cooljarloo heavy mineral deposit. Geological Survey of Western Australia Annual Report for 1980, 44.

Kendrick G W, Wyroll K-H & Szabo B J 1991. Pliocene-Pleistocene coastal events and history along the western margin of Australia. *Quaternary Science Reviews* **10**, 419–439.

Lewis S E, Sloss C R, Murray-Wallace C V, Woodruff C D & Smitheres S G 2012. Post-glacial sea-level changes around the Australian margin: a review. *Quaternary Science Reviews* **74**, 115–138.

Lisiecki L E & Raymo M E 2005. A Pliocene-Pleistocene stack of 57 globally distributed benthic $\delta^{18}O$ records. *Paleoceanography and Paleoclimatology* **20**, PA1003, doi: 10.1029/2004PA001071.

Lipar M & Webb J A 2014. Middle–late Pleistocene and Holocene chronostratigraphy and climate history of the Tamala Limestone, Cooloongup and Safety Bay Sands, Nambung National Park, southwestern Western Australia. *Australian Journal of Earth Sciences* **61(8)**, 1023–1039.

Lipar M, Webb J A, Cupper M L & Wang N 2017. Aeolianite, calcrete/microbiolite and karst in southwestern Australia as indicators of Middle to Late Quaternary palaeoclimates. *Palaeogeography Palaeoclimatology Palaeoecology* **470**, 11–29.

Lowry D C 1965. Geology of the Southern Perth Basin. Geological Survey of Western Australia Record 1965/17.

Lowry D C 1967. Busselton and Augusta. Geological Survey Western Australia 1:250 000 Geological Series Explanatory Notes.

Marnham J R, Hall G J & Langford R L 2000. Regolith–landform resources of the Cowaramup–Mentelle 1:50 000 sheet. Geological Survey of Western Australia Record 2000/18.

McArthur W M & Bettenay E 1960. The development and distribution of soils on the Swan coastal plain. *CSIRO Australia Soil Publication* **16**, 1–55.

McCulloch M T & Mortimer G E 2008. Applications of the ^{238}U–^{230}Th decay series to dating fossil and modern corals using MC-ICPMS. *Australian Journal of Earth Sciences* **55**, 955–965.

Miller K G, Browning J V, Schmelz J, Kopp R E, Mountain G S & Wright J D 2020. Cenozoic sea-level and cryospheric evolution from deep-sea geochemical and continental margin records. *Science Advances* **6**, doi:10.1126/sciadv.aaz1346

McGoldrick P 1990. Report on PLA 70/845-7, Ludlow Pines Project, RGC Exploration Pty Ltd, Geological Survey of Western Australia WAMEX A31001 (Open file).

Mory A J, Haig D W, McLoughlin S, Hocking R M 2005. Geology of the northern Perth Basin, Western Australia – a field guide, Geological Survey of Western Australia Record 2005/9.

Murray-Wallace C V, Belperio A P, Dosseto A, Nicholas W A, Mitchell C, Bourman R P, Eggis S M & Grun R 2016. Last interglacial (MIS 5e) sea-level determined from a tectonically stable, far-field location, Eyre Peninsula, southern Australia. *Australian Journal of Earth Sciences* **63(5)**, 611–630.

Mylroie J, Humphreys W, Brooks D & Middleton G 2017. Flank margin cave development and tectonic uplift, Cape Range, Australia. *Journal of Cave and Karst Studies* **79**, 35–47.

Norvick M S 2004. Tectonic and stratigraphic history of the Perth Basin. Geoscience Australia Record 2003/16, 30p.

Passmore J R 1962. Report on Busselton Shire Council water bore, Milne Street, Busselton. Geological survey of Western Australia Record 1962/19.

Pidgeon R T, Brander T & Lippolt H J 2004. Late Miocene (U+Th)–^{4}He ages of ferruginous nodules from lateritic duricrust, Darling Range, Western Australia. *Australian Journal of Earth Sciences* **51**, 901–909.

Pillans B 2005. Geochronology of the Australian regolith, Pages 41–61 *in* R R Anand & P de Broekert, editors, *Regolith landscape evolution across Australia: a compilation of regolith-landscape case studies and landscape evolution models,* Cooperative Research Centre for Landscape Environments and Mineral Exploration (CRC LEME) Monograph. http://crcleme.org.au/RegLandEvol/Geochron_of_%20Aust_Regolith.pdf

Playford P E & Low G H 1972. Definitions of some new and revised rock units in the Perth Basin. Geological Survey of Western Australia Annual Report 1971, 44–46.

Playford P E, Cockbain A E & Low G 1976. Geology of the Perth Basin. Geological Survey of Western Australia, Bulletin 124.

Prider R T 1948. The geology of the Darling Scarp at Ridge Hill. *Journal of the Royal Society of Western Australia* **32**, 105–129.

Rovere A, Raymo M E, Mitrovica K X, Hearty J, O'Leary M J & Inglis J D 2014. The Mid-Pliocene sea-level conundrum: glacial isostasy, eustasy and dynamic topography. Earth and Planetary Science Letters **387**, 27–33.

Sandiford M 2007. The tilting continent: a new constraint on the dynamic topographic field from Australia. *Earth and Planetary Science Letters* **261**,152–163.

Schafer D B, Johnson S L & Kern A M 2008. Hydrogeology of the Leederville aquifer in the western Busselton-Capel Groundwater Area. Department of Water, Hydrogeological Record Series, HG31.

Schmidt P W & Clark D A 2000. Palaeomagnetism, apparent polarwander path and palaeolatitude. Pages 12–17 *in* J J Veevers, editor, *Billion-Year Earth History of Australia and Neighbours in Gondwanaland,* Gemoc Press, Sydney.

Semeniuk V, Cresswell I D & Wurm P A 1989. The Quindalup Dunes: regional system, physical framework and vegetation

habitats. *Journal of the Royal Society of Western Australia* **71**, 23–47.

Słodkowska B, Kramarska R & Kasiński J R 2013. The Eocene Climatic Optimum and the formation of the Baltic amber deposits. Pages 28–31 *in* B Kosmowska-Ceranowicz, W Gierlowski & E Sontag, editors, The International Amber Research Symposium: Amber Deposits-Collections-The Market: Amberif Fair, 22–23 March 2013, Gadańsk, Poland.

Spratt R M & Lisiecki LE 2016. A Late Pleistocene sea level stack. *Climate of the Past* **12**, 1079–1092, doi: 10.5194/cp-12-1079-2016.

Stewart S 2007. Annual report for the period 30/4/2006 to 29/4/2007 Busselton Project, Olympia Resources, Geological Survey of Western Australia WAMEX A75706 (open file).

Stirling C H, Esat T M, McCulloch M T & Lambek K 1995. High-precision U-series dating of corals from Western Australia and implications for the timing and duration of the Last Interglacial. Earth and Planetary Science Letters **135**, 115–130.

Thomas C M 2018. Regional seismic interpretation and structure of the Southern Perth Basin. Geological Survey of Western Australia, Report 184.

Twiggs E J & Collins L B 2010. Development and demise of a fringing coral reef during Holocene environmental change, eastern Ningaloo Reef, Western Australia. *Marine Geology* **275**, 20–36.

Welch B K 1964. The ilmenite deposits of Geographe Bay. *Australian Institute Mining and Metallurgy, Proceedings* **277**, 25–48.

Wells M A, Danisik M & McInnes B I A 2018. (U–Th)/He dating of ferruginous duricrust, Boddington gold mine, Western Australia. Geological Survey of Western Australia Record 2018/13, 14p.

Wharton P H 1982. Geology and hydrology of the Quindalup boreholes. Record Geological Survey of Western Australia 1982/2.

White L T, Gibson G M & Lister G S 2013. A reassessment of paleogeographic reconstructions of eastern Gondwana: Bringing geology back into the equation. *Gondwana Research* **24**, 984–998, doi: 10.1016/j.gr.2013.06.009.

Whitney B B & Hengesh J V 2015. Geomorphological evidence for late Quaternary tectonic deformation of the Cape Region, coastal west central Australia. *Geomorphology* **241**, 160–174.

Wilde S A & Backhouse J 1976. Fossiliferous Tertiary deposits on the Darling Plateau. Annual Report Geological Survey Western Australia 1975, 49–52.

Wilde S A & Walker I W 1982. Collie 1:250 000 Geological Series Explanatory Notes. Geological Survey of Western Australia.

Anne Brearley

BSc, PhD (UWA)

18th September 1949 – 12th February 2022

A personal tribute

Anne was a UWA student, research fellow and associate of the Schools of Plant Biology and Biological Sciences, as well as a founding member of The University of Western Australia's Oceans Institute and a long-term member of the Royal Society of Western Australia. She made an outstanding contribution to the University and to the wider community, which was recognised by the award of a Chancellor's Medal in 2006. Anne Brearley passed away surrounded by her family in Albany after a long illness aged 72 on Saturday 12th February 2022.

Annie was a mature age student in the first undergraduate class I taught in 1988. She was special even then. Initially I had little idea of her already impressive skills. Her early fieldtrips with the Western Australia Museum in the 1960s through the State included parts of the Kimberley and the South Coast. Her experience in London in 1974, at the British Museum of Natural History and the Far Eastern Section of the Victoria and Albert Museum gave her a breadth of knowledge and understanding of the natural world, as well as dealing with people and different systems, both natural and organizational. She was lovely and great fun to be with. Most of all she wanted everyone to share in her wonder at the underwater world and her passion for learning.

At Cottesloe Beach in 2015 (photo: Angela Rossen).

Although already well versed in invertebrate biodiversity, she followed me into the depths of seagrass and algae, joining Gary Kendrick (then a fellow student) and myself on research diving trips up and down the coast, from the Pilbara to Shark Bay, down to estuaries on the South Coast to Esperance, Cape Arid and beyond, always keen to see more. More than anything she wanted to make sure everyone gained as much as possible out of a trip and did not miss anything, pointing out all the things we might not have seen—she was a true naturalist.

Her work on seagrass leaf grazing was breakthrough research in our understanding of limnoriid and lynseiid crustacean feeding on seagrass meristems in southern Australia. Her first postdoctoral appointment was with a program studying the ecological significance of seagrasses and their associated invertebrate communities in Cockburn Sound and Owen Anchorage (1997–1999).

She became a well-respected expert on natural systems, particularly estuaries. Her most significant contribution was 'Ernest Hodgkin's Swanland: Estuaries and Coastal Lagoons of South-western Australia'. A magnificent book, which she wrote as single author, clearly showcasing her affiliation with UWA. Published in 2005 it is still the text for understanding wave influenced estuaries in Australia.

Anne was also involved in undergraduate teaching and research supervision. She freely shared her detailed knowledge of marine invertebrate taxonomy and ecology with colleagues, staff and students. As an honorary research fellow she coordinated laboratories and lectured on seagrass ecology and estuaries of Western Australia. She co-supervised several Honours students on the reserve status on invertebrate assemblages, impact of grazers on seagrasses and intertidal invertebrate communities. She stimulated students to think critically, and added significantly to inputs made by formal supervisors.

Anne was also active as a volunteer in the Western Australian Naturalist Club, the Rottnest Island Voluntary Guides, Mandurah Coast Care, Cottesloe Fish Habitat Protection Area & Coast Care, Friends of Allen Park Bushland, Coastal and urban bushland restoration, and undertook community investigations in Esperance Bay. She was a regular attendee and contributor to the Society's talks and symposia.

Professor John Raven, University of Dundee, FRS, FRSE, made frequent visits to UWA in the 1990s. At a dinner at the home of Anne (and husband Reg) in Swanbourne, John commented to Annie, then a PhD

At the microscope during a 2015 Albany fieldtrip (photo: Angela Rossen).

student, on how impressed he was. She had a life. Not only was she a brilliant student, but she ran a household, organising and bringing up two wonderful boys, Winston and Charlie (then 12 and 10), entertaining in spectacular style, whilst discussing science and literature. When I told him she had died, he observed she was 'one of the best'.

The scale of Annie's output on my bookshelves is substantial. Besides her two theses, she contributed to eight Marine Biology Workshops and ten Seagrass Workshop volumes. There are also about ten other books or volumes she added immeasurably to, as well as her own publications. She collaborated with everyone she met and left a substantial legacy as an eminent natural historian.

Annie had an unbridled curiosity about everything and a passion to learn even more—characteristics that stayed with her until late in her life. I am honoured to have had the opportunity to share much of her life over the last 34 years. I will treasure the memories underwater and on land as well as her lasting scientific legacy.

Vale Anne Brearley.

Em Prof D I Walker
The University of Western Australia

Competition for space drives morphological abnormalities in the epiphytic foraminifer *Vertebralina striata* in Mangles Bay, Western Australia

CLÉMENT M. TREMBLIN [1*], JUSTIN H. PARKER [2] & DAVID W. HAIG [1]

[1] *Oceans Graduate School, The University of Western Australia, 35 Stirling Highway, Perth, WA 6009, Australia.*

[2] *14 Westminster St, Perth, WA 6101, Australia.*

[*] *Corresponding author: ✉ 23126169@student.uwa.edu.au*

Abstract

Aberrant morphologies are common in a foraminiferal assemblage living on the ribbon-like seagrass *Posidonia* in the shallow waters (<3 m) of Mangles Bay, Cockburn Sound, Western Australia. *Vertebralina striata* is one of the most conspicuous and abundant foraminifers living in the seagrass meadows. Although abnormal tests occur throughout the year, a sample collected in the Australian Summer contained an unusually high abundance of *Vertebralina* with deformed tests living amongst the dense tufted brown alga *Sphacelaria,* epiphytic on mature parts of *Posidonia* leaves. Many mature specimens of *V. striata* have deformed final uniserial chambers with earlier trochospiral chambers unaffected. Abnormalities include bifurcation and trifurcation of chambers, as well as cavities and depressions in the walls. These are associated with *Sphacelaria* thalli which obstruct chamber addition in adult tests by restricting living space. Seasonal growth patterns in both *Posidonia* and its epiphytic *Sphacelaria* may result in natural increases in the abundance of abnormal *Vertebralina* tests in summer.

Keywords: Miliolida, abnormal growth, *Sphacelaria*, algal–foraminiferal interaction, *Posidonia* epiphytes

Manuscript received 15 February 2022; accepted 28 April 2022

INTRODUCTION

Seagrass meadows are common on sand banks in the inner neritic zone of southwest Australian coastal waters (McMahon *et al*. 1997; Graham 2000; Carruthers *et al*. 2007). The ribbon grass *Posidonia* (including *Posidonia australis* and *Posidonia sinuosa*) is one of the major constituents among the phytocenosis described in these meadows (Gobert *et al*. 2006; Carruthers *et al*. 2007). *Posidonia* is a photosynthetic organism that undergoes vigorous growth over summer and a low growth rate in winter when there is lower light intensity and the water is colder (Cambridge 1975; Walker & McComb 1988). During late spring to autumn, their leaves start shedding from the root, forming extensive areas of floating wrack (McComb *et al*. 1981; Silberstein 1985). *Posidonia* leaves are host to a diverse epiphytic biota including algae, minute diatoms with siliceous frustules, benthic foraminifers, sponges, hydrozoans, bryozoans, micro-bivalves, micro-gastropods, ostracods and other minute crustacea, and *Spirorbis* tubeworms (Gordon & Parker 1991; Trautman & Borowitzka 1999; Semeniuk, 2001; Brown, 2005; Prado *et al*. 2008). Common algae include the tufted brown alga *Sphacelaria,* and scale-like encrustations of calcareous coralline algae.

In summer, at water depths <3 m, *Posidonia* in Mangles Bay (Fig. 1a, b) commonly has a dense cover of *Sphacelaria,* at least on the upper portions of many leaves (Fig. 1c). *Sphacelaria* consists of very short, branching upright, elongate and moderately angled thalli (filaments) that vary from dark to light brown (Tsuda 1972; Huisman & Walker 1990; Ateweberhan & Prud'homme van Reine 2005). Associated with the short tuft-like *Sphacelaria* are many living foraminifers—eukaryotic unicellular microorganisms with tests revealing different chamber structures and shapes. Among the most common foraminifers living in spaces between thalli, are the porcelaneous *Vertebralina striata* d'Orbigny and *Peneroplis planatus* Fichtel & Moll. These species can be seen without magnification. Examination of *Posidonia* leaves during January 2022 yielded an unusually high abundance of *V. striata* with morphological deformities and less-common deformed *P. planatus*.

In Shoalwater Bay, just south of Mangles Bay, Trautman & Borowitzka (1999) documented a great increase in abundance of *Sphacelaria* and some other algae on *Posidonia* leaves from low levels during winter, after shedding of leaves during autumn (April–May), to dense growths in late summer (March). Our observation of abundant deformed *V. striata* was made at the height of the Australian summer, when the epiphytic algal growths were dense on the upper portions of *Posidonia* leaves (Fig. 1b, c).

Morphological abnormalities and inhibited shell growth in benthic foraminifers have mostly been attributed to pollution and heavy metal contamination (Alve 1995 and references within; Yanko *et al*. 1998; Le Cadre & Debenay, 2006; Eliahu *et al*. 2020). Boehnert *et al*. (2020), however, found that test deformations did not correspond to historic heavy metal contamination and suggested that other environmental stressors were

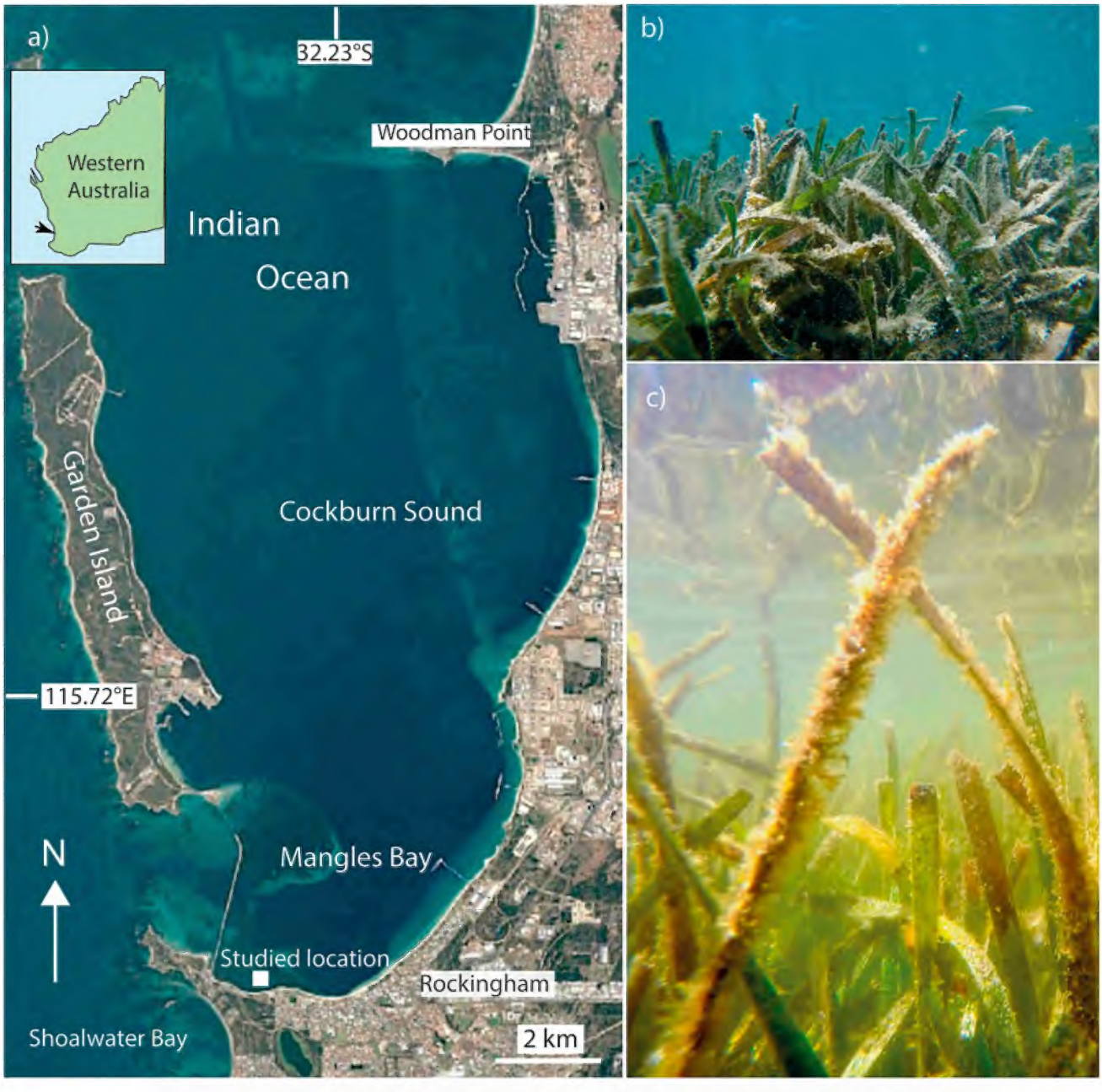

Figure 1. a) Google Earth image of Mangles Bay in the Cockburn Sound region, showing the locality investigated in January 2022 (represented by the white square 32.2744°S; 115°7054°E); b) Underwater photo of the *Posidonia australis* seagrass meadow; and c) closeup view of *Posidonia australis* leaves covered by epiphytic algae and other micro-benthic biota.

responsible. Similarly, Sagar *et al*. (2021a, b) cultured the porcelaneous foraminifer *Amphisorus hemprichii* under different levels of heavy metal contamination and did not find any significant test abnormalities. Several studies have shown relationships between natural salinity, oxygen, temperature, and/or pH variability and increased incidence of test aberrations in foraminifers (e.g. Boltovskoy *et al*. 1991; Geslin *et al*. 2002; Meriç *et al*. 2009; Li *et al*. 2020). Geslin *et al*. (2002) further showed that abnormalities could form during the reconstruction of tests damaged by hydrodynamic processes. Consorti *et al*. (2020) considered abnormalities in the tests of *P. planatus* to be a response to incrustation of filamentous cyanobacteria covering the tests and impeding the protoplasmic stream during the addition of new chambers. The interaction between algal epiphytes and foraminifera on seagrasses and competition for space, however, have not been considered as forming morphological irregularities in any foraminifer.

To better understand the morphological deformities in the porcelaneous foraminifer *Vertebralina*, this paper (1) describes its occurrence on *Posidonia* leaves in Mangles Bay; and (2) examines the relationship between *Vertebralina* and the epiphyte *Sphacelaria* on the leaves. It also compares the deformities with those described for the species elsewhere.

LOCATION, MATERIAL AND METHODS

Cockburn Sound is home to a diverse marine biota with shared habitats (including seagrass meadows) for many fish and invertebrates (Dybdahl 1979; Johnston *et al.* 2008). Mean monthly water temperature ranges from about 24 °C in summer (December–February) to below 16 °C in winter (June–August). Normal-marine salinity prevails throughout the year (Coulson *et al.* 2016). Mangles Bay is a protected bay in the southern part of Cockburn Sound (Fig. 1a), 47 km south of Perth. The bay has a low-energy shoreline and is microtidal (diurnal, with a mean tidal range <0.5 m; Hegge *et al.* 1996; Masselink & Pattiaratchi 2001; Travers 2007). Rockingham, which borders the southern shoreline of the bay, is a popular recreational area for marine activities including fishing, snorkelling, and boating in summer. The high maritime boat activity has led to the contamination of the area with Tributyltin $C_{12}H_{27}Sn$ (TBT), a product that was applied on boats to avoid incrustations of living organisms (D A Lord & Associates Pty Ltd 2001; Department of Fisheries 2016). Its release into the aquatic environment was responsible for numerous anomalies especially in shellfish, notably oysters, and other marine invertebrates (Alzieu *et al.* 1986; Alzieu 2000; Higuera-Ruiz & Elorza 2011). In Western Australia, use of Tributyltin in protected parts of Cockburn Sound was banned in 2003.

During an ongoing study of benthic foraminifers from the seagrass meadow in southern Cockburn Sound, small lengths of fresh *Posidonia* leaf and sediment from depths down to 6 m have been examined and foraminifera counted (Tables 1, 2). Live *Vertebralina striata* and *Peneroplis planatus* are particularly abundant, especially in shallower parts of the meadow, and are clearly detected without magnification by their large flat tests that are white and purple, respectively. These species are also common constituents of the sediment sampled within the meadow. During a recent excursion in Mangles Bay (January 2022) specimens of living foraminifers from seagrass leaves intensely covered by algae were carefully picked, counted and stored in a small plastic container filled with local sea water. The foraminifers were photographed using reflected light microscopy and images rendered with Helicon focus software. Photographs were used for measuring test and chamber dimensions. An environmental scanning electron microscope under low vacuum was used to image selected uncoated specimens. Figured specimens are curated in the collection of the Earth Science Museum at The University of Western Australia.

POSIDONIA HABITAT

Posidonia australis and *P. sinuosa* form a dense meadow at the study site (Fig. 1b). In January–February 2022, the seagrass leaves were about 30 to 50 cm long and many had been cropped at the top (Fig. 1b, c). The seagrass grows on a medium to coarse sandy bottom and forms a relatively dense meadow punctuated by sandy patches caused mainly by boat moorings. At the time of study, mature leaves were covered by a dense growth of predominantly epiphytic algae (Fig. 1b, c).

On the small leaf segments examined for this study, scale-like calcareous coralline algae cover about 50% of the surface. Tufts of *Sphacelaria* occur at frequencies from <2 per cm^2 on long young (clean) leaves to 11–12 per cm^2 on mature densely covered leaves (Table 1). Much very fine detritus (mud and organic particles, including transparent gelatinous material) accumulates around the thalli. Also present are very thin, flexible, agglutinated worm tubes which run through the *Sphacelaria* growths and calcareous serpulid worm tubes. Rare bryozoans, sponges and hydrozoans also encrust on the leaf segments.

The most conspicuous foraminiferal species living among *Sphacelaria* on the *Posidonia* leaves are *V. striata* and *P. planatus*. These porcelaneous foraminifers are characterised by an imperforate wall composed of high-magnesium calcite crystallites (Parker 2017). They are easily distinguishable, without magnification, in the field by colour. The test of *V. striata* is white with the faint dull grey protoplasm evident, particularly in inner chambers, through the translucent wall. It also has a brown organic lining to the inner whorl of chambers (Fig. 2). In contrast, the purple–violet protoplasm, due to rhodophyte symbionts (Lee 1990; Walter *et al.* 1992), of *P. planatus* is highly visible through the very thin parts of its wall between septa.

Other living foraminifers found amongst the *Sphacelaria* include common smaller miliolids (such as *Quinqueloculina*, *Triloculina*, and *Miliolinella*), and the smaller rotaliids *Elphidium* and *Planorbulina*. Other less common foraminifers include the attached *Cornuspiramia*, *Lamellodiscorbis* and *Nubeculina*. The thalli also host a diverse range of very rare other smaller rotaliids as well as buliminids. The observed forms are well-known from other Western Australian coastal sites (Parker 2009, and personal observations of the authors).

Figure 2. Live *Vertebralina striata* among epiphytes including the tufted brown alga *Sphacelaria* on *Posidonia* leaves; note the strongly grooved ornament of this specimen, grey colour of the protoplasm and brown internal organic lining in the initial whorl. A tuft of *Sphacelaria* is present near the *V. striata*. A large *Peneroplis planatus* is in the background.

Table 1. Frequencies of live *Vertebralina* on leaf segments of *Posidonia* examined in January–February 2022 and May 2020 from Mangles Bay. The area was calculated from the length and width of the segment. Minor deformities include small incisions and cavities in the wall (e.g. Fig. 3a, h–j). Major deformities include several incised subdivisions of final chambers (e.g. Fig. 3b, c, f, g, k–m).

A. Leaf segments examined January–February 2022

Leaf area: 23 cm², with heavy epiphyte cover

Live specimen count	**Total**	**per cm²**
Vertebralina	116	5
"*Sphacelaria*" tufts	278	12
***Vertebralina* test growth stage**	**Total**	**%**
Trochospiral only	50	43
Adult - with uniserial stage	66	57

***Vertebralina* test deformities**	**Normal**	**Minor**	**Major**
Trochospiral (only) tests - total count	45	5	
% Trochospiral (only)	90	10	
Adult tests — total count	11	38	17
Adult tests — % adults	17	57	26

Leaf area: 45 cm², with heavy epiphyte cover

Live specimen count	**Total**	**per cm²**
Vertebralina	75	2
"*Sphacelaria*" tufts	491	10.9
***Vertebralina* test growth stage**	**Total**	**%**
Trochospiral only	15	20
Adult - with uniserial stage	60	80

***Vertebralina* test deformities**	**Normal**	**Minor**	**Major**
Adult tests — total count	19	18	23
Adult tests — % adults	32	30	38

Leaf area: 48 cm², with moderate epiphyte cover

Live specimen count	**Total**	**per cm²**
Vertebralina	108	2
"*Sphacelaria*" tufts	229	4.8
***Vertebralina* test growth stage**	**Total**	**%**
Trochospiral only	66	61
Adult - with uniserial stage	42	39

***Vertebralina* test deformities**	**Normal**	**Minor**	**Major**
Adult tests — total count	26	13	3
Adult tests — % adults	62	31	7

Leaf area: 46 cm², with light epiphyte cover

Live specimen count	**Total**	**per cm²**
Vertebralina	40	87
"*Sphacelaria*" tufts	76	2
***Vertebralina* test growth stage**	**Total**	**%**
Trochospiral only	25	63
Adult — with uniserial stage	17	37

***Vertebralina* test deformities**	**Normal**	**Minor**	**Major**
Adult tests — total count	6	9	2
Adult tests — % adults	0	30	38

B. Leaf segments scanned May 2020

Clean leaf segments with few epiphytes

leaf area: 61.5 cm²

Live specimen count	**Total**	**per cm²**
Vertebralina	32	0.5
***Vertebralina* test growth stage**	**Total**	**%**
Trochospiral only	28	88
Adult — with uniserial stage	4	12

***Vertebralina* test deformities**	**Normal**	**Minor**	**Major**
Trochospiral (only) tests — total count	28	1	3
% Trochospiral (only)	88	3	9

Leaf segments with heavy epiphytes cover (including *Sphacelaria*)

leaf area: 34 cm²

Live specimen count*	**Total**	**per cm²**
Vertebralina	215	6

* Test were identified in photographic scans of leaves and were partly hidden under epiphytes. Therefore, counts of deformities could not be made.

Table 2. Frequencies of *Vertebralina striata* in sediment samples from under *Posidonia* seagrass meadows at Mangles Bay. n = number of specimens. Sediment samples were washed in freshwater, the water decanted, and the sediment dried. The volume of dry sediment was measured in a calibrated cylinder.

Sample	**Water Depth (m)**	**Volume (cm³)**	**n *V. striata***	**n/cm³**	**n Adults (>4 chambers)**	**n Bifurcated**	**n indented**
24112018-01	0.8	1.1	65	59	41	2	32
24112018-02	2.3	1.2	44	37	23	2	23
24112018-03	2.5	1.6	23	14	14	0	13
10112018	4	1.8	8	4	6	0	5
10112018-04	4	1.7	7	4	5	0	2
10112018-05	5	1.6	33	21	8	0	3
10112018-06	6	1.5	15	10	5	0	2
11022022-01	1	0.8	37	46	5	1	20

MORPHOLOGICAL VARIATION IN *VERTEBRALINA STRIATA*

Vertebralina striata has a low trochospiral test with flattened broadly elongate chambers and a broad apertural slit that lies on the flat umbilical side along the terminal face of the last chamber (Fig. 3). The aperture is bordered by a thickened lip. An abnormal Y-shaped aperture is present in one large, deformed test (Fig. 3m). Most descriptions of the species show specimens with final chambers still part of a trochospiral coil (Loeblich & Tappan 1987; Haig 1988; Hottinger *et al.* 1993; Parker 2009). However, some of the specimens from Mangles Bay have up to five uncoiled adult chambers (Fig. 3). A similar uncoiled morphotype from Oyster Harbour next to Albany in southern Western Australia, was attributed to *Vertebralina* sp. by McKenzie (1962, pl. 1 fig. 21). In our studied assemblage, tests vary from a juvenile trochospiral morphotype of 288 μm maximum diameter to a gerontic test with five uniserial chambers and a

Figure 3. *Vertebralina striata* extracted from around *Sphacelaria* on *Posidonia* leaves at studied locality; views of the dorsal/spiral (a–c, f, g, i, j) and ventral/umbilical (d, e, h) sides showing morphological modifications of final chambers in response to development among thalli (brown fibre-like growths) of *Sphacelaria* brown algae. Rendered reflected-light micrographs. Scale bars = 200 μm. a) UWA181398; b) UWA181399; c) UWA181400; d) UWA181401; e) UWA181402; f) UWA181403; g) UWA181404; h) UWA181405; i) UWA181406; j) UWA181407; k) UWA181408; l) UWA181409; m) UWA181410.

maximum length of 1192 µm (Fig. 4a). Considerable variation exists in the lengths of adult (uniserial) tests, e.g. at the three uniserial chamber stage, tests vary from 577–962 µm (Fig. 4a). In undeformed tests with uniserial stages, the growth pattern of chamber addition is, however, markedly irregular (Fig. 4b).

Wall ornamentation is highly variable between specimens and even between adjacent chambers. It can vary from unornamented and smooth (e.g. early parts of test in Figs. 3c and i), to finely striate as is typical of the species and most specimens (Figs. 3d–i). The striae extend the length of the chamber and are 2–4 µm wide (mean ~3 µm). In many large specimens, large grooves may be present that are typically parallel to the direction of growth and extend for most of the height of the chamber (Fig. 3). The grooves are much larger than the striate ornament, ranging in width from 12 to 20 µm (mean = ~15 µm) and are superimposed by the fine striae. The shapes of the grooves vary and may be linear (Fig. 3e), irregular (Fig. 3h), sinuous (Fig. 3h), broken (Fig. 3b), or curved (Fig. 3f), which is in part due to the chamber shape and tightness of coiling at the stage of chamber development. The wall of the test is thinner at the grooves, exposing parts of the chamber lumen and the foraminifer to increased light intensity, as observed in live specimens (see Fig. 2). In some specimens, numerous long thin irregular marks that are perpendicular to the coiling direction and wall ornament were observed under SEM (e.g. Fig. 5d). The nature of these is uncertain but given that they show no distinct excavation of the test wall, are parallel to the apertural face and appear to be restricted to the last chamber, they are possibly wrinkles in an organic lining. Further study is required to confirm the nature of these marks.

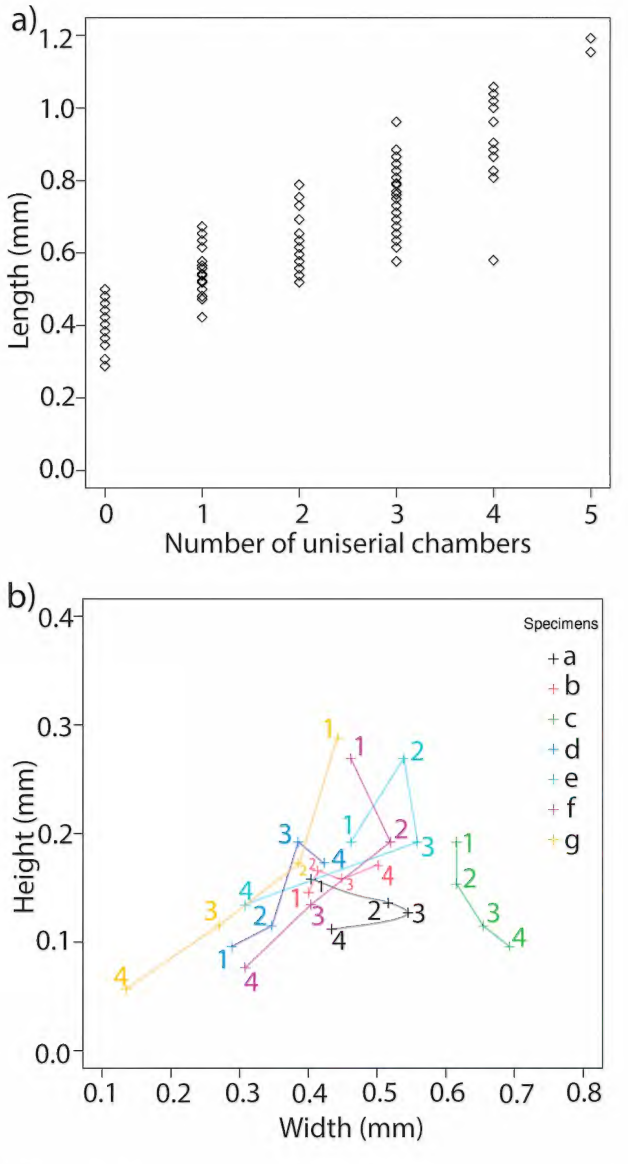

Figure 4. Measurements on tests of *V. striata* collected from small leaf segments (23 cm^2 of leaf surface): a) Length of test against number of uniserial chambers with '0' being tests with only trochospiral development; and b) Highly irregular growth patterns in the uniserial stages of seven tests that lack abnormalities; progressive changes (1–4, added uniserial chambers) are represented by a plot of maximum chamber height vs maximum chamber width.

The final chambers of some tests bifurcate (Fig. 3b, c, h, j, l, m) or trifurcate (Fig. 3f, g, k). Small cavities and indentations also exist in the wall of many tests (Fig. 3g). Some indentations are clearly the linear impressions of *Sphacelaria* thalli (Fig. 5b). These abnormalities, particularly branched chambers, are found mainly in large specimens with uniserial mature stages (Fig. 3j). The abnormalities are much less common in the earlier trochospiral chambers and were not observed in tests with less than four final chambers. The causes of abnormalities mainly influenced chamber growth during the final stages of test development in mature specimens.

Chamber addition has been observed in several specimens (Fig. 6). A transparent gelatinous sheath encases the extruded protoplasm and forms a template for the new chamber. Incipient calcification takes place in patches on the inside of the sheath and is marked by whitish areas (Fig. 6b, c). These are presumably concentrations of minute calcite crystallites (Angell 1980; Hemleben *et al.* 1986; de Nooijer *et al.* 2009). The striate ornament, as occurs in previous chambers, is already imprinted in the transparent sheath (Fig. 6c). As suggested by Parker (2017), ornament in the miliolid foraminifers is a genetic function of wall formation, rather than added afterwards.

The presence of abnormal *V. striata* living on *Posidonia* has been observed throughout the year. On *Posidonia australis* leaf segments with few epiphytes collected during May 2020, living *V. striata* was present at frequencies of 0.5 specimens per cm^2, but on leaf segments with dense epiphyte growth the frequencies were six specimens per cm^2, comparable to frequencies found in our January 2022 observations (Table 1). This suggests that the maximum abundance of *V. striata* occurs when there is a heavy epiphyte load on the *Posidonia* leaves.

Examination of mainly discarded *V. striata* tests in sediments from Mangles Bay yielded 4–60 specimens per cm^3 (Table 2). The highest abundances are in the shallow (<2 m) western parts of the seagrass meadow, and the lowest in deeper (>4 m) on the outer edges. Within the sediment, bifurcate and trifurcate specimens are rare, with only two specimens per cm^3 encountered in samples

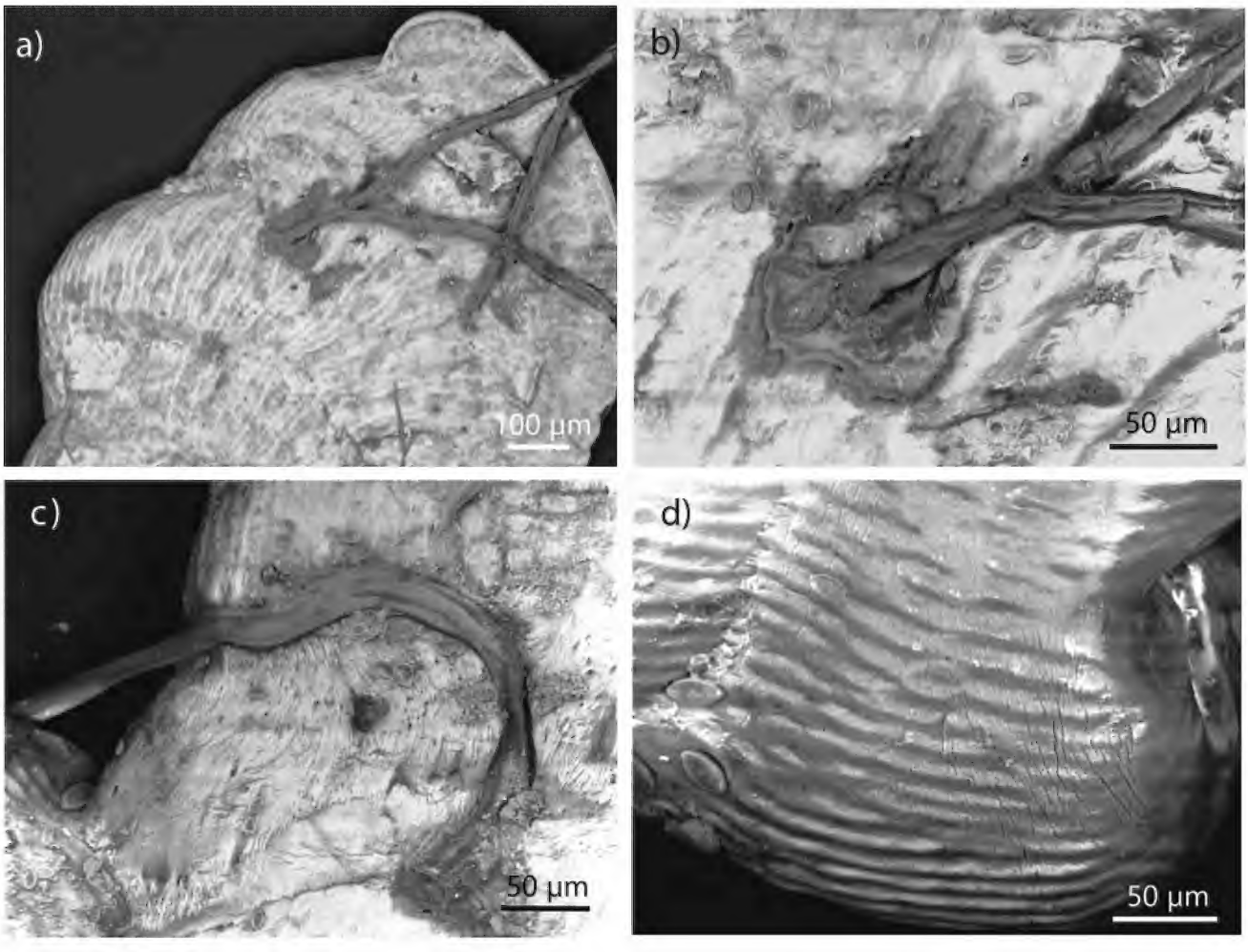

Figure 5. *Vertebralina striata* with thalli of *Sphacelaria* and abnormal surface microstructure; SEM micrographs taken of uncoated specimens in an environmental scanning electron microscope. a, b) lateral views of UWA181398 (Fig. 3a); b) closeup view of the base of a protruding thallus; c) lateral views of UWA181400 (Fig. 2c); and c, d) lateral view of UWA181404 (Fig. 3g). Note long thin irregular marks that are perpendicular to the striate ornament. Diatoms are common on most of the tests.

with the highest abundances of *V. striata*—at the same locality as the observed abundance of abnormal *V. striata* living amongst *Sphacelaria*. Minor deformities, such as indentations and the propensity to uncoil, can make up to >50% of the adult population in the sediment.

INFLUENCE OF *SPHACELARIA* ON GROWTH IN *V. STRIATA*

On *Posidonia* leaves, *V. striata* are common in small, enclosed spaces among the tufted *Sphacelaria* (Fig. 2). They are much more common around *Sphacelaria* growths than on younger leaves and lower parts of leaves that lack a dense epiphytic community. In normal growth position, *V. striata* lives with its broad flat umbilical side downwards on the substrate. In Mangles Bay, they are commonly found on the surface of *Posidonia* leaves—an observation that contrasts with that of Langer (1993) who suggested *Posidonia* rarely hosts *V. striata* in meadows within the Mediterranean. The aperture, through which food is ingested, is normally just above the leaf surface enabling pseudopodia to gather diatoms and other very fine organic detritus, and to stream this material to the internal cytoplasm. However, where there are dense *Sphacelaria* thalli on the *Posidonia,* this life position is impossible to maintain. The confinement to small inter-thalli spaces impedes the normal addition of new chambers. This is evident in the observed relationship between *V. striata* and *Sphacelaria* tufts on *Posidonia* leaves, i.e. the tufts occur within shallow grooves in the peripheries of tests, between bifurcating and trifurcating branches, extending through narrow holes in the test, and growing attached to first-formed parts of large mature *V. striata*.

We suggest that morphological abnormalities present in mature specimens of *V. striata* living on *Sphacelaria*-encrusted leaves, are the result of *Sphacelaria* thalli obstructing the flexible transparent sheath (Fig. 6) that forms the template for the new chamber. Figure 7 shows a model for adult chamber addition. Normal development (Figs 3d, i; 6a–c) takes place where no thalli are present in the area where the new chamber is forming (Fig. 7a, b). Bifurcations (Fig. 3 c, h, j) and trifurcations (Fig. 3f, g) develop where *Sphacelaria* thalli impede the normal development of the transparent sheath encasing the

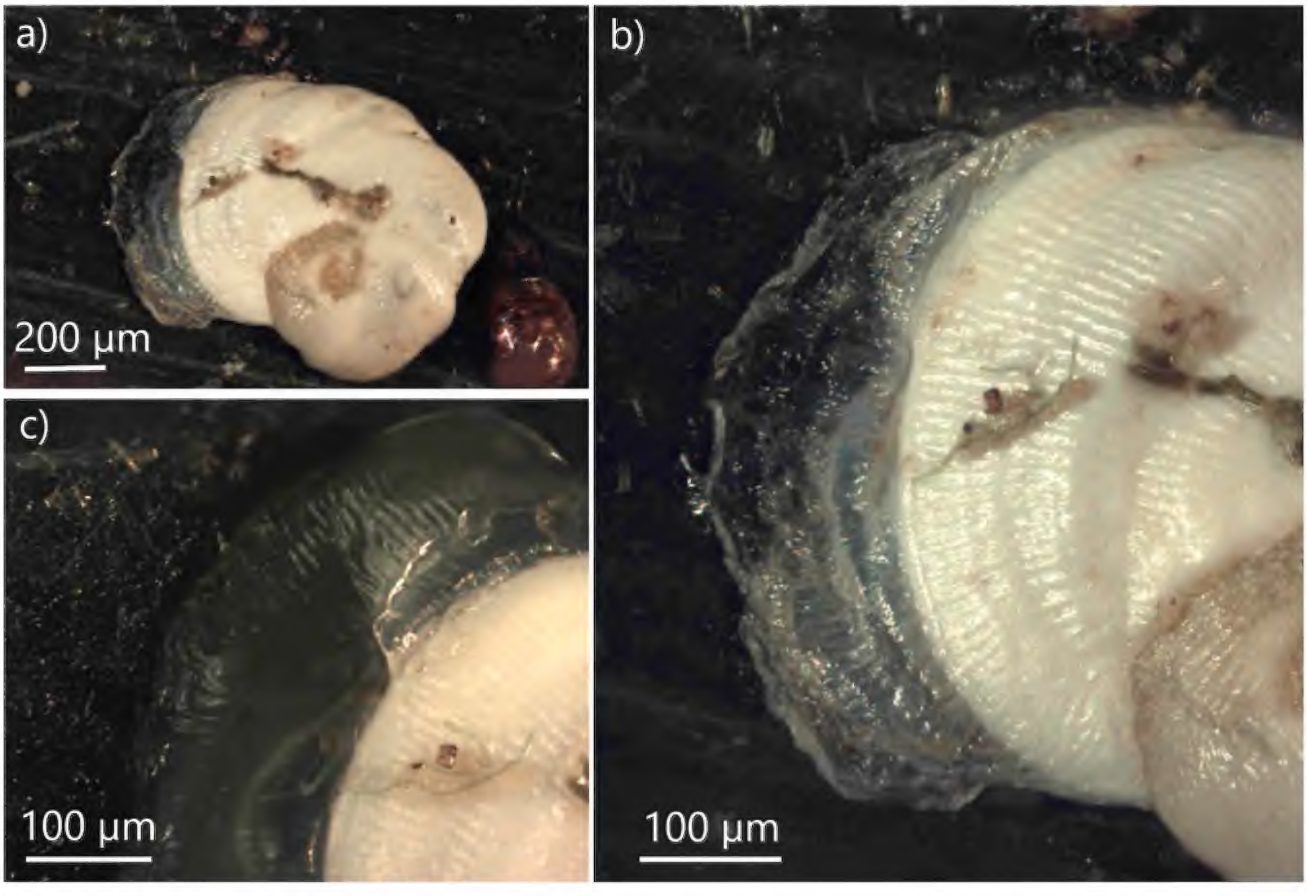

Figure 6. The addition of a new uniserial chamber in *Vertebralina striata* living on a *P. australis* leaf free of dense epiphytic algae. Note: (1) cytoplasm is enveloped by a transparent sheath that outlines the position of the new chamber; (2) striate ornament is already present in the transparent sheath before calcification; (3) white areas on the sheath indicate incipient concentrations of minute calcite crystallites that form the mineralised wall. Specimen collected from Mangles Bay seagrass meadow in 2018.

protoplasm of the new chamber (Fig. 7c, d). Small cavities and depressions, and peripheral grooves are also formed where the transparent sheath encloses or is indented by *Sphacelaria* thalli (Fig. 7e, f). The effects of algal filaments that encrust on the wall surface, other than indentation of the test wall, require further study (Fig. 5).

DISCUSSION

Morphological aberrations in *V. striata*, similar to those reported here, have been described in the Gulf of Izmir, northern coast of Karaburun Peninsula, Turkey by Meriç *et al*. (2009, 2012, 2019). Their specimens were collected from sand near a thermal spring, but the living habitat was not described. Several studies conducted around the same locality have described prolific shallow-water seagrass meadows, where *Posidonia oceanica* is abundant (Dural *et al*. 2012, 2013). The epiphytic community on *P. oceanica* comprises brown macroalgae including *Sphacelaria* (Taşkin & Öztürk 2013; Taşkin 2014). The assemblage in sand likely includes many dead specimens from many generations of the species. Some of the *V. striata* tests figured by Meriç *et al*. (2019, e.g. figs 2, 4a, b, c), appear to have scars on the walls caused by embedded algal thalli. The morphology may not be related to influences on the environment by thermal springs as this would cause noticeable deformities in the tests throughout ontogeny. Based on our observations in Mangles Bay of *V. striata* with similar deformities, we suspect that the Turkish deformed assemblages of *V. striata* may also be the result of interaction with *Sphacelaria* epiphytes on *Posidonia*.

Consorti *et al*. (2020) suggested that abnormal test development in *Peneroplis planatus* from Pete's Pond at Lake McLeod, Western Australia, was linked to cyanobacterial growth. They postulated that *P. planatus* gets entangled in fine cyanobacterial filaments growing on mangrove roots inhibiting growth, forcing the foraminifers to adapt the shape of new chambers around the filaments. This results in bifurcation and trifurcation of chambers. As in *Vertebralina*, such deformities were only observed in the later chambers of adult specimens. At Mangles Bay, the association of *V. striata* with the brown algae thalli appears to be similar and results in wide variations in the shape of adult chambers. On the examined seagrass leaves, deformed *V. striata* were observed abutting other less common epiphytes, such as other algae and bryozoans. The interactions were not as striking as observed with the denser *Sphacelaria*, but overall, our observations demonstrate that by deforming its chambers during growth, *V. striata* is able to successfully compete for living space amongst other epiphytic organisms.

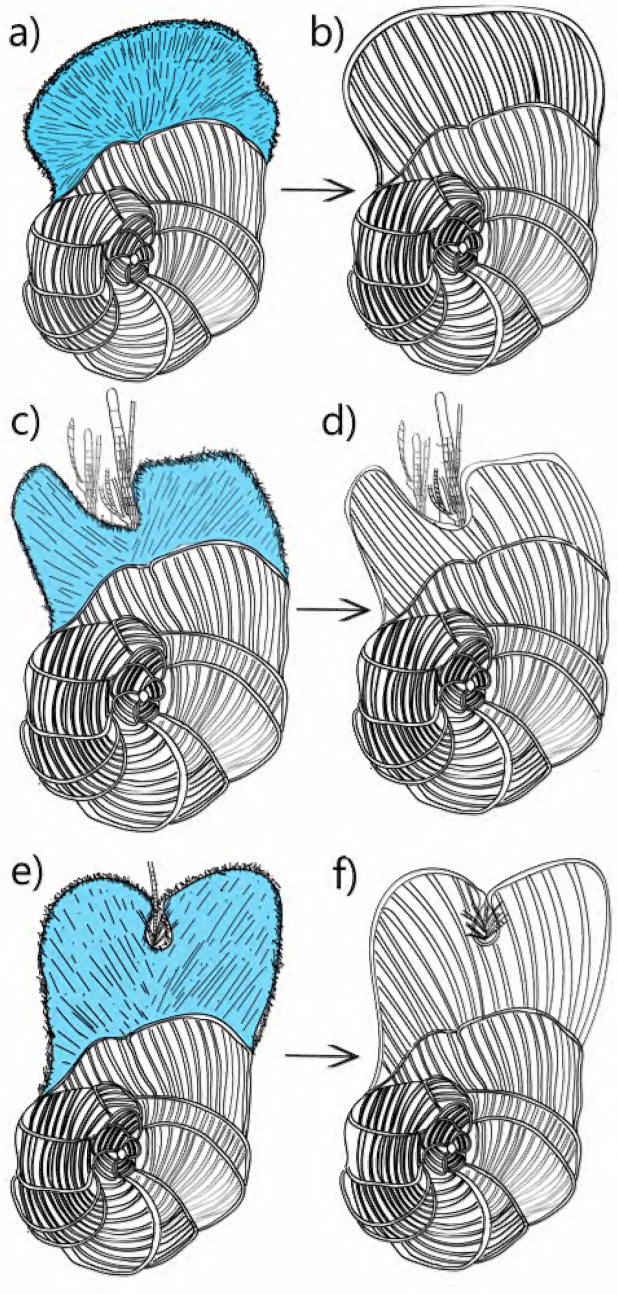

Figure 7. Diagrams showing possible scenarios for development of morphological abnormalities in *Vertebralina striata*. The blue areas shown on a, c, e) are cytoplasm extruded from the aperture covered by a transparent flexible sheath (Fig. 6) that forms the template for the new chamber; a, b) normal unimpeded growth; c, d) chamber addition when dense tufted *Sphacelaria* causes bifurcation of the final chamber; e, f) initial chamber divergence around *Sphacelaria* thalli is repaired leaving the thalli protruding through the test.

We suspect that the seasonal shedding of leaves by *Posidonia* (Silberstein 1985) and changes in intensity of *Sphacelaria* incrustation (Trautman & Borowitzka 1999) results in the seasonal variation in the abundance of deformed tests of *Vertebralina* and possibly of other foraminifers. As *Posidonia* sheds leaves in Autumn (April–May) and the build-up of *Sphacelaria* reaches a maximum density in Summer (December–February), the maximum number of deformed tests would be expected during Summer. This also suggests that there may be increased abundances of dead deformed tests in sediment where seagrass wrack is deposited, which could be away from meadows. However, investigation of these is outside the scope of the present study, and demonstrations of seasonal and transported increases in the abundance require further study.

CONCLUSIONS

Up to 80% of mature specimens of *Vertebralina striata* in the fauna described here, living among the brown tufted algae *Sphacelaria* on *Posidonia* leaves, show abnormalities in their adult chambers. During chamber addition, due to obstruction mainly by thin cylindrical algal thalli, deformities occur in the growth of the flexible transparent sheath that forms a template for the new chamber. Thus, after calcification, some specimens have bifurcated or trifurcated final chambers, and/or have embedded thalli in the chamber walls forming depressions or cavities. The abnormalities are mainly in the adult chambers of mature specimens; juvenile stages show normal growth patterns.

This study demonstrates that some foraminiferal species, when competing for space with epiphytic algae, can adapt the shape of new chambers to deflect around or accommodate the epiphyte, resulting in structural abnormalities in the test that need not be linked to pollution. It also shows an increase in *V. striata* with deformed tests may be linked to seasonal growth patterns in both *Posidonia* and its epiphytic *Sphacelaria*. More detailed studies of living *V. striata* on *Posidonia* should include: (1) sampling and examination of the meadows and their epiphytes at short regular intervals through the year to chart seasonal variations in more detail; (2) determine if the abundance of foraminiferal species such as *V. striata* is linked to abundance of food particles (e.g. diatoms) in the dense *Sphacelaria* growths; and (3) recording abnormalities in other foraminifers living in Cockburn Sound, particularly in other habitats.

ACKNOWLEDGEMENTS

Marion Cambridge provided valuable information on *Posidonia* and *Sphacelaria* and made comments on the manuscript. Two anonymous reviewers are thanked for their useful comments and suggestions that have helped improve the manuscript. Aleksey Sadekov assisted with the SEM study of selected specimens. Netramani Sagar gave advice on the effects of heavy-metal pollution on foraminifers. Jenny Bevan and Eckart Håkansson kindly read an early version of the manuscript. Kailah Thorn of The University of Western Australia Earth Science Museum is thanked for curatorial assistance. We thank the Oceans Graduate School at The University of Western Australia for facilitating the voluntary research internship of Clément Tremblin and the Honorary Senior Research Fellowship of David Haig. The authors acknowledge the facilities, and the scientific and technical assistance of Microscopy Australia at the Centre for Microscopy, Characterisation & Analysis, The University of Western Australia, a facility funded by the University and state and commonwealth governments.

REFERENCES

Alve E 1995. Benthic foraminiferal responses to estuarine pollution; a review. *The Journal of Foraminiferal Research*, **25**, 190–203.

Alzieu C 2000. Impact of Tributyltin on marine invertebrates. *Ecotoxicology* **9**, 71–76.

Alzieu C, Sanjuan J, Deltreil J P & Borel M 1986. Tin contamination in Arcachon Bay: Effects on oyster shell anomalies. *Marine Pollution Bulletin* **17**, 494–498.

Angell R W 1980. Test morphogenesis (chamber formation) in the foraminifer *Spiroloculina hyalina* Schulze. *Journal of Foraminiferal Research* **10**, 89–101.

Ateweberhan M & Prud'homme van Reine W F 2005. A taxonomic survey of seaweeds from Eritrea. *BLUMEA* **50**, 65–111.

Boehnert S, Birkelund A R, Schmiedl G & Kuhnert H 2020. Test deformation and chemistry of Foraminifera as response to anthropogenic heavy metal input. *Marine Pollution Bulletin*. **155**, 111112. Doi: 10.1016/j.marpolbul.2020.111112

Boltovskoy E, Scott D B & Medioli F S 1991. Morphological variations of benthic foraminiferal tests in response to changes in ecological parameters: A review. *Journal of Paleontology* **65**, 175–185.

Brown K M 2005. Calcareous epiphytes on modern seagrasses as carbonate sediment producers in shallow cool-water marine environments, South Australia. PhD Thesis, The University of Adelaide, University of Adelaide Library (unpublished).

Cambridge M L 1975. Seagrasses of south-western Australia with special reference to the ecology of *Posidonia australis* Hook. f. in a polluted environment. *Aquatic Botany* **1**, 149–161.

Carruthers T J B, Dennison W C, Kendrick G A, Waycott M & Cambridge M L 2007. Seagrass of south-west Australia: A conceptual synthesis of the world's diverse and extensive seagrass meadows. *Journal of Experimental Marine Biology and Ecology* **350**, 21–45.

Consorti L, Kavazos C R J, Ford C, Smith M & Haig D W 2020. High productivity of *Peneroplis* (Foraminifera) including aberrant morphotypes, in an inland thalassic salt pond at Lake MacLeod, Western Australia. *Marine Micropaleontology* **160**, 101919. doi: 10.1016/j.marmicro.2020.101919.

Coulson P G, Leporati S, Chandler J, Hart A & Caputi N 2016. Determining the dynamics of WA squid populations through research and recreational fishing. Department of Fisheries, Government of Western Australia, Recreational Initiative fishing Fund Project 2012/002, 1–86.

D A Lord & Associates Pty Ltd 2001. The State of Cockburn: a pressure-state-response report. Cockburn Sound. Prepared for Department of the Environment by Oceanica Consulting Pty Ltd. Report No. 457/1. (https://www.der.wa.gov.au/images/documents/about/committees/CSMC/2001_State_CockburnSound_Report.PDF)

De Nooijer L J, Toyofuku T & Kitazato H 2009. Foraminifera promote calcification by elevating their intercellular pH. *PNAS* **106**, 15374–15378.

Department of Fisheries 2016. Fish kill incident: Cockburn Sound, Western Australia November-December 2015. Government of Western Australia (unpublished). http://www.fish.wa.gov.au/Documents/corporate_publications/fish-kill-incident-cockburn-sound-2015.pdf

Dural B, Aysel V, Demir N, Yazici I & Erdugan H 2012. The status of sensitive ecosystems along the Aegean Coast of Turkey: *Posidonia oceanica* (L.) Delile meadows. *Journal of Black Sea/Mediterranean Environment* **18**, 360–379.

Dural B, Aysel V & demir N. 2013 *Posidonia oceanica* (L.) Delile on the coast of Turkey. Pages 1–19 *in* Y Aktan & V Aysel, editor, 2013. First National workshop on *Posidonia oceanica* (L.) Delile on the Coasts of Turkey. *Turkey Marine Research Foundation* **39.**

Dybdahl R E 1979. Technical Report on fish productivity – An assessment of the marine faunal resources of Cockburn Sound. Cockburn Sound Study 1976-1979. Department of Conservation and Environment Report **4**, 1–87.

Eliahu N B, Herut B, Rahav E & Abramovich S 2020. Shell growth of large benthic Foraminifera under heavy metals pollution: Implications for geochemical monitoring of coastal environments. *International Journal of Environmental Research and Public Health* **17**, 3741.

Geslin E, Debenay J P, Duleba W & Bonetti C 2002. Morphological abnormalities of foraminiferal tests in Brazilian environments: comparison between polluted and non-polluted areas. *Marine Micropaleontology*, **45**, 151–168.

Gobert S, Cambridge M L, Velimirov B, Pergent G, Lepoint G, Bouquegneau J-M, Dauby P, Pergent-Martini C & Walker D I 2006. Biology of *Posidonia*. Pages 387–408 *in* A W D Larkum, R J Orth & C M Duarte, editors, *Seagrasses: Biology, Ecology and Conservation*, Springer, The Netherlands.

Gordon D P & Parker S A 1991. An aberrant new genus and subfamily of the spiculate bryozoan family Thalamoporellidae epiphytic on *Posidonia*. *Journal of Natural History* **25**, 1363–1378.

Graham J E 2000. *Australian Marine Life: The Plants and Animals of Temperate Waters*. New Holland Publishers, Sydney.

Haig D W 1988. Miliolid foraminifera from inner neritic sand and mud facies of the Papuan Lagoon, New Guinea. *Journal of Foraminiferal Research* **18**, 203–236.

Hegge B J, Eliot I & Hsu J 1996. Sheltered sandy beaches of southwestern Australia. *Journal of Coastal Research* **12**, 748–760.

Hemleben C, Anderson O R, Berthold W & Spindler M 1986. Calcification and chamber formation in Foraminifera—a brief overview. Pages 237–249, *in* B S C Leadbeater & R Riding, editors, Biomineralization in Lower Plants and Animals: *The Systematics Association Special Publication* **30**.

Higuera-Ruiz R & Elorza J 2011. Shell thickening and chambering in the oyster *Crassostrea gigas*: natural and anthropogenic influence of tributyltin contamination. *Environmental Technology* **32**, 583–591.

Hottinger L, Halicz E & Reiss Z 1993. Recent Foraminiferida from the Gulf of Aquaba, Red Sea. *Slovenska akademija znanosti in umetnosti, Razred za naravoslovne vede - Opera, Academia Scientiarum et Artium Slovenica, Classis IV, Historia Naturalis* **33**, 1–179.

Huisman J M & Walker D I 1990. A catalogue of the marine plants of Rottnest Island, Western Australia, with notes on their distribution and biogeography. *Kingia* **1**, 349–459.

Johnston D J, Wakefield C B, Sampey A, Fromont J & Harris D C 2008. Developing long-term indicators for the sub-tidal embayment communities of Cockburn Sound. *Western Australian Fisheries Research Report* **181**.

Langer M R 1993. Epiphytic foraminifera. *Marine Micropaleontology* **20**, 235–265.

Le Cadre V & Debenay J P 2006. Morphological and cytological responses of *Ammonia* (foraminifera) to copper contamination: Implication for the use of foraminifera as bioindicators of pollution. *Environmental pollution*, **143**, 304–317.

Lee J J 1990. Fine structure of the rhodophycean *Porphyridium purpureum* in situ in *Peneroplis pertusus* (Forskal) and *P. acicularis* (Batsch) and in axenic culture. *Journal of Foraminiferal Research* **20**, 162–169.

Li M, Lei Y, Tiegang L & Dong S 2020. Response of intertidal Foraminiferal assemblages to salinity changes in a laboratory culture experiment. *Journal of Foraminiferal Research* **50**, 319–329.

Loeblich A R & Tappan H 1987. *Foraminiferal Genera and their Classification*. Van Nostrand Reinhold Company, New York.

Masselink G & Pattiaratchi C B 2001. Seasonal changes in beach morphology along the sheltered coastline of Perth, Western Australia. *Marine Geology* **172**, 243–263.

McComb A J, Cambridge M L, Kirman H & Kuo J 1981. The Biology of Australian Seagrasses. *University of Western Australia Press*, Nedlands, Western Australia.

McKenzie K G 1962. A record of Foraminifera from Oyster Harbour, near Albany, Western Australia. *Journal of the Royal Society of Western Australia* **45**, 117–133.

McMahon K, Young E, Montgomery S, Cosgrove J & Wilshaw Walker, D I (1997). Status of a shallow seagrass system, Geographe Bay, south-western Australia. *Journal of the Royal Society of Western Australia* **80**, 255–262.

Meriç E, Yokeş M B, Avşar N & Bircan C 2009. A new observation of abnormal development in benthic foraminifers: *Vertebralina-Cornuspira* togetherness. *Marine Biodiversity Records* **2**, 1–6.

Meriç E, Avşar N, Nazik A, Yokes B, Dora O, Barut I F, Eryilmaz M, Dinçer F, Kam E, Aksu A, Taskin H, Bassari A, Bircan C & Kaygun A 2012. The influences of oceanographical characteristics of the north coasts of Karaburun Peninsula on the benthic foraminiferal and ostracod assemblage. *Mineral Research and Exploration Bulletin* **145**, 22–47.

Meriç E, Avşar N, Yokeş M B & Dinçer F 2019. Morphological anomalies observed on *Vertebralina striata* d'Orbigny, 1826 test in the northern coast of Karaburun Peninsula (Izmir-Turkey). *Natural and Engineering Sciences* **4**, 163–173.

Parker J H 2009. Taxonomy of Foraminifera from Ningaloo Reef, Western Australia. *Memoirs of the Association of Australian Palaeontologist* **36**, 1–810.

Parker J H 2017. Ultrastructure of the test wall in modern porcelaneous Foraminifera: Implications for the classification of the Miliolida. *Journal of Foraminiferal Research* **47**, 136–174.

Prado P, Alcovero T & Romero J 2008. Seasonal response of *Posidonia oceanica* epiphyte assemblages to nutrient increase. *Marine Ecology Progress Series* **359**, 89–98.

Sagar N, Sadekov A, Scott P, Jenner T, Vadiveloo A, Moheimani N R & McCculloch M 2020a. Geochemistry of large benthic foraminifera *Amphisorus hemprichii* as a high-resolution proxy for lead pollution in coastal environments. *Marine Pollution Bulletin*, **162**, 111918. doi: 10.1016/j.marpolbul.2020.111918

Sagar N, Sadekov A, Jenner T, Chapuis L, Scott P, Choudhary M & McCulloch M 2021b. Heavy metal incorporation in foraminiferal calcite under variable environmental and acute level seawater pollution: multi-element culture experiments for *Amphisorus hemprichii*. *Environmental Science and Pollution Research* **29**, 3826–3839.

Semeniuk T A 2001. Epiphytic Foraminifera along a climatic gradient, Western Australia. *Journal of Foraminiferal Research* **31**, 191–200.

Silberstein K 1985. The effects of epiphytes on seagrass in Cockburn Sound. *Department of Conservation and Environment*, Bulletin **135**.

Taşkin E & Öztürk M 2013 Epiphytic macroalgal assemblages of *Posidonia oceanica* (L.) Delile in Turkey. Pages 68–76 *in* Y Aktan & V Aysel, editors, First National workshop on *Posidonia oceanica* (L.) Delile on the Coasts of Turkey. *Turkey Marine Research Foundation* **39.**

Taşkin E 2014. Comparison of the brown algal diversity between four seacoasts of Turkey. *Journal of Academic Documents for Fisheries and Aquaculture* **3**, 145–153.

Trautman D A & Borowitzka M A 1999. Distribution of the epiphytic organisms on *Posidonia australis* and *P. sinuosa*, two seagrasses with differing leaf morphology. *Marine Ecology Progress Series* **179**, 215–229.

Travers A 2007. Low-energy beach morphology with respect to physical setting: A case study from Cockburn Sound, southwestern Australia. *Journal of Coastal Research* **232**, 429–444.

Tsuda R T 1972. Marine benthic algae of Guam. I. Phaeophyta. *Micronesica* **8**, 87–115.

Walker D I & McComb A J 1988. Seasonal variation in the production, biomass and nutrient status of *Amphibolis antactica* (Labill.) Sonder ex Aschers. and *Posidonia australis* Hook.f. in Shark Bay, Western Australia. *Aquatic Botany* **31**, 259–275.

Walter W, Faber J R & Lee J J 1992. Pathways of carbon in the *Peneroplis planatus* (Foraminifer)–*Porphyridium purpureum* (Rhodophyte) Endosymbiosis. *Symbiosis* **14**, 439–463.

Yanko V, Ahmad M & Kaminski M 1998. Morphological deformities of benthic foraminiferal tests in response to pollution by heavy metals: implications for pollution monitoring. *Journal of Foraminiferal Research* **28**, 177–200.

Origin of the Western Australian land boundary

PAUL WHINCUP [1*] & ANTONIO C. CAMPO LÓPEZ [2]

[1] *Environmental consultant, Jakarta, Indonesia.*
[2] *Historian, Universidad Nacional de Educación a Distancia, Madrid, Spain.*

* *Corresponding author:* ✉ *paul.whincup@yahoo.com*

ABSTRACT

The internal political boundaries of Australia, according to common belief, were derived from the *Treaty of Tordesillas* in 1494, which divided the New World between Spain and Portugal along a western meridian in the Atlantic. Later, when the lucrative Spice Islands in the Moluccas of Indonesia were discovered by the Portuguese sailing east in 1512 and the Spanish Magellan expedition sailing west in 1521, the *Treaty of Zaragoza* in 1529 attempted to clarify the anti-meridian of the eastern hemisphere to designate who could rightly claim possession. Because the Moluccas are close to the anti-meridian it was inevitable that both Spain and Portugal would vigorously defend their rights to occupation under the terms of the treaty such that to this day the anti-meridian has never been fully agreed upon. Within the Australian context, and supposedly based on the *Treaty of Tordesillas*, the three anti-meridians of 135°E, 129°E and 141°E in that order have been used to designate Australia's internal political boundaries, but uncertainty remains on the origin of each. Historical maps and documents from the 16th and 17th centuries clarify the credibility of the various anti-meridians and show that the only valid contender is the Portuguese anti-meridian of 135°E. This line was used by Tasman in 1644 to divide the Australian continent between Hollandia Nova and Terra Australis, and later by Governor Darling in 1785 to designate the boundary between New Holland and New South Wales. The derivation of the Western Australian border at 129°E appears to have been a convenient choice to protect New South Wales settlements at Port Essington and Melville Island, west of the 135°E Portuguese anti-meridian, rather than to any speculative alternative Portuguese anti-meridian derived from the *Treaty of Tordesillas*.

Keywords: Western Australia, Tordesillas, Zaragoza, Spice Islands, Moluccas, Meridians

Manuscript received 18 April 2022; accepted 23 May 2022

INTRODUCTION

In his classic work 'The Fatal Shore' Robert Hughes (2003, p. 575) has a short footnote on the eastern boundary of the newly declared colony of Western Australia: 'The common boundary was the meridian of 129°E—not that this represented any "natural" boundary, but simply because it was the convenient fossil of the "Pope's Line", fixed in the fifteenth century by the "*Treaty of Tordesillas*", which divided the world into Spanish and Portuguese hemispheres'. King (1988) and Marchant (2011) described the origins of the Western Australian boundary and alluded to the treaty as did Carney (2013) in his comprehensive presentation, from a legal perspective, on Australia's land boundaries made to the High Court of Australia. As Carney (2013, p. 2) stated 'a significant determinate of a nation's boundary is of course, international law', and 'In this respect, many may be surprised by the fact that the first land boundary created by the British on this continent in 1786 can be traced to a treaty between Portugal and Spain in 1494'. In this context, the meridian refers to the *Treaty of Tordesillas* and the anti-meridian to the *Treaty of Zaragoza*, which effectively split the globe into two supposedly equal hemispheres.

THE *TREATY OF TORDESILLAS*

After Columbus discovered America in 1492 exploration and colonialization of the New World expanded rapidly driven by Spain and Portugal, the two great maritime powers at that time, both catholic and with allegiance to the pope. After a *Papal Bull* in 1493 was rejected by Portugal, Pope Alexander VI signed the *Treaty of Tordesillas* in Spain in 1494. The treaty established a line of demarcation in the westernmost Atlantic (Fig. 1) 370 leagues west of the Cape Verde Islands. Exactly where in the islands was not specified with Spain gaining most of the Americas, except for the Brazilian bulge of South America, and Portugal claiming lands discovered to the east. However, because the line was not defined by degrees of longitude, nor did the line encircle the globe, different interpretations regarding its practical implementation arose. The exact position of the line of demarcation, the Papal Line, was inexact because of the limits of navigation particularly in respect to longitude, its disputed provenance within the Cape Verde Islands, and different interpretations of the length of a league.

MAGELLAN

In the years immediately after the signing of the *Treaty of Tordesillas* the attention of Portugal and Spain became

Figure 1. The Tordesillas meridian – The *Papal Line*. Antonio de Herrera (1621), courtesy the Library of Congress.

fixed on the fabled Spice Islands in the Moluccas, specifically the two tiny volcanic islands of Ternate and Tidore (Fig. 2). Portugal first reached the Moluccas in 1512 by sailing eastward from Malacca whereas the Magellan expedition funded by the King of Spain discovered the first westward route across the Pacific in 1521, landing first in the Philippines where Magellan, a Portuguese, was killed and the remainder of his crew eventually reached Tidore. Magellan had sailed westwards through the Straits of Magellan and across the Pacific with the expectation he could claim the Spice Islands for the King of Spain. Prior to his voyage he had calculated the earth's circumference to be 34,882 km (Mazon 2020) but found it be approximately 40,000 km (the actual distance around the equator is 40,007.863 km) creating a wide, previously unknown gap covering both Australia and the Moluccas. Before his voyage he had estimated that the Moluccas would lie east of a meridian between what became New Zealand and Australia but afterwards moved the meridian a distance equivalent to 5,253 km westward crossing Borneo to match the 40,000 km circumference he calculated. Both his meridians supported his justification of the Moluccas (and the Philippines) as being under the jurisdiction of Spain.

THE *TREATY OF ZARAGOZA*

After Juan Sebastián Elcano's return to Spain in 1522 with information from the first round-the-world trip, the cartographer Nuño García Torreño made a map of South Asia on which he drew the equator and the anti-meridian of the *Treaty of Tordesillas*: the *"Línea divisionis castellanorum et portugalliensium"*. This was the first time the anti-meridian of Tordesillas had been drawn (Sanchez M 2009). The anti-meridian crossed Sumatra and the Indochina peninsula, reflecting the Spanish position that Portuguese rights only reached as far as Malacca.

Given the dispute between Spain and Portugal over the jurisdiction of the Moluccas, the *Treaty of Zaragoza* was endorsed by Pope Clement VII in 1529 dividing the world into two hemispheres with the anti-meridian being designated as 297 leagues east of the Moluccas. A degree longitude was later agreed to be equivalent to 17.5 leagues placing the anti-meridian 17° east of those islands. We now know that both Ternate and Tidore are near 127°E, which would have placed the anti-meridian at 144°E implying that the two hemispheres, were not equal, which was not the intent of the treaty. Spain strongly argued their rights to the Moluccas during the several years of treaty negotiation but ultimately with the signing of the treaty the king of Spain agreed to cede his rights to the Spice Islands to Portugal for 350,000 ducats (1,260 kg) of gold (Sánchez G 1993, p. 306). It was not until the *Treaty of Madrid* in 1750 that Spain agreed the Moluccas were within Portugal's jurisdiction. After the treaty, numerous calculations were made based on

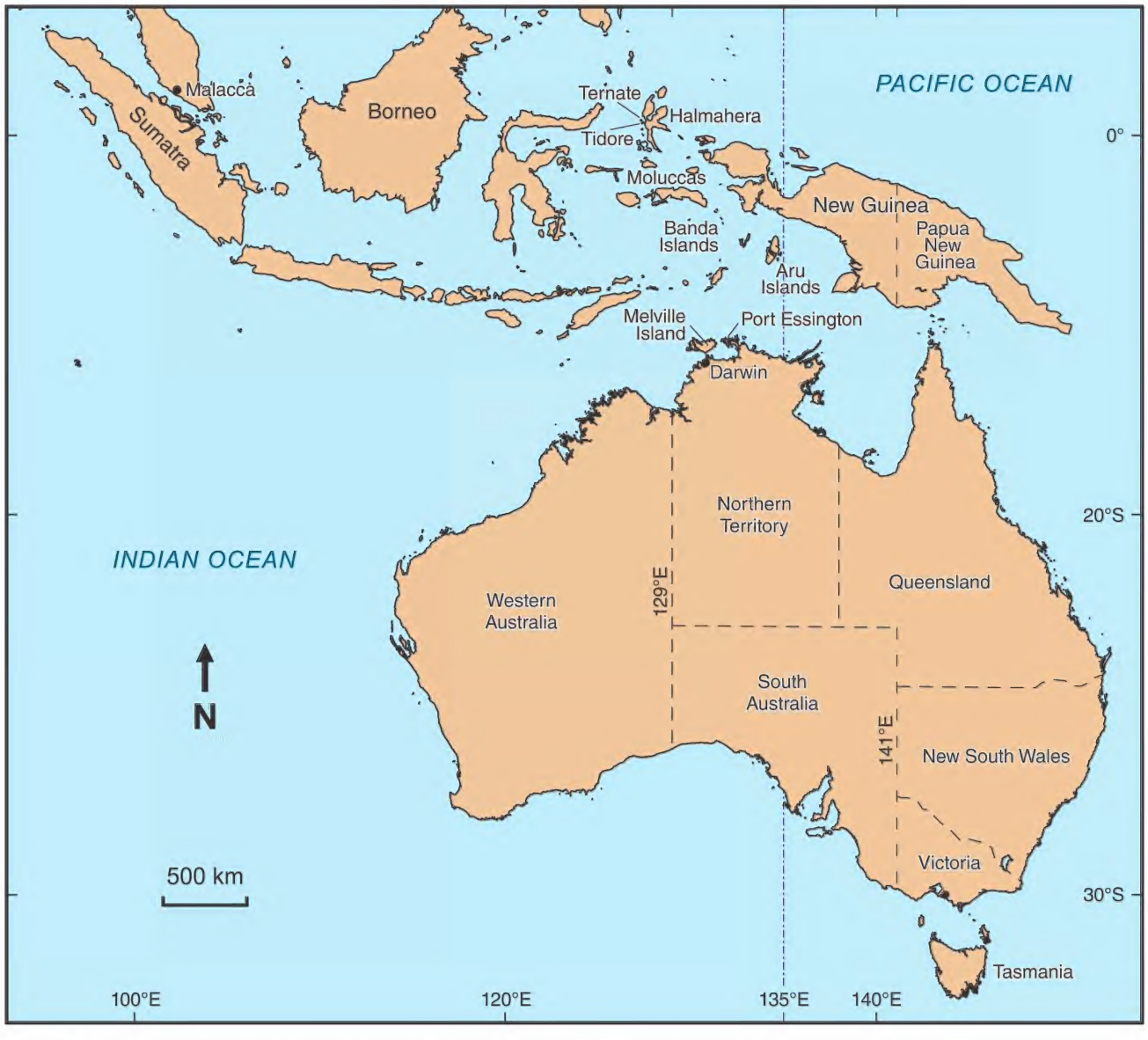

Figure 2. The internal political boundaries of Australia and localities mentioned in the text.

equal hemispheres with the Tordesillas line as the origin. According to Gammage (1981, p. 524), and quoted by Carney (2013), Portugal calculated the Tordesillas Line effectively as 51°W, the anti-meridian of which is 129°E. Perhaps because Spain had calculated the Tordesillas Line as 45°W, the anti-meridian of which is 135°E, this may be where the mistaken 129°E Portuguese anti-meridian and a 135°E Spanish anti-meridian originated. However, this would not have given Spain any claim to the Moluccas and no justification for Gammage's statement can be found. It merely confirms the inaccuracies in determining longitudes in the early 16th century. As longitudes were not normally represented on the early maps reference to locations such as Malacca and the Moluccas is considered a much more reliable indicator of where each party thought the anti-meridian should be but strongly influenced on where they wanted it to be, justifiably so by Portugal.

LONGITUDES

All longitudes now describing the meridian and anti-meridian are based on the Greenwich meridian, which was adopted by England in 1721. Although informally accepted by many countries it was not until 1884 that this meridian was ratified internationally, but more than a dozen countries still do not recognise it. The Spanish had used a meridian centred on the Canary Islands at 15°41'W, whereas from 1509 Portugal fixed zero longitude in the Madeira Islands at 16°96'W. Both of these meridians were in the Atlantic, as are the Cape Verde Islands, which were the reference origin for the *Treaty of Tordesillas*, with the meridian defined in leagues from those islands. In terms of the Cape Verde Islands, at the Badajoz-Elvas Conferencia in 1524 the Portuguese wanted to put the easternmost island 'Isla de la Sal' as the source, but at the second meeting in 1682, after the Moluccas had already

been lost, they took the opposite position to try to access more of America, in particular Sacramento–Uruguay. In this meeting the Spaniards nominated the central island of San Nicolás (24°18′W), which was then agreed as the demarcation line (Rumeu de Armas 1992). The discrepancy between the westernmost and easternmost islands is 2°13′ of longitude, which is several degrees less than apparently used to define the 45°W and 51°W papal lines previously claimed.

THE ANTI-MERIDIANS

Estimates of the longitude of the Tordesillas meridian in the years following the signing of the two treaties ranged between 42°25′ and 47°37′W with 46°37′W (Rumeu di Armas 1992, p. 219) being agreed at the *Treaty of Madrid* in 1750, by which time the Moluccas were of no further interest to either party. The agreement was more to finally settle Spain's right to the Philippines and no anti-meridian was nominated. Had this been agreed to earlier, and had the intent of the treaty had been to create two equal hemispheres, it would have corresponded to an anti-meridian of 133°30′E thereby placing the Moluccas firmly within Portugal's jurisdiction, which is not too different from the 135°E anti-meridian adopted in the early 16th century. In 1524 at the Badajoz-Elvas conference, Juan Vespucci, a cartographic expert, produced a map showing a proposed anti-meridian passing through Malacca. Inside his book *Descripcion d[e] las Indias Ocidentales* Antonio de Herrera y Tordesillas (1601) included a map called *Descripcion de las Indias del Poniente* made by Juan López de Velasco around 1575 (Fig. 3), which repeats the Spanish official position of the anti-meridian passing through Malacca. No longitudes were shown on this map, but such an anti-meridian would have given Spain rightful claim to the Philippines and the Moluccas. Spain would never have accepted any anti-meridian farther to the east and there is no reference or map to indicate they ever did so. Suggesting that the Spanish anti-meridian was 135°E is not credible and a 121°E anti-meridian is even less so, as it would have implied unequal hemispheres.

Lopo Homem, the cartographer who defended Portugal in the Junta de Badajoz-Elvas in 1524, which was the prelude to the *Treaty of Zaragoza,* prepared a map (dated 1554), now in the Museo Galileo in Florence, implying a Portuguese anti-meridian of 135°E. The 1571 map by Vaz Dourado (Fig. 4) repeats this showing the Portugese and Castille flags on either side of the anti-meridian passing directly east of the island of Aru (134°28′E). Annotations on this map are proof of Portuguese early interest in New Guinea. All Portuguese maps from that

Figure 3. The Spanish anti-meridian passing through Malacca—a present day longitude of 121°E. López de Velasco (1575, *in* de Herrera 1601). Held by Princeton University Library, NJ, USA.

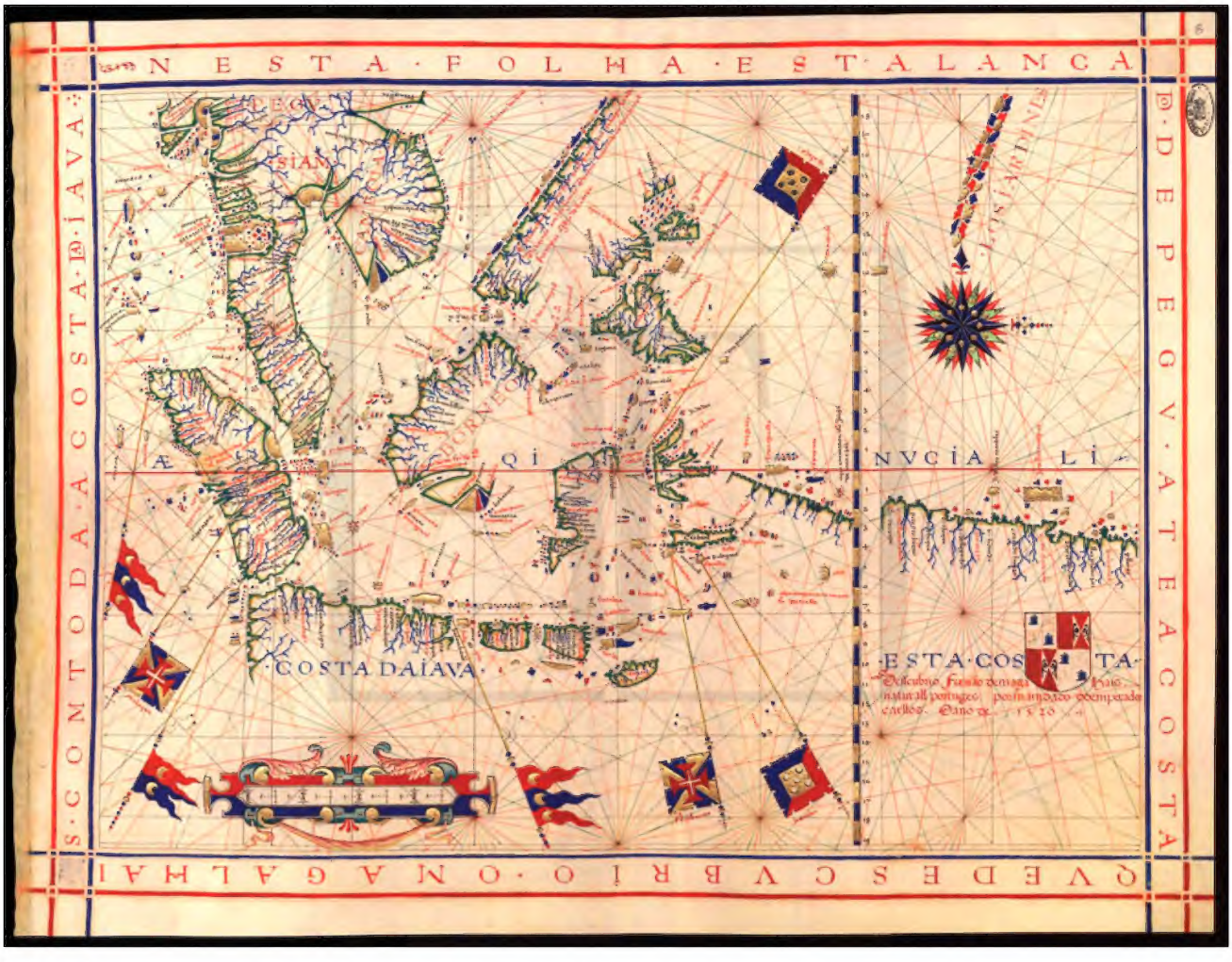

Figure 4. The Portuguese Anti-Meridian at 135°E by Vaz Dourado (1571). Held by Torre do Tombo, National Archive, Lisbon.

period display the same anti-meridian of 135°E, so there can be no doubt of its authenticity as the Portuguese anti-meridian. The 1630 map by Texeira Albernaz (Fig. 5) shows both the Tordesillas and Zaragoza meridians at 45°W and 135°E, and demonstrates the limited knowledge of the Southern Hemisphere and the northern coast of Australia at that time.

RELEVANCE TO AUSTRALIA

The Dutchman, Abel Tasman was the first to explore and chart the northern coast of Australia as shown on the Tasman map of 1644, now in the Mitchell Library, Sydney. He subdivided Australia along a 135°E meridian naming the western half of the new continent as Hollandia Nova and left the eastern half as Terra Australis within the dominion of Spain. This avoided any additional conflict with Spain, against whom Holland was fighting for independence, while at the same time assuming control of the East Indies from the Portuguese. Maps by Texeira Albernaz in 1649, reproduced by the Frenchman Thevenaux (1663), by the Englishman Bowen (1744) and Anon (1786), adopted the 135°E meridian from the Tasman map. The Bowen map (Fig. 6) appears to explain why the English selected 135°E in 1786 as the western boundary of New South Wales, thereby leaving the western half of the continent as New Holland. Governor Darling's commission of 16 July 1825 moved the boundary of the colony with New Holland westwards to 129°E. The British, Dutch and French, who were actively exploring the coast of Australia in the late 18th to early 19th century, had never accepted the *Treaties of Tordesillas or Zaragoza*. As the interior of Australia was largely unexplored there were no geographical features that could be adopted and, as explained by Carney (2013), it was convenient to accept the status quo determined by Tasman as an international line of demarcation (135°E) without delving into the basis for its designation. Despite an exhaustive review of historical maps, no reference has been found to a 129°E meridian as deriving from the Treaties of Tordesillas or Zaragoza. The selection of this meridian most likely was to accommodate the new settlements at Port Essington and Melville Island, rather than any adherence to the invoked Portuguese anti-meridian, and remained in place when the Governor of New South Wales declared Western Australia as a colony to replace New Holland.

The derivation of the 141°E meridian by the Netherlands when dividing New Guinea between their interests on the west from those of England and Germany on

Figure 5. Texeira Albernaz's (1630) map showing the meridian (45°W) and anti-meridian (135°E). Held by Library of Congress, Washington D.C., USA.

Figure 6. The English map used by the Colonial Authorities to define the 135°E anti-meridian (Bowen 1744). Held by National Library of Australia.

the east in 1828 and later by Indonesia in 1974 is loosely attributed to the *Treaty of Tordesillas* and is even more obscure (van de Veur 1966, p. 10). It does fall within the potential range of anti-meridians, which had been variously promoted, but no historical maps or documents have been uncovered to support it. Australia initially adopted 141°E to define all the eastern states and Northern Territory boundaries a few years after the subdivision of New Guinea commenced in 1834. This was adjusted to 138°E in 1862 for the Queensland border with the Northern Territory (Fig. 2). The history of the changing boundaries discussed herein is summarized in Table 1.

CONCLUSIONS

The common understanding in Australian literature is that the internal political boundaries of the continent are based on a '*Papal Line*' originating from the 1494 *Treaty of Tordesillas* and subsequently the 1529 *Treaty of Zaragoza* to resolve the dispute between Spain and Portugal over their respective claims over the Spice Islands (the Moluccas). The initial subdivision between New Holland and Terra Australis by Tasman in 1644 was along the 135°E anti-meridian, which has incorrectly been termed the Spanish anti-meridian, whereas the subsequent inland boundary of Western Australia proclaimed in

Table 1. Timeline for the definition of Western Australia's eastern boundary.

Year	Comment
1492	Columbus discovers America triggering the age of colonialism driven by Spain and Portugal.
1493	Papal line proposed by Pope Alexander VI 100 leagues west of Cape Verde Islands in the Atlantic to divide the western world between Spain and Portugal.
1494	Treaty of Tordesillas agreed between Spain and Portugal signed by Pope Alexander VI. The line of demarcation is designated as 370 leagues west of Cape Verde Islands in the Atlantic.
1512	Portuguese expedition sails eastward from Malacca to Ternate, Moluccas.
1521	Spanish expedition under Magellan sails westward across the Pacific to Tidore.
1524	The world map made by Juan Vespucci in 1524 places the anti-meridian at 135°E (for the first time) thereby putting Moluccas within Spain's domain.
1529	Treaty of Zaragoza signed by Pope Clement VII sets the anti-meridian at 297.5 leagues east of the Spice Islands. Portugal pays 350,000 ducats of gold to Spain to secure possession of the Spice Islands.
1529 onward	Estimates of the eastern anti-meridian range between 121°E and 147°E based either on leagues, as intended, or on an equal division of the globe between Spain and Portugal along the Tordesillas line.
1575	Spain proposes an anti-meridian passing through Malacca, for which the moderm equivalent longitude is 121°E.
1605	The Dutch East India Company take possession of the Moluccas.
1611	Calculation of Portuguese anti-meridian by Joao Bautista Lavanha indicates that Gilolo (Halmahera) is the most eastern island within the Portuguese zone. Approximate derived longitude is 129°E.
1644	Abel Tasman designates the 135°E meridian as the boundary between Hollandia Nova and Terra Australis.
1660	Dutch East Indies Company recognises the Sultan of Tidore's sovereignty over New Guinea.
1663	Map by the Frenchman Thevenot shows 135°E as the anti-meridian.
1713	Spain cedes New Guinea to Netherlands under the Treaty of Utrecht.
1730	First design of Harrisons marine chronometer allows the first accurate measurement of longitude. The Moluccas are accurately defined as spanning 127°E (Ternate) to 129°E (Halmahera and Banda Islands).
1747	Emmanuel Bowen shows 135°E as the anti-meridian, probably based on the Thevenot map of 1663. This was the first time it was recognised by the English.
1750	The Zaragoza anti-meridian is annulled by Spain and Portugal under the Treaty of Madrid.
1786	The Governor of NSW designates 135°E as the western boundary of NSW with New Holland, the meridian proposed by Tasman more than a 100 years earlier.
1825	The Governor of NSW claims possession of north coast of Australia between 129°E and 135°E establishing settlements at Port Essington and Melville Island.
1826	Establishment of a military base at King George Sound (Albany) by Governor Darling.
1828	Dutch expedition to New Guinea results in formal annexation eastwards to the 141°E meridian, recognising the Sultan of Tidore and informally the Treaty of Tordesillas. Ratified in 1848.
May 1829	Captain Fremantle reaches the Swan River and takes formal possession of whole west coast of New Holland.
June 1829	Captain James Stirling sails up the Swan River on the Parmelia on 1 June 1829 to take formal possession of Western Australia by proclamation on 18 June 1829.
1832	The governor of NSW proclaims Western Australia as a colony using the 129°E meridian as the common boundary.
1834–1861	South Australia and Northern Territory eastern boundaries, and Victoria, Queensland and NSW's western boundaries designated as the 141°E meridian.
1862	Queensland boundary with NSW shifted westwards from 141°E to 138°E.

1831 is the 129°E meridian, also incorrectly referred to as the Portuguese anti-meridian. A further meridian of 141°E was the common boundary between the eastern states and Northern Territory later moved westwards by Queensland.

An exhaustive review of historical maps and documents finds that the relationship of the 135°E anti-meridian to the papal line is justified as a Portuguese rather than Spanish anti-meridian although it no longer forms a political boundary. The Spanish used Malacca as the origin of their anti-meridian, but this position was never widely promoted. This meridian was used to reinforce Spain's jurisdiction over the Philippines and has never been considered in the Australian political context. The Spanish had no reason to accepted an anti-meridian of 135°E and never did so as it would have placed the Moluccas firmly within the Portuguese sphere of influence. The Portuguese at one time suggested the west coast of the island of Halmahera in the Moluccas constituted the easternmost extent of their influence. As this is close to 129°E it may have been the source of speculation that this was the Portuguese anti-meridian, but if so it was a short-lived diversion and detracted from their early interest in New Guinea to the east. No Portuguese maps, of which there are several, depict a 129°E meridian but instead exclusively and consistently show 135°E. There should be little question that the first political boundary in Australia was the 135°E Portuguese anti-meridian, although the English, French or Dutch never accepted the two treaties. The anti-meridian was a convenient line of demarcation given there was no exploration of the western half of the continent and hence no knowledge of geographical features that could have been used. Setting the eastern boundary of Western Australia at 129°E was likely related to protecting the settlements of Port Essington and Melville Island by shifting the boundary of New South Wales westwards because it was convenient to set a meridian parallel to 135°E. The inference that 129°E was in some way related to 135°E gives a tenuous connection to the *Treaty of Zaragoza*, but it was not an anti-meridian that Spain or Portugal ever promoted.

REFERENCES

Anon 1786. A General Chart of New Holland including New South Wales & Botany Bay with The Adjacent Countries and New Discovered Lands, *published in* An Historical Narrative of the Discovery of New Holland and New South Wales, Fielding and Stockdale, London, UK.

Bowen E 1744. A Complete Map of the Southern Continent. Survey'd by Capt. Abel Tasman & Depicted by Order of the East India Company in Holland in the Stadt House at Amsterdam. Page 325 *in* J Harris, editor, *Navigantium atque itinerantium bibliotheca. or, A complete collection of voyages and travels*. Printed by Royal Order of George the Second for Citizens and Booksellers of London.

Carney G 2013. The Story behind the Land Borders of the Australian States - A Legal and Historical Overview, Public Lecture Series, High Court of Australia, 10 April 2013 (unpublished).

Cerezo Martínez R 1994. El Meridiano y el Antimeridiano de Tordesillas en la Geografía, la Náutica y la Cartografía. *Revista De Indias* **54 (202)**, 509–542.

de Herrera Y Tordesillas A 1601. *Descripción de las Indias Occidentales*, Madrid, (ed. 1751), Princeton University Library, NJ, USA. https://catalog.princeton.edu/catalog/9953536023506421

Gammage B 1981. Early Boundaries of New South Wales, *Historical Studies* **19 (77)**, 524–531.

Hughes R 2003. *The Fatal Shore*, Vintage Publishing, London UK. ISBN 0 099 45915 9

King R J 1998. Terra Australis, New Holland and New South Wales: The Treaty of Tordesillas and Australia, *The Globe* **47**, 35–55.

Lopo H 1554. Unamed world map, Planisphere, https://catalogue.museogalileo.it/gallery/PlanisphereInv946.html Galileo Museum, Florence, Italy.

Marchant L R 2000. The Political Division of Australia 1479-1829: The historical development of the Western Australian border, *Cartography*, **29 (2)**, 1–22.

Mazón Serrano T 2020. *Elcano, Viaje a la historia*, Ed. Encuentro. Madrid.

Rumeu de Armas A 1992. El Tratado de Tordesillas. Rivalidad hispano-lusa por el dominio de océanos y continentes. Editorial Mapfre (Colecciones Mapfre 1492. Colección América 92), Madrid.

Sánchez Gonzalez D M 1993. Aspectos jurídicos de la negociación de las Molucas, BFD: *Boletín de la Facultad de Derecho de la UNED* **3**, 293–310.

Sánchez Martínez A 2009. De la cartografía oficial' a la 'cartografía jurídica, la querella de las Molucas reconsiderada, 1479-1529. Mundos Nuevos, Debates, doi: 10.4000/nuevomundo.56899

Texeira Albernaz J 1630. Taboas geraes de toda a navegação divididas e emendadas por Dom Jeronimo de Attayde. Com todos os portos principaes das conquistas de Portugal. Delineadas por João Teixeira. Cosmographo de Sua Majestade. Anno 1630, Library of Congress, Washington D.C., USA. https://www.loc.gov/resource/g3200m.gct00052/?sp=4&st=image&r=-0.241,0,1.482,0.596,0

Thevenot M 1663. Chart, Hollandia Nova—Terre Australe, published in Relation de divers voyages curieux qui n'ont point est publiées ou qui ont est traduites d'Hacluyt, de Purchas et d'autres voyageurs anglois, hollandois, portugues, allemands, espagnols et de quelques persans, arabes et autres auteurs orientales 1663–1696, Paris.

Tous Meliá J 2001. La isla de El Hierro y el meridiano origen. *Estudios Canarios, Anuario del Instituto de Estudios Canarios* **46,** 249–288.

van der Veur P W 1966. *Search for New Guinea's Boundaries, From Torres Strait to the Pacific*, Australian National University Press, Canberra, 176 pp.

Vaz Dourado 1571. https://hdl.huntington.org/digital/collection/p15150coll7/id/46319 Huntington Library, San Marino, California, USA.

Vespucci J 1524. *Totius orbis descriptio tam veterum quam recentium geographorum traditionibus observata novum* [map] Liechtenstein Map Collection *held by* Houghton Library, Harvard University, Cambridge, USA https://curiosity.lib.harvard.edu/scanned-maps/catalog/44-990088492040203941 .

Aspects of the geological development of the Makassar Strait, Indonesia

PETER BAILLIE [1*] & JOHN DECKER [2]

[1] *School of Earth Sciences, University of Western Australia, Perth, Western Australia.*
[2] *Oro Negro Exploration LLC, Cambria, California, USA.*

**Corresponding author: ✉ peter.baillie@uwa.edu.au*

ABSTRACT

The Makassar Strait is a Cenozoic extensional deep-water basin bounded to the east by Borneo and the Mahakam Delta system, to the west by Sulawesi, to the north by a zone of deformation associated with strike-slip movements and the North Sulawesi Fold-and-Thrust Belt, and to the south by the Paternoster Platform. It comprises a maximum of 7 km of Paleogene shallow- to non-marine synrift sedimentary rocks and volcanics, and Paleogene to Neogene post-rift deep-water sediments overlying a basement of attenuated continental crust with volcanics.

Early Miocene uplift of Borneo resulted in the deposition of large volumes of Neogene sediment in the Kutai Basin, some of which was remobilised from the Mahakam Delta and deposited in east-directed fan systems in the Makassar Strait. Pliocene tectonic events in west Sulawesi formed the West Sulawesi Fold Belt and west-directed turbidites in the central and eastern Makassar Strait. Current turbidite sedimentation in the central part of the strait is north directed through the Makassar Fan, and primarily sourced from the Lariang River in west Sulawesi.

Keywords: Indonesia, tectonics, deep-water sedimentation

Manuscript received 5 April 2022; accepted 20 May 2022

INTRODUCTION

The Makassar Strait (Fig. 1) between Borneo and Sulawesi (formerly Celebes) in eastern Indonesia is a north–south seaway approximately 600 km long and 100–200 km wide with water depths greater than 2,000 m. It is an important oceanic gateway allowing the main branch of the Indonesian Throughflow, which transports water from the Pacific into the Indian Ocean. It is the spiritual heartland of Wallacea—the series of islands stretching between the Eurasian and Australian continents—(Fig. 1 inset), as it was here that Alfred Russell Wallace first recognised the spectacular divide between Asian and Australo-Pacific biogeography, and established the 'Wallace Line' (Wallace 1863; Fig. 1).

Although numerous studies examined the onshore geology of Borneo and Sulawesi during the twentieth century, it was not until the advent of marine seismic acquisition and the discovery of major hydrocarbon deposits in the Mahakam Delta in the 1970s that any attention was given to the offshore geology of the Makassar Strait. This paper utilises petroleum industry seismic and high-resolution bathymetric data to illustrate aspects of the geological development of the Makassar Strait.

Geological setting and development

The formation of the Makassar Strait and nature of the underlying crust have long been the subject of scientific debate. One of the earliest observations was by Wallace in 1858:

> *In this Archipelago there are two distinct faunas rigidly circumscribed, which differ as much as those of South America and Africa, and more than those of Europe and North America: yet there is nothing on the map or on the face of the islands to mark their limits. The boundary line often passes between islands closer than others in the same group. I believe the western part to be a separated portion of continental Asia, the eastern the fragmentary prolongation of a former Pacific continent.* (Letter to Henry Bates 1858).

The Makassar Strait (Fig. 1) lies within a highly complex and dynamic plate tectonic setting where 3 major tectonic plates meet the oceanic/continental Indo–Australian Plate, the predominantly continental Eurasian Plate, and oceanic Pacific/Philippine Sea plates. Rapid geographic changes have occurred over the past 100 million years; biogeographic complexity reflects significant changes in the vertical and horizontal distribution of land and sea during the Neogene, which in turn reflects the complex geological history, largely driven by subduction and strike–slip fault movements (Hall 2011, 2012 and references therein). The region is extremely susceptible to seismic activity, primarily because the compressional tectonic boundaries are lined by volcanic arcs.

The Makassar Strait, within Sundaland (the south-eastern extension of the continental portion of Southeast Asia), is bounded to the west by the island of Borneo, to the east by Sulawesi, and to the north by a zone of tectonic disturbance which terminates in the North

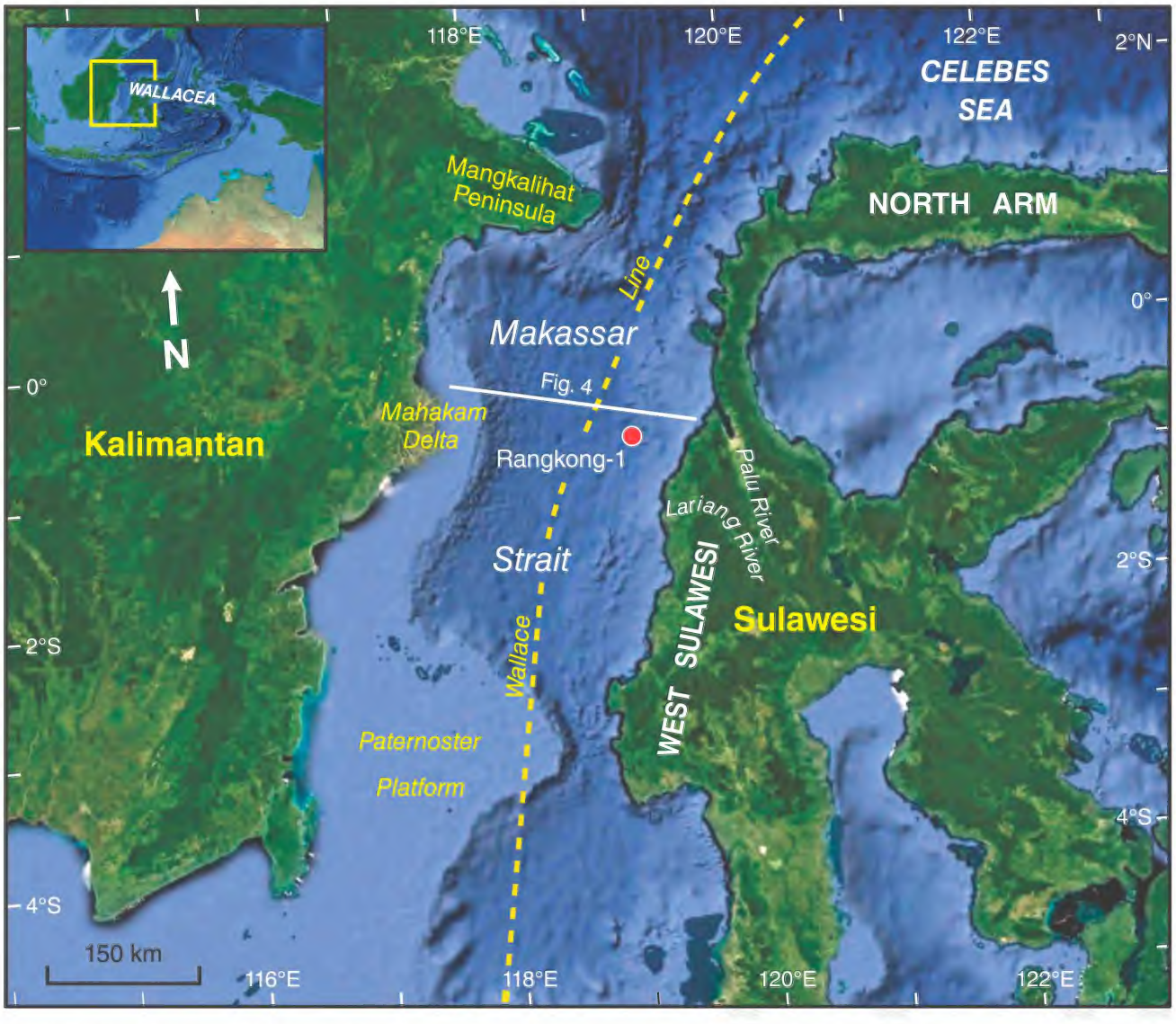

Figure 1. Locality map of Makassar Strait; inset shows regional position (Google Earth).

Sulawesi subduction system. To the south is the relatively stable Paternoster Platform, which is the northern boundary of the South Makassar Basin (Fig. 1). Water depths range from 0 to 2,500 m with gentle topography and broad shelves on the Borneo side of the basin and rugged terrain and a narrow shelf on the Sulawesi side. Five distinct morphotectonic units (geomorphic units having a distinct and common tectonic origin) are recognised (Fig. 2) and described below. Seismic images from various parts of the Makassar Strait are illustrated in Figure 3, and a geoseismic section from the Mahakam Delta to western Sulawesi is shown as Figure 4.

Hamilton (1979) interpreted the Makassar Strait as being underlain by oceanic crust, an interpretation supported by modelling of the gravity data (Cloke *et al*. 1999). Based on considerable anomalies in gravity and limited seismic data availability, other workers (e.g. Situmorang 1989) considered the basement to consist of extended continental crust that had been subjected to Paleogene rifting. Although Hall *et al*. (2009) considered the southern part of the strait to be underlain by extended continental crust, they also suggested the northern parts were likely to overlie middle Eocene oceanic crust with the junction between continental and oceanic crust beneath the Mahakam Delta.

Where it can be observed, the top of acoustic basement in the Makassar Strait is marked by a strong, distinctly hummocky, seismic reflector that possibly encompasses volcanic mounds or carbonate build-ups (Fig. 5a). These features locally display weak internal structuring and may have vertical relief of over one second TWT, although typically in the range of 200–300 milliseconds. During Cenozoic deformation, they acted as points of anisotropy, the focus for small-scale polygonal faults (see fault patterns above interpreted volcanoes, Fig. 5a). 3D seismic data from the central Makassar Strait clearly shows sedimentary packages within the basement succession, thus ruling out basement being oceanic crust. We interpret that the northern Makassar Strait is floored by thinned continental crust and that apparent conical structures are volcanic edifices analogous to those found in the Lake Kivu region of the Great African Rift (Fig. 5b).

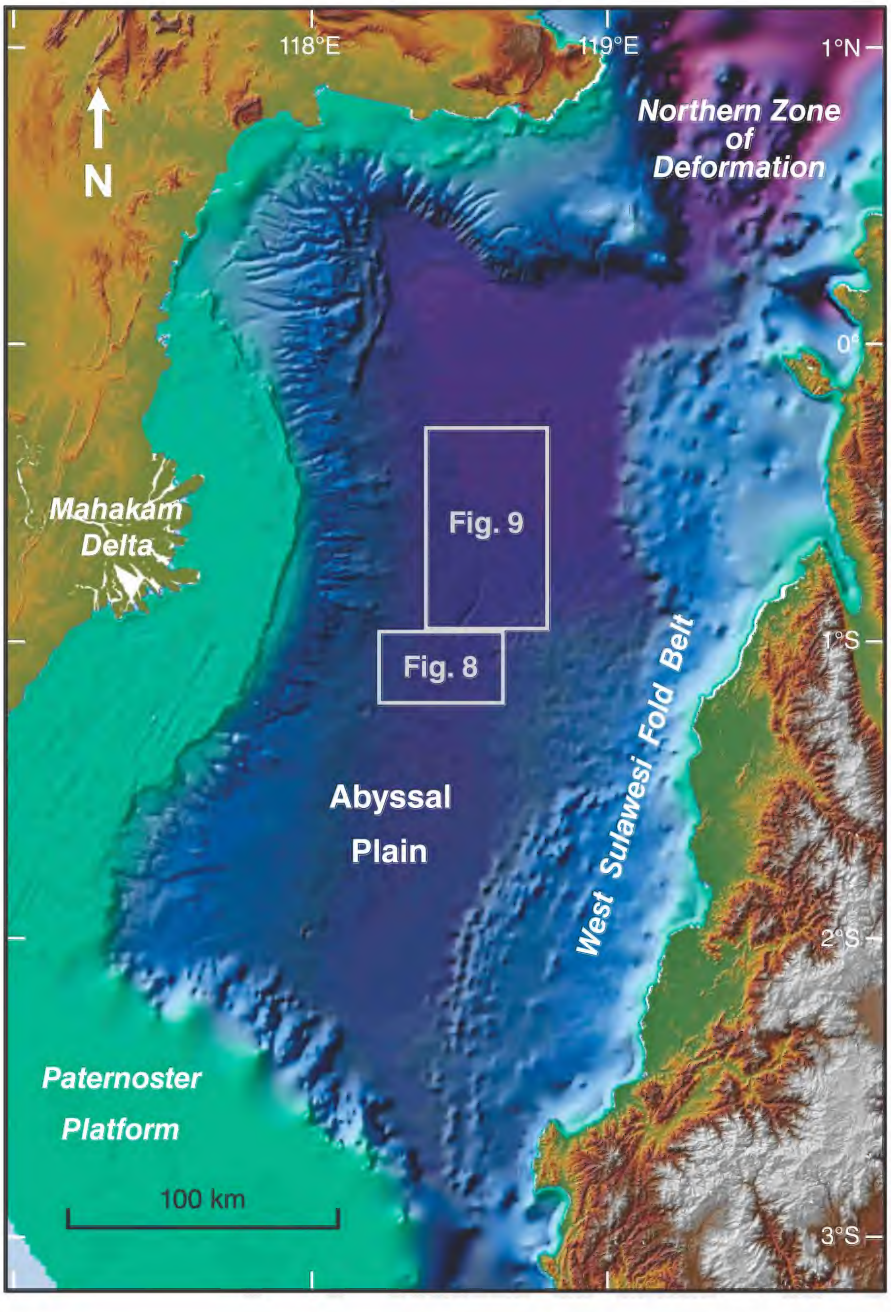

Figure 2. Makassar Strait bathymetric image (after Teas *et al.* 2004) with tectonomorphic areas indicated.

West of the Makassar Strait, Borneo has experienced a complex tectonic history from the Late Cretaceous to the present and was assembled from Gondwana fragments by the early Mesozoic (Longley 1997; Moss *et al.* 1997; Cloke *et al.* 1999; Moss & Chambers 1999; Hall 2013). To the east, western Sulawesi developed in a continental margin setting during the Late Cretaceous and Paleogene (e.g. Parkinson *et al.* 1998; Hall 2012).

The Kutai Basin of eastern Borneo (the Indonesian province of Kalimantan) is the largest and deepest basin in Indonesia. Basin development commenced in the Paleogene (middle Eocene) with subsequent late Eocene – early Oligocene deltaic to marine siliciclastic deposition in the Mahakam Delta depocentre with major lowstand influxes during the middle to late Miocene in the deep-water Makassar Strait (Fraser *et al.* 2003; Saller *et al.* 2004). Chronostratigraphy of the Kutai Basin and Makassar Strait (the deep-water portion outboard of the Mahakam Delta is also known as the North Makassar Basin) is shown as Figure 6.

Western Sulawesi forms the (rifted) continental margin of eastern Sundaland and comprises microcontinental fragments together with abundant Cenozoic calc-alkaline igneous (volcanic and intrusive) rocks (Hall 2002; Nugraha *et al.* 2022; Baillie & Decker 2022). In the Lariang–Karama region (Fig. 7), all the Neogene sediments that unconformably overlie pre-Neogene rocks were considered to belong to the 'Celebes Molasse' comprising early to late Miocene shallow marine carbonate and mudstone overlain by early Pliocene shelf sediments and the Plio-Pleistocene syn-orogenic Pasangkayu Formation (Calvert & Hall 2007). Nugraha

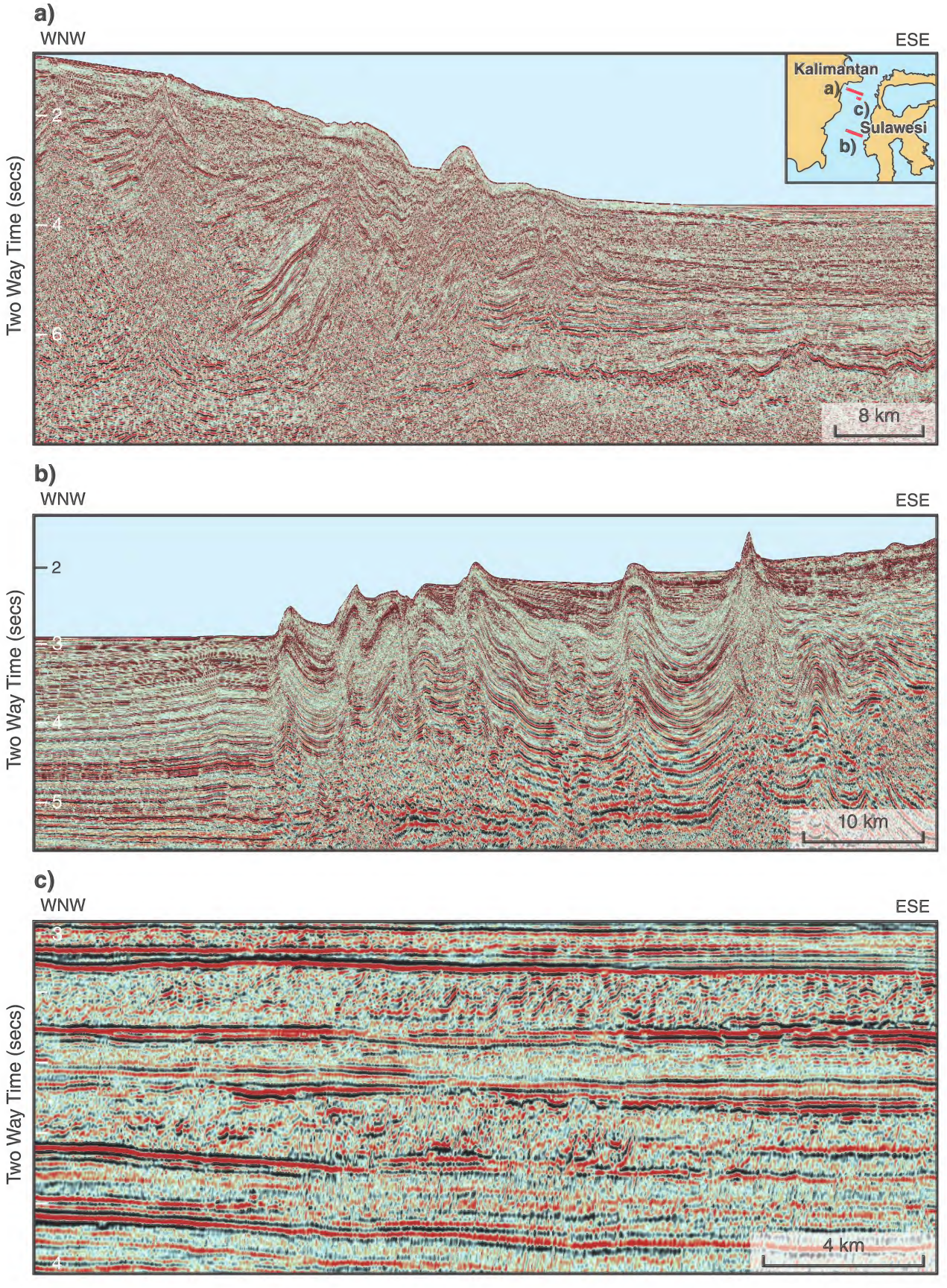

Figure 3. Makassar Strait seismic images: a) outer part of Mahakam Delta showing large growth faults, outer fold-and-thrust belt; abyssal plain with prominent acoustic basement reflector with conical features interpreted as volcanic edifices (after Baillie *et al*. 1999); b) West Sulawesi Fold Belt; c) central Makassar Strait with mass transport deposits at several horizons (after Baillie & Decker 2012).

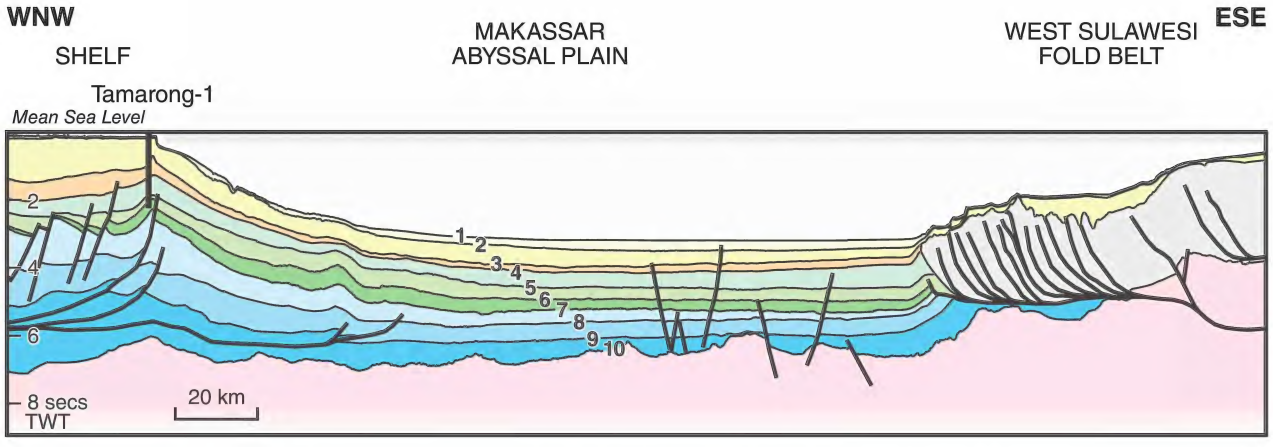

1. Seabed
2. Top Pleistocene
3. Top Pliocene
4. Top Upper Miocene
5. Top Miocene
6. Maximum Flooding Surface Intra Upper Miocene
7. Top Middle Miocene
8. Top Oligocene
9. Top Eocene
10. Top Basement

Figure 4. Makassar Strait geoseismic section though Tamarong1 well to west Sulawesi (modified after Fraser *et al*. 2003); approximate location shown as Line A–B on Figure 1.

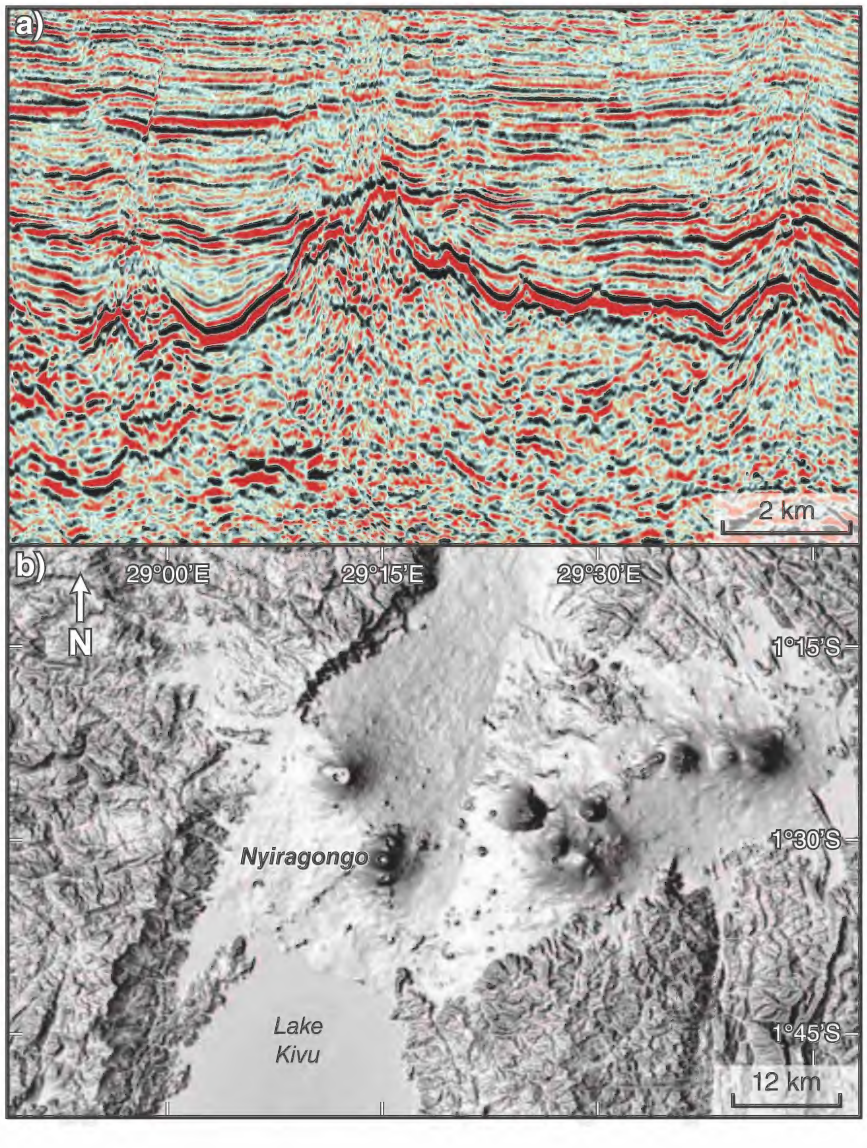

Figure 5. a) seismic section (detail of Fig. 3a) showing prominent basement reflector interpreted as a volcanic feature; b) Google Earth image (SRTM) of Lake Kiva (East African Rift) showing modern volcanoes that are possible (subaerial) analogues of Makassar volcanic features.

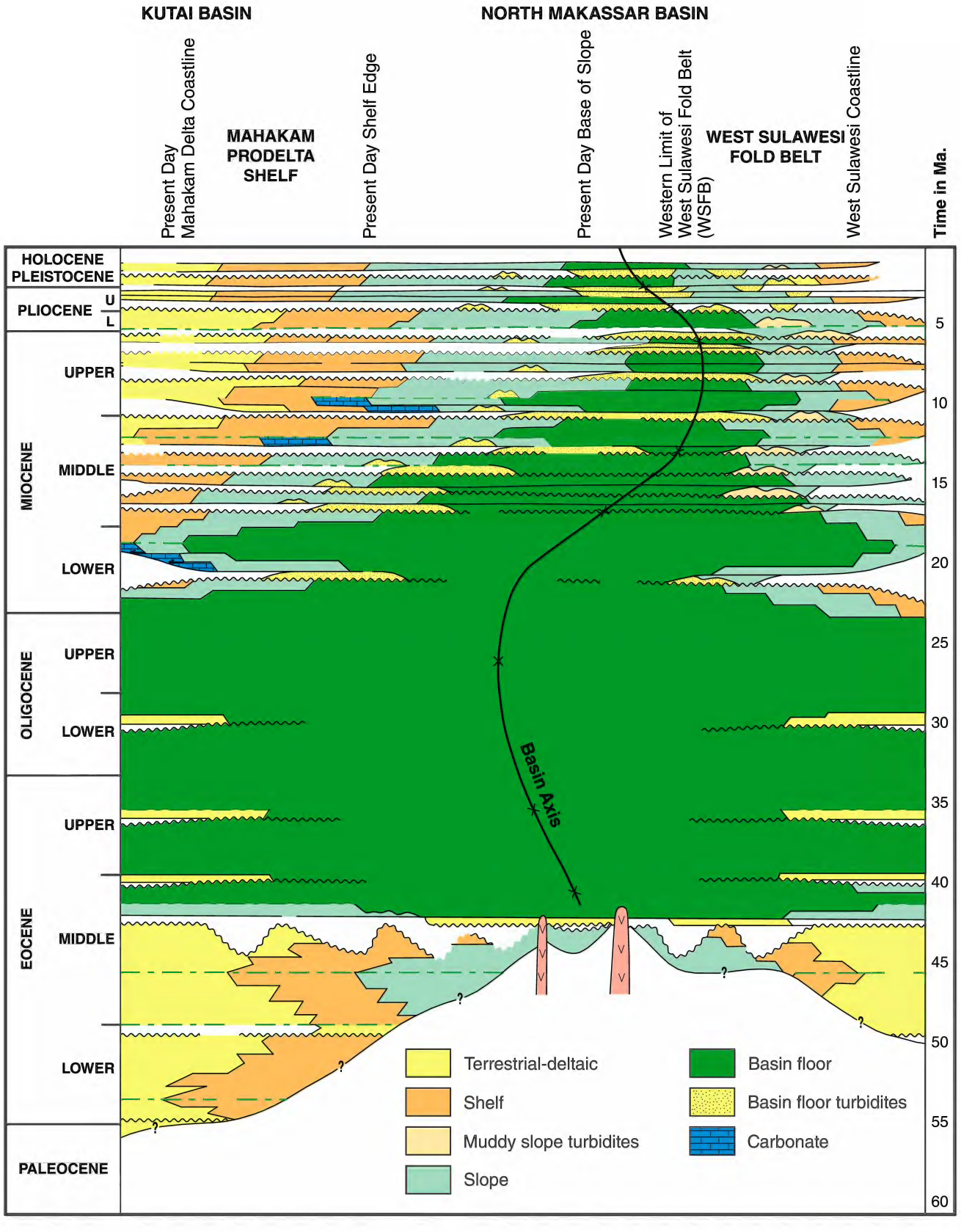

Figure 6. Makassar Strait chronostratigraphy (after Fraser *et al*. 2003).

et al. (2022) provided a new stratigraphy for the Celebes Molasse with sediments showing significant variations in age and depositional environment, and identified unconformities ranging in age from early Miocene to Pleistocene.

MAKASSAR STRAIT MORPHOTECTONIC UNITS

Paternoster Platform

The Paternoster Platform is a shallow-water (less than 200 m deep) area of basement rocks overlain by a veneer of Cenozoic shelf-margin carbonates and patch reefs, lowstand clastic sediments, and highstand muds. It forms the southern boundary of the Makassar Strait (Fig. 2). Seismic lines across the northern margin of the Paternoster Platform indicate at least 1 km of subsidence on reactivated faults close to Sulawesi in the north of the basin at the end of the Miocene (Hall 2011). There is a deep channel between the platform and South Sulawesi (Fig. 2).

The Mahakam Delta

The Mahakam Delta is a major depocentre containing over 14 km of fluvio-deltaic sediment, which started accumulating in the Oligocene; and represents the bulk since the main phase of clastic sedimentation commenced in the early to middle Miocene (van de Weerd & Armin 1992; Moss *et al*. 1997; Allen & Chambers 1998). The delta is characterised by an onshore proximal deformed zone, the modern delta and shallow shelf, a zone dominated by growth faults that may extend down the delta slope, and a deep-water outer zone of folding and associated thrust faults, leading to the abyssal plain (Fig. 4a; Moss *et al*. 2000). The current delta is dominated by fluvial and tidal processes with low wave energy (Allen 1996).

Northwest-directed contractional deformation, producing reactivation and inversion of older extensional faults, began around 14 Ma and continues to the present (Moss *et al*. 2000; McClay *et al*. 2000). The Mahakam fold belt ('Samarinda Anticlinorium') is characterised by tight, asymmetric anticlines separated by broad synclines cored by over-pressured shales and formed by contractional reactivation of early delta-top extensional growth faults. The axial traces of these structures are long (20–50 km in strike length) and linear to gently curved. Formation of the fold belt caused the Mahakam River to incise across the structures and thus become 'locked', which also diminished the influence of fluvial floods in the delta (Allen & Chambers 1998). The contraction has produced inversion and uplift of the western part of the Mahakam Delta, and caused reactivation of extensional growth faults in outer parts of the delta to produce detached, uplifted anticlines, as well as tightening and amplifying the delta-toe fold-and-thrust belt (McClay *et al*. 2000; Fraser *et al*. 2003).

The Makassar Abyssal Plain

The seafloor in the central Makassar Strait is relatively flat and undeformed; it dips gently to the north with few or no structural features (Fig. 2). In the deepest part, the north, the water depth is approximately 2,500 m. The sedimentary section underlying the northern sector of the Makassar abyssal plain (also known as the North Makassar Basin) is contiguous with the Kutai Basin (Mahakam Delta) to the west (Fig. 6). The sedimentary history of the abyssal plain is discussed below.

The West Sulawesi Fold Belt

In the eastern Makassar Strait, the seafloor shallows towards western Sulawesi where a fold-and-thrust belt is currently emerging (West Sulawesi Fold Belt, WSFB) and extends onshore to the Palu–Koro Fault (Figs 4b, 5, 7, 8). Contraction began in Sulawesi during the early Miocene with thrusting, uplift and foreland basin development in western Sulawesi from the early Pliocene (Hall 2002). Rapid uplift and exhumation provided sediment to the broadly west-verging fold-and-thrust belt (Hall 2002, 2011) with significant volumes of sediment beginning to

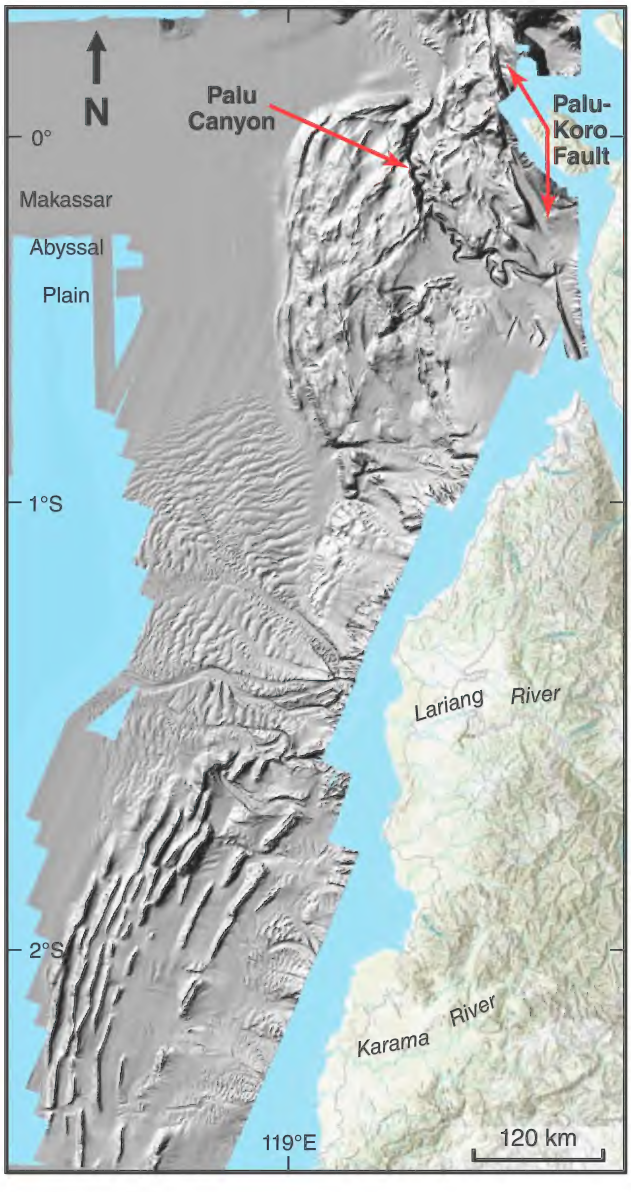

Figure 7. Bathymetric image showing offshore West Sulawesi Fold Belt.

enter the Makassar Strait from Sulawesi during the early Pliocene (Nur'Aini *et al*. 2005; Puspita *et al*. 2005).

The offshore WSFB is not a single fold belt and is divided into 3 structural provinces (Puspita *et al*. 2005). These comprise the Southern Structural Province (SSP), a west-verging thin-skinned fold-and-thrust belt with thrust faults detaching on different decollement layers; the Central Structural Province (CSP) with less deformation, at least offshore; and the Northern Structural Province (NSP), which is strongly deformed.

The age of folding is well constrained onshore where continental alluvial plain and marine deposits of the Plio-Pleistocene Pasangkayu Formation (part of the 'Celebes Molasse') formed in response to uplift of the hinterland to the east. Continuing deformation is recorded on offshore seismic sections and syn-depositional folding of younger parts of the Pasangkayu Formation (Calvert & Hall 2003, 2007; Fraser *et al*. 2003).

Northern Zone of Deformation

The Northern Zone of Deformation, a bathymetrically complex zone between the Mangkaliat Peninsula and the North Arm of Sulawesi (Fig. 1), is the southern sector of the North Sulawesi Fold-and-Thrust Belt (Tiranda & Hall *in prep*; Baillie & Decker 2022). Seismic evidence suggests several flower structures are present, representing periods of transpression along 'structural freeways' (Fraser *et al*. 2003). The Palu–Koro fault zone (Fig. 1), a NNW–SSE-trending strike–slip fault connecting with the North Sulawesi subduction trench in the Celebes Sea, is relatively active: 5 years of GPS measurements across the fault showed left lateral strike–slip movement of 3.4 cm/year with a small normal component of 0.4 cm/year (Walpersdorf & Vigny 1998).

The sinistral wrench systems are the western extremity of one of the most important and longest structural elements in the Western Pacific and Southeast Asia. The eastern end is the Sorong Fault System, which forms the southern boundary of both the Molucca Sea and the Philippine Sea plates with the Indo-Australian Plate (Hall & Wilson 2000). This fault system was initiated no later than the early Miocene by oblique convergence of the Indo-Australian and Pacific plates, and has continued to be active to the present day.

MAKASSAR STRAIT SEDIMENTARY FEATURES

The Mahakam Delta, and its resulting broad shelf, limits modern-day sedimentation from Borneo into the deep basin. Little sediment is currently being received from the Mahakam system and the main sediment flow into the deep marine basin today is from Sulawesi (Palu, Lariang and Karama rivers; Fig. 7). There is almost no shelf or delta on the Sulawesi side but 2 deep-marine fold-belt lobes trap and deflect sediment from going into the deep basin.

In the central part of the Makassar Strait, up to 4 km of sedimentary infill is present above the top synrift unconformity (Late Eocene, ~36 Ma). This section, which is entirely deep-water in origin, comprises pelagic and hemipelagic oozes and muds, sands of turbidite origin, mass-transport complexes, and carbonates. Sediment was fed into the system primarily during lowstands of relative sea level and the resultant erosion, incision and reworking of the delta plain, delta front and shelf (Moss *et al*. 2000).

Bacheller *et al*. (2011) described the stratigraphy of the deep-water Makassar Strait, as encountered in the Rangkong-1 exploration well drilled by ExxonMobil in 2009. Basement of altered continental volcanics is overlain by 2 m of deep-water carbonate of probable late Eocene to earliest Oligocene age. The succeeding highly condensed, but continuous, upper to middle bathyal, calcareous mudstones range in age from early Miocene to early Oligocene. The bulk of the section comprises an upper

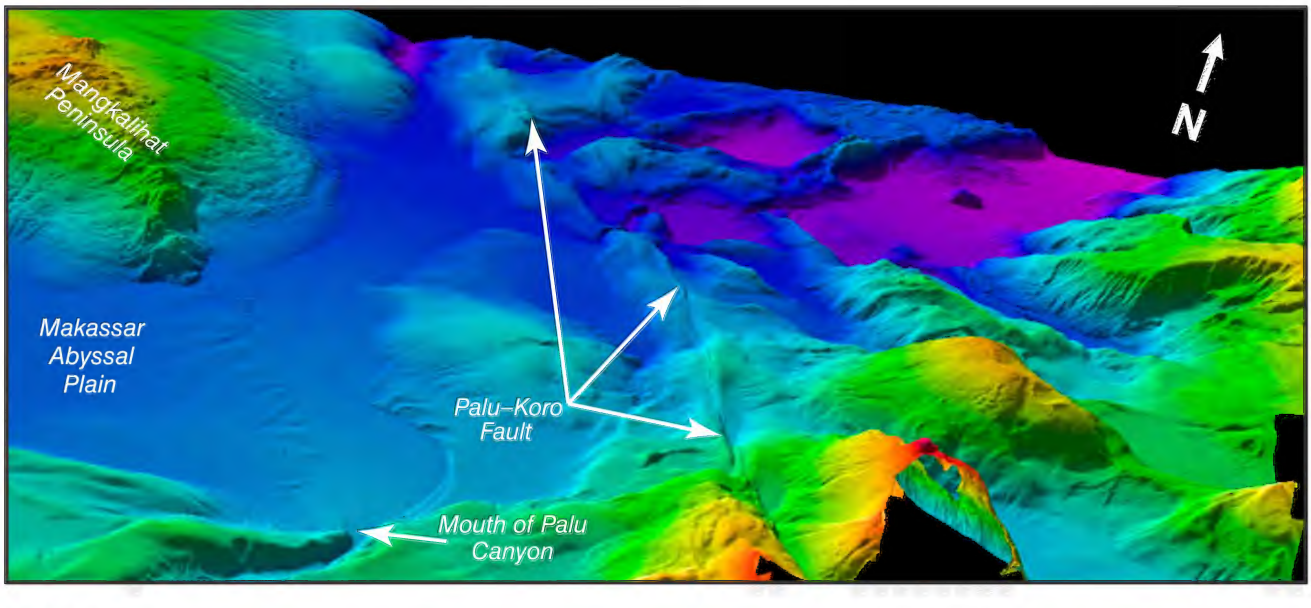

Figure 8. Rotated bathymetric image of Northern Zone of Deformation; view looking down towards the northwest; Palu–Koro fault trace indicated.

to middle bathyal distal Neogene (middle Miocene to Recent) turbiditic succession.

Turbidite sediments are both west- and east-directed; the major Borneo-derived pulse took place during the early–middle Miocene (Fig. 9), whereas Pliocene sediment was largely derived from Sulawesi. Because the Mahakam River has been locked for the past 4 million years (McClay *et al*. 2000), little coarse clastic material has entered the present Mahakam Delta and so the only material available for incorporation into west-derived turbidity currents has been material already in the system.

Makassar Fan and Sulawesi Sediment Apron

Turbidite deposition is continuing in the Makassar Strait. High-resolution bathymetric data show an active fan system—the Makassar Fan—in the central part of the basin (Fig. 10). The subtle bathymetric expression of the fan and its components are observable only via quantitative multibeam backscatter. Details of the fan are well imaged by backscatter (because of the strong returning sonar signal and the hardness and roughness of the seafloor), which allows differentiation of various sediment types subsequently confirmed by shallow coring (Fig. 10b). The Makassar Fan, which spans 65 × 50 km close to and orthogonal to the Mahakam Delta, is aggrading to the north and predominantly sourced from the Lariang River (Fig. 1) in western Sulawesi. The gradient from the channel to the end of the fan is about 0.05° and the relief across the outer fan is less than 2 m.

Interpretation of fan components from multibeam backscatter (Fig. 10c) allows recognition of:

a) a subdued outer fan with minimal relief and elongate lobes composed of interbedded sand and mud, and shallow relic channels extending nearly to the fan's limit;

b) a mid-fan with bifurcating sand-filled shallow channels generally less than 2 m deep and levees less

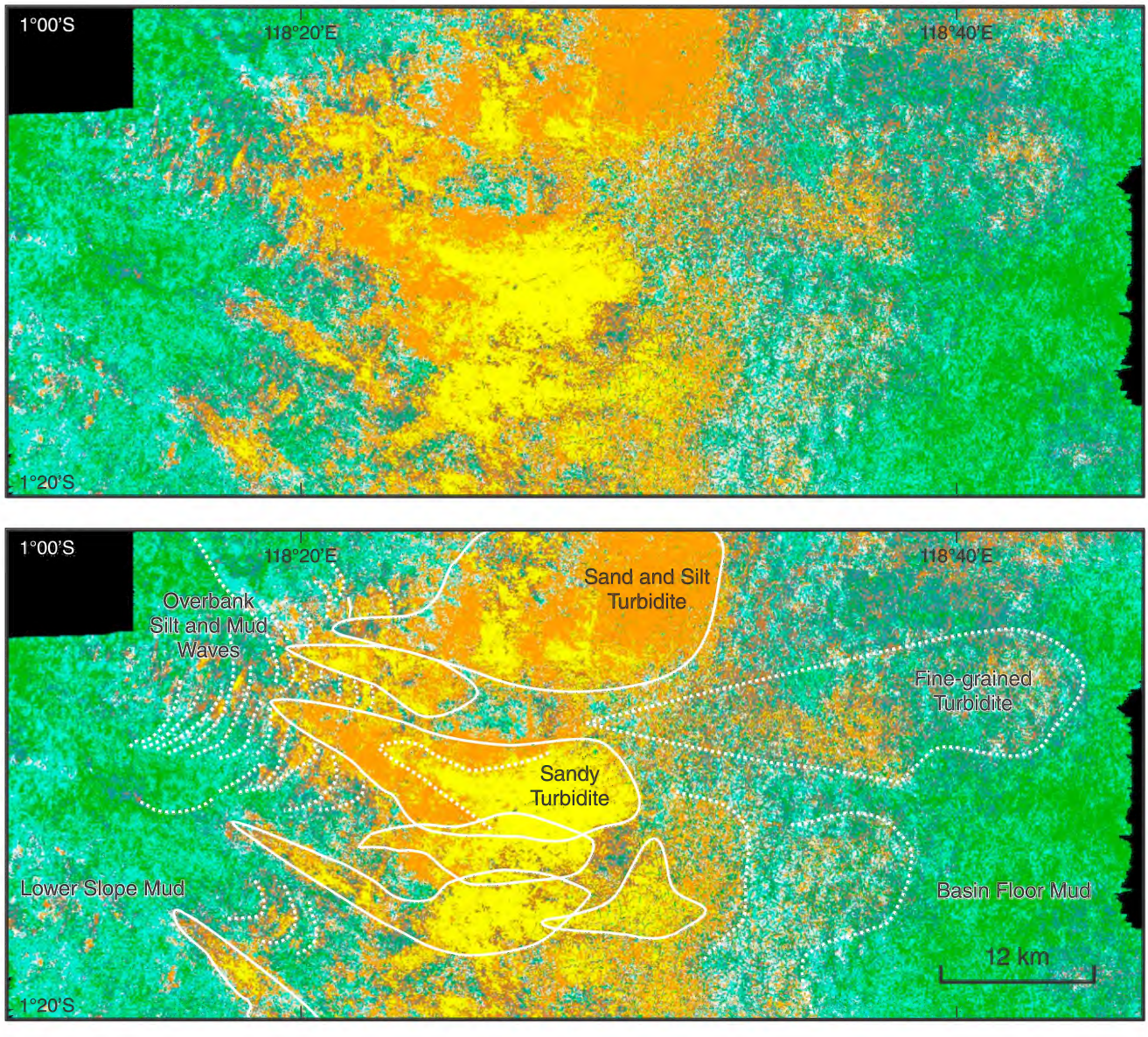

Figure 9. Uninterpreted and interpreted amplitude extraction from 3D seismic dataset showing 12 Ma turbidite sands in central Makassar Strait (after Baillie & Decker 2012); location shown on Figure 2.

than 1 m high, if present at all, with a sandy overbank and inter-channel area; and

c) an inner fan comprising a single incised straight channel up to 40 m deep with levees up to 3 m high.

The presence of sand up to coarse or medium grade was confirmed by coring (Fig. 10d–f) with the coarsest deposits being related to channels; some gravels are also present (Decker *et al*. 2008).

The fan is fed from a single channel within the basin but includes sediment almost certainly derived from both sides of the basin. It is likely that turbidites are initiated by both earthquakes and hyperpycnal currents produced when density of the water entering the basin is greater than the density of the standing water in the basin (Baillie *et al*. 2008). The hyperpycnal currents are related to climate and are triggered from high water discharge following high rainfall. The climate of South Sulawesi is tropical with 2 seasons: 'dry', from March to September, and 'rainy', from October to February; the average rainfall at the city of Makassar (formerly Ujung Pandang) is 1,000–1,500 mm/year on average.

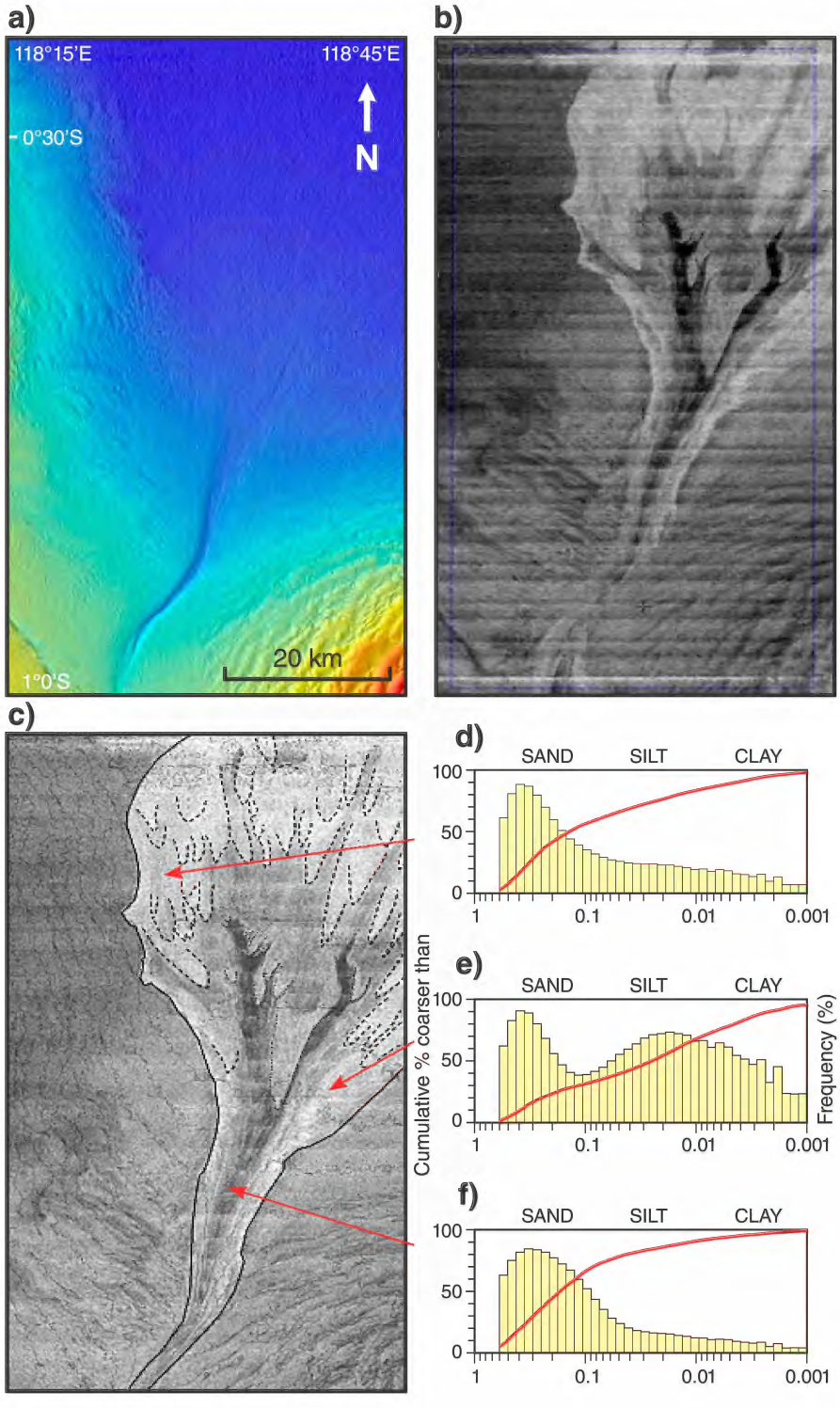

Figure 10. Makassar Fan (after Decker *et al*. 2004): a) colour-coded bathymetric image (note sand-waves in bottom (southeast) corner; b) bathymetry with greyscale backscatter; c) previous image with depositional units interpreted; d, e, f) sediment distribution curves, sample points indicated. Location shown on Figure 2.

An area with prominent sediment waves, the Sulawesi Sediment Apron, occurs east of the basin axis outboard of the Lariang River and adjacent to the Makassar Fan (Fig. 7). Coring found fine- to very-fine-grained sands and silts on the crests of the sediment waves with finer material in the troughs (Decker *et al*. 2008). Thinning of sedimentary layers occurs on the lee of individual waves.

The direction of the currents forming the sediment waves is orthogonal to the coast so a contourite origin is unlikely as sediment transport direction would be north to south and related to the Indonesia Throughflow. We believe the trigger to the formation of the Makassar Fan and Sediment Wave Field was a massive influx of sediment related to continuing tectonism in Sulawesi. As previously noted, there has been little sedimentary input into the Mahakam Delta since it became 'locked' by local tectonism during the late Miocene and therefore sediment entering the Makassar deep-water basin would largely have been recycled from the delta. With increased discharge from Sulawesi since the Pliocene, discharge from the Lariang River fed a significant volume of sediment into the basin from the east and swamped the existing submarine depositional system. The Makassar Fan developed in a northerly direction because the regional slope is to the north. Its sedimentary system is confined to the west by the Mahakam Delta and the associated small, deep-water fold-and-thrust belt (Fig. 4a), and to the east by the developing WSFB (Fig. 4b).

Mass-Transport Deposits

Mass-transport deposits (MTDs) is a general term for underwater landslide accumulations that undergo a combination of creeping, sliding, slumping and/or plastic flow in a marine or freshwater lacustrine environment to form an intergradational continuum (Nardin *et al*. 1979; Moscardelli & Wood 2008; Posamentier & Martinsen 2011). Slope-derived MTDs are readily observable on both 2D and 3D seismic data; these predominate west of the Makassar Basin's axis and throughout the deep-water sedimentary section (Fig. 4c).

Brackenridge *et al*. (2020) identified several moderate (>10 km^3) to giant (up to 650 km^3) MTDs within the North Makassar Basin Pleistocene–Recent section. Most submarine landslides that formed these deposits originated from the Mahakam pro-delta, the largest being skewed to the south.

Along the northwest margin of Borneo west of the basin axis, deep-water mass transport complexes form a large proportion of the total sedimentary column. They are not local failures but are large-scale transported deposits (Algar *et al*. 2011). South of the Paternoster Platform a large, coherent slope-attached MTD covering an area of at least 9,000 km^2 with a total volume of 2,438 km^2 has undergone relatively low internal translation and is interpreted to have been triggered by uplift of the adjacent platform area and/or basin subsidence (Armandita *et al*. 2015).

DISCUSSION AND CONCLUSIONS

The Makassar Strait is an asymmetric structural and geomorphic depression initially formed by mid-Eocene (~42 Ma) extension within a typical Sundaland continental synrift setting of graben and half-graben with common volcanoes, particularly in the northern sector. The volcanoes are probably analogous to those of the Kivu Rift (albeit subaerial) of the Great African Rift, where a combination of Cenozoic doming and crustal deformation in the eastern sector of the African Plate associated with upper-mantle activity has produced an array of hyperthermal anomalies, volcanism and local intrusions (Fig. 5b; Varet 2018).

The Makassar Strait has been the site of continuous deep-water deposition since the late Eocene with pulses of clastic sedimentation in response to tectonic events in adjacent Borneo and western Sulawesi. The sudden deepening was probably the result of extension or hyperextension related to rifting and subsequent seafloor spreading in the Celebes Sea to the north (~40 Ma; Hall, 2002). Timing of this event is constrained by the Rangkong-1 well, in which basement of altered continental volcanics is overlain by 2 m of deep-water carbonate of probable late Eocene to earliest Oligocene age (38–33 Ma; Bacheller *et al*. 2011).

Plate reorganisation around 25 Ma (latest Oligocene – earliest Miocene) caused major changes in regional tectonics and resulted in the setting up of a major left-lateral strike–slip fault system. This restructuring was responsible for transporting continental fragments along the northern margin of the Australian Plate (i.e. the Bird's Head of New Guinea) to the outer edge of Sundaland, as well as the uplift and probable rotation of Borneo, and the subsequent shedding of voluminous detritus into Neogene delta systems around the northern, western and eastern peripheries of Borneo (Hutchison 1996; Hall 2002, 2011). The increase in clastic sedimentation is expressed in the Makassar Strait through a prominent pulse of quartzose turbidites (Fig. 9).

There was a major change during the middle Miocene, around 15 Ma, when widespread extension and major subsidence began in Wallacea. Extension occurred in several phases, one of which was caused by development of the North Sulawesi subduction zone at about 5 Ma (Hall 2013). Pliocene and younger deformation in western Sulawesi was associated with metamorphism and magmatism due to extension and crustal thinning, which led to uplift in central and western Sulawesi and resultant inversion, thrusting, folding and subsidence in the WSFB (Hennig *et al*. 2016, 2017). Rapid Pliocene uplift and exhumation provided sediment to the developing fold-and-thrust belt, which has grown (and continues to grow) into a pre-existing deep-water area. The trend of fold axes indicates radial transport of material away from the mountains, which terminate relatively abruptly to the south at the northern edge of a stable carbonate platform (Hall 2011).

Continuing tectonic activity will produce geohazards, notably earthquakes and tsunamis. The Makassar Strait has the highest frequency of tsunamis in Indonesia (Prasetya *et al*. 2001). Historical records show that most are caused by earthquake-generated fault ruptures of the seafloor, except for the September 2018 Palu event, which probably had a landslide component (Jamelot *et al*. 2019). However, there are numerous other factors in the Strait that could make it susceptible to submarine landslide-triggered tsunamis, including over-steepening

of the continental slope due to carbonate growth and faulting, or sediment influx from the Mahakam Delta (Brackenridge *et al*. 2020).

ACKNOWLEDGEMENTS

Aspects of this paper have been presented previously at numerous conferences and industry presentations. These include Indonesia Petroleum Association (IPA) annual and specialist technical events; South East Asia Exploration Society (SEAPEX) exploration conferences; American Association of Petroleum Geologists (AAPG) 2008 Hedberg Conference on 'Sediment Transfer from Shelf to Deepwater – Revisiting the Delivery Mechanisms'; AAPG International Conference and Exhibition, Singapore 2012; Royal Holloway University of London 2008 'Southeast Asian Gateway Evolution Conference'; and the Royal Society of Western Australia 2020 Wallacia Symposium. This paper is a consolidation of that work.

The authors thank the Government of Indonesia for its support for various projects we were involved with over 1995–2012 and the many colleagues with whom we worked and collaborated, in particular: Paul Gilleran and Tanya Johnstone (TGS, Perth); Phil Teas and Dan Orange (Black Gold Energy, Jakarta); Paul Carter and the late Pete Barber (Isis Petroleum Consultants, Perth); and Steve Moss (Ikoda, Perth). We thank Robert Hall (Royal Holloway, University of London) and Tom Fraser for numerous discussions over many years, together with Peter Purcell for discussions and information about volcanism in the African rift system. Paul Carter and Andrew Mulder helped with seismic and bathymetry imaging. We also acknowledge Eujay McCartain, an anonymous reviewer and the RSWA editorial team for their numerous suggestions, which significantly improved the manuscript.

REFERENCES

Algar S, Milton C, Upshall H, Roestenburg J & Crevello P 2011. Mass-transport deposits of the deepwater northwestern Borneo margin – Characterization from seismic-reflection, borehole, and core data with implications for hydrocarbon exploration and exploitation. Pages 351–366, *in* R C Shipp, P Weimer & H W Posamentier, editors, Mass-Transport Deposits in Deepwater Settings, *Society for Sedimentary Geology (SEPM) Special Publication* **96**.

Allen G P 1996. Sedimentary facies and reservoir geometry in a mixed fluvial and tidal system – the Mahakam delta, Indonesia. *Journal Petroleum Exploration Society of Australia* **24**, 140–155.

Allen G P & Chambers, J L C 1998. *Sedimentation in the Modern and Miocene Mahakam Delta*. Indonesian Petroleum Association, Jakarta, Indonesia, 236pp.

Armandita C, Morley C K & Rowell P 2015. Origin, structural geometry, and development of a giant coherent slide: The South Makassar Strait mass transport complex. *Geosphere* **11**, 1–28.

Bacheller J, Buck S P, Cahyono A B, Polis S R, Helsing C E, Zulfitriadi, De Man E M, Hillock P M, Ruf A S & Toxey J K 2011. Early deepwater drilling results from a new exploration play, Offshore West Sulawesi, Indonesia. Proceedings Indonesian Petroleum Association, 35th Annual Convention, Paper IPA11-G-243.

Baillie P & Decker J 2012. Geological Development of the Straits of Makassar, Indonesia. AAPG Search & Discovery Article 30251.

Baillie P & Decker J 2022. Enigmatic Sulawesi: The Tectonic Collage. *Berita Sedimentologi*, **48(1)**. doi: 10.51835/bsed.2022.48.1.388

Baillie P, Gilleran P, Clark W, Moss S, Stein A, Hermantoto A E & Oemar, S 1999. New insights into the geological development of the deepwater Mahakam Delta and Makassar Straits. Proceedings Indonesian Petroleum Association, 27th Annual Convention & Exhibition, Jakarta, October 1999 (abstract and poster).

Baillie P, Teas P A, Decker J, Orange D & Widjanarko 2008. Contrasting deepwater sediment feeder systems, Sulawesi, Indonesia. 2008 Hedberg Conference: Sediment Transfer from Shelf to Deepwater – Revisiting the Delivery Mechanisms. Ushuaia – Patagonia, Argentina, March 3–7, 2008 (abstract and presentation).

Brackenridge R E, Nicholson U, Sapiie B, Stow D & Tappin, D R 2020. Indonesian Throughflow as a preconditioning mechanism for submarine landslides in the Makassar Strait. Pages 195–217, *in* A Georgiopoulou, L A Amy, S Benetti, J D Chaytor, M A Clare, D Gamboa, P D W Haughton, J Moernaut & J J Mountjoy, editors, Subaqueous Mass Movements and their Consequences: Advances in Process Understanding, Monitoring and Hazard Assessments. *Geological Society, London, Special Publications* **500**.

Calvert S J & Hall R 2003. The Cenozoic geology of the Lariang and Karama regions, western Sulawesi: New insight into the evolution of the Makassar Strait region. Proceedings Indonesian Petroleum Association 29th Annual Convention, Jakarta, October 14–16, 2003, 501–518.

Calvert S J & Hall R 2007. Cenozoic evolution of the Lariang and Karama regions, North Makassar Basin, western Sulawesi, Indonesia. *Petroleum Geoscience* **13**, 353–368.

Cloke I R, Milsom J & Blundell, D J B 1999. Implications of gravity data from East Kalimantan and the Makassar Strait: a solution to the origin of the Makassar Strait? *Journal of Asian Earth Sciences* **17**, 61–78.

Decker, J, Teas P A, Schneider R D, Saller A H & Orange D 2004. Modern deep-sea sedimentation in the Makassar Strait: Insights from high-resolution multibeam bathymetry and backscatter, sub-bottom profiles, and USBL-navigated cores. Pages 377–387, *in* R A Noble, A Argenton & C A Caughey, editors, *Deepwater and Frontier Exploration in Asia & Australasia*. Proceedings of the International Geoscience Conference, Indonesian Petroleum Association, Jakarta, DFE-04-PO-042.

Decker J, Teas, P A, Baillie P, Orange D L, Widjanarko 2008. Sediment dispersal in the Makassar Strait, Indonesia. 2008 Hedberg Conference: Sediment Transfer from Shelf to Deepwater – Revisiting the Delivery Mechanisms. Ushuaia – Patagonia, Argentina, March 3–7, 2008 (abstract and presentation).

Fraser T H, Jackson B A, Barber P M, Baillie P & Myers K 2003. The West Sulawesi Fold Belt and other new plays within the North Makassar Strait – a prospectivity review. Proceedings Indonesian Petroleum Association 29th Annual Convention, Jakarta, 14–16 October 2003, 431–450.

Hall R 2002. Cenozoic geological and plate tectonic evolution of SE Asia and the SW Pacific: Computer-based reconstructions, model and animations. *Journal of Asian Earth Sciences* **20**, 353–431.

Hall, R 2011. Australia–SE Asia collision: plate tectonics and crustal flow. Pages 75–109, *in* R Hall, M A Cottam & M E J Wilson, editors, The SE Asian Gateway: History and Tectonics of the Australia–Asia Collision. *Geological Society, London, Special Publications*, **355**.

Hall R 2012. Sundaland and Wallacea: Geology, plate tectonics and palaeogeography. Pages 32–78, *in* D J Gower, K G Johnson, J E Richardson, B R Rosen, L Ruber & S T Williams,

editors, *Biotic evolution and environmental change in Southeast Asia*, Cambridge University Press.

Hall R 2013. The palaeogeography of Sundaland and Wallacea since the Late Jurassic. *Journal of Limnology* **72**, 1–17.

Hall R & Wilson M E J 2000. Neogene sutures in eastern Indonesia. *Journal of Asian Earth Sciences* **18**, 781–808.

Hall R, Cloke I R, Nur'aini S, Puspita S D, Calvert S J & Elders C F 2009. The North Makassar Straits: What lies beneath? *Petroleum Geoscience* **15**, 147–158.

Hamilton W 1979. *Tectonics of the Indonesian Region*. U.S. Geological Survey Professional Paper 1078. 345pp. Washington, D.C., U.S.A.

Hennig J, Hall R & Armstrong, R A 2016. U-Pb zircon geochronology of rocks from west Central Sulawesi, Indonesia: Extension-related metamorphism and magmatism during the early stages of mountain building. *Gondwana Research*, **32**, 41–63.

Hennig J, Hall R Forster M A, Kohn B P & Lister G S 2017. Rapid cooling and exhumation as a consequence of extension and crustal thinning: Inferences from the Late Miocene to Pliocene Palu Metamorphic Complex, Sulawesi, Indonesia. *Tectonophysics*, **712-713,** 600–622.

Hutchison C S 1996. *South-East Asian Oil, Gas and Mineral Deposits*. Oxford Monographs on Geology and Geophysics, 36. Clarendon Press, Oxford. 265 pp.

Jamelot A, Gailler A, Heinrich P, Vallage A & Champenois J 2019. Tsunami simulations of the Sulawesi M w 7.5 event: Comparison of seismic sources issued from a tsunami warning context v. post-event finite source. *Pure and Applied Geophysics* **176**, 3351–3376.

Longley I M 1997. The tectonostratigraphic evolution of Southeast Asia. Pages 311–340, *in* A J Fraser, S J Matthews & R W Murphy, editors, Petroleum Geology of Southeast Asia. *Geological Society, London, Special Publication* **126**.

McClay K, Dooley T, Ferguson A & Poblet J 2000. Tectonic evolution of the Sanga Sanga Block, Mahakam Delta, Kalimantan, Indonesia. *American Association of Petroleum Geologists Bulletin* **84**, 765–786.

Moscardelli, L & Wood L 2008, New classification system for mass transport complexes in offshore Trinidad. *Basin Research* **20**, 73–98.

Moss S J & Chambers J L C 1999. Tertiary facies architecture in the Kutai Basin, Kalimantan, Indonesia. *Journal of Asian Earth Sciences* **17**, 157–181.

Moss S J, Chambers J, Cooke I, Satria D, Ali J, Milsom J & Carter A 1997. New observations on the sedimentary and tectonic evolution of the Tertiary Kutai Basin, East Kalimantan. Pages 395–416, *in* A J Fraser, S J Matthews & R W Murphy, editors, Petroleum Geology of Southeast Asia. *Geological Society, London, Special Publication* **126**.

Moss S J, Clark W, Baillie P W, Hermantoro A E & Oemar S 2000. Tectono-stratigraphic evolution of the North Makassar Basin, Indonesia. AAPG 2000 International Conference and Exhibition, Bali, abstract A-63.

Nardin T R, Hein F J, Gorsline D S & Edwards B D 1979. A review of mass movement processes, sediment and acoustic characteristics, and contrasts in slope and base-of-slope systems versus canyon–fan–basin floor systems. Pages 61–73, *in* L J Doyle & O H Pilkey, editors, *Geology of continental slopes.* Society of Economic Paleontologists and Mineralogists Special Publication **27**.

Nugraha, A M S, Hall R & BouDagher-Fadel M 2022. The Celebes Molasse: A revised Neogene stratigraphy for Sulawesi, Indonesia. *Journal of Asian Earth Sciences* **228**. doi: 10.1016/j.jseaes.2022.105140

Nur'Aini S, Hall R & Elders C F 2005. Basement architecture and sedimentary fill of the North Makassar Straits Basin. Proceedings Indonesian Petroleum Association Thirtieth Annual Convention, Jakarta, August 2005, Paper IPA05-G-161.

Parkinson C D, Miyazaki K, Wakita K, Barber A J & Carswell D A 1998. An overview and tectonic synthesis of the pre-Tertiary very-high pressure metamorphic and associated rocks of Java, Sulawesi and Kalimantan, Indonesia. *The Island Arc* **7**, 184–200.

Posamentier H W & Martinsen O J 2011. The character and genesis of submarine mass-transport deposits: insights from outcrop and 3D seismic data. Pages 7–38, *in* R C Shipp, P Weimer & H W Posamentier, editors, Mass-transport Deposits in Deepwater Settings. *Society for Sedimentary Geology (SEPM) Special Publication* **96**.

Prasetya G S, De Lange W P & Healy T R 2001. The Makassar Strait tsunamigenic region, Indonesia. *Natural Hazards* **24**, 295–307.

Puspita S D, Hall R. & Elders C F 2005. Structural styles of the offshore West Sulawesi Fold Belt, North Makassar Straits, Indonesia. Proceedings Indonesian Petroleum Association Thirtieth Annual Convention, Jakarta, August 2005, 519–542.

Saller A H, Noah J T, Ruzuar A P & Schneider R 2004. Linked lowstand delta to basin-floor fan deposition, offshore Indonesia: An analog for deep-water reservoir systems. *American Association of Petroleum Geologists Bulletin* **88**, 21–46.

Situmorang B 1989. Crustal structure of the Makassar basin as interpreted from gravity anomalies: Implications for basin origin and evolution. Lemigas Scientific Contributions on Petroleum Science & Technology **1/89**, 10–24.

Teas P A, Decker J, Nurhono A & Isnain A 2004. Exploration significance of high resolution bathymetry in the Makassar Straits. Indonesian Petroleum Association Proceedings, Deepwater and Frontier Exploration in Asia & Australasia Symposium, December 2004. Paper DFE04=OR-044.

Tiranda H & Hall R In prep. Structural and stratigraphic development of Offshore NW Sulawesi, Indonesia. EarthArxiv non-peer reviewed preprint. doi: 10.31223/X5WC89.

van de Weerd A & Armin R 1992. Origin and evolution of the Tertiary hydrocarbon-bearing basins in Kalimantan (Borneo), Indonesia. *American Association of Petroleum Geologists Bulletin* **76**, 1778–1803.

Varet J 2018. Geothermal resource along borders: The Rwanda-DRC case. Proceedings, 7th African Rift Geothermal Conference, Kigali, Rwanda 31st October – 2nd November 2018.

Wallace A R 1863. On the Physical Geography of the Malay Archipelago. *Journal of the Royal Geographical Society* **1863**, 217–234.

Walsperdorf A & Vigny C 1998. Monitoring of the Palu-Koro Fault (Sulawesi) by GPS. *Geophysical Research Letters* **25(13)**, 2313–2316.

A new subspecies of Tyto owl (Aves: Strigiformes: Tytonidae) from Alor and Pantar islands, Lesser Sundas, Indonesia

RONALD E. JOHNSTONE[1]*, JOHN C. DARNELL[1] & GAYNOR DOLMAN[1]

[1] *Department of Terrestrial Zoology, Western Australian Museum, 49 Kew Street, Welshpool, WA 6016, Australia.*

* *Corresponding author:* ✉ *ron.johnstone@museum.wa.gov.au*

ABSTRACT

We describe a new subspecies of Barn Owl, *Tyto javanica fallens*, from Alor and Pantar islands in the Lesser Sunda islands of eastern Indonesia. This subspecies differs significantly in morphology and colouration from other members of the *Tyto alba* complex, namely the Common or Western Barn Owl *Tyto alba* from Africa and Eurasia; the Eastern or Australian Barn Owl *Tyto javanica* (including *T. j. delicatula*, *T. j. sumbaensis* and the Sulawesi Owl *Tyto j. rosenbergii*) restricted to southern and South-East Asia, Australia, New Zealand, New Guinea and parts of Polynesia; and the American Barn Owl *Tyto furcata* from North to South America. It also differs from the Lesser or Moluccan Masked Owl *Tyto sororcula* and the Australian Masked Owl *Tyto novaehollandiae*. These differences are corroborated by molecular analyses. Four specimens were collected, one from Pantar and 3 from Alor, in April 1991 during joint Western Australian Museum and Museum Zoologicum Bogoriense vertebrate surveys in eastern Indonesia. These are the first *Tyto* specimens recorded from these islands.

Key words: speciation, morphology, DNA sequencing, Wallacea, *Tyto javanica fallens* ssp. nov.

Manuscript received 4 November 2021, accepted 27 May 2022

INTRODUCTION

The Indonesian archipelago, consisting of many thousands of islands, encompasses the Oriental–Australian faunal interface (see Fig. 1). The islands of eastern Indonesia (Wallacea) form a major contact overlap or transition zone between Asia and Australia. Since Alfred Russel Wallace's time this region has attracted the attention of biogeographers who have sought to delineate the Australian–Oriental divide (Simpson 1977). The biogeographic affinities of some of the birds of this region continue to be equivocal. Wallacea contains biogeographic subregions with relatively high levels of endemism and evidence of incipient speciation following changes in sea levels and climate during the Pleistocene. Within southern Wallacea are 2 island chains, the Banda Arcs, of different geological age and composition. The inner Banda Arc islands (including Sumatra and Java, and the islands from Bali through Lombok, Sumbawa, Flores, Pantar, Alor, Wetar to Banda) are principally volcanic, whereas the outer Banda Arc islands (including Sumba, Savu/Sabu, Roti, Timor, Tanimbar, Kai and Seram), are chiefly sedimentary in origin and represent outliers of the Australian Plate (Veevers 1991). The Banda Arcs formed during the collision and subduction of the Australian and Pacific plates beneath the Asian Plate in the mid- to late Pliocene. Sea levels in the region fluctuated because of alternating glacial maxima and minima during the subsequent Pleistocene (Roy *et al.* 1996). The islands also experienced changes in the seasonality of precipitation and fluctuations in mean temperatures (Morley & Flenley 1987). It is highly likely that local extinctions followed volcanic activity (Diamond 1974).

There has been considerable uncertainty about the biogeographic affinities of the Wallacean fauna. Wallace changed the position of his line of demarcation between the Asian and Australasian regions several times between 1859 and 1876 (Wallace 1876). Some assemblages of butterflies, bats and birds from islands within the region show different distributions depending on whether they originated from either Oriental or Australian forms (Holloway & Jardine 1968). There is now abundant evidence indicating Wallacea has a high proportion of endemic species with considerable speciation because the islands have been variously isolated in both space and time (Vane-Wright 1991; Kitchener & Suyanto 1996; How & Kitchener 1997).

Until recently the avifauna of many of the smaller islands in the Lesser Sundas, including Alor and Pantar, was poorly known. The relatively recent descriptions of several taxa (e.g. Mees 1973; Rozendaal 1987; Olsen *et al.* 2002; Sangster & Rozendaal 2004) and a new subspecies of the Sunda Bush Warbler *Cettia vulcania kolichisi* from Alor (Johnstone & Darnell 1997a) indicate higher levels of speciation within the region than previously recognised. Noteworthy among these are 2 taxa of Boobook Owl. That from Roti (Johnstone & Darnell 1997b), recently elevated to species status, and a new species from Sumba (Olsen *et al.* 2002), highlighting that speciation has taken place on both large and small Banda Arc islands. More recently, Jønsson *et al.* (2013) described a new species of owl, *Tyto almae*, from Seram. No endemic bird species are known from Alor or Pantar whereas there are 4 on Flores, 7 on Sumba and 10 on Timor/Semau; however, there are

urn:lsid:zoobank.org:pub:6485F171-FF4A-4ABB-85E6-569C48B-2BA6D

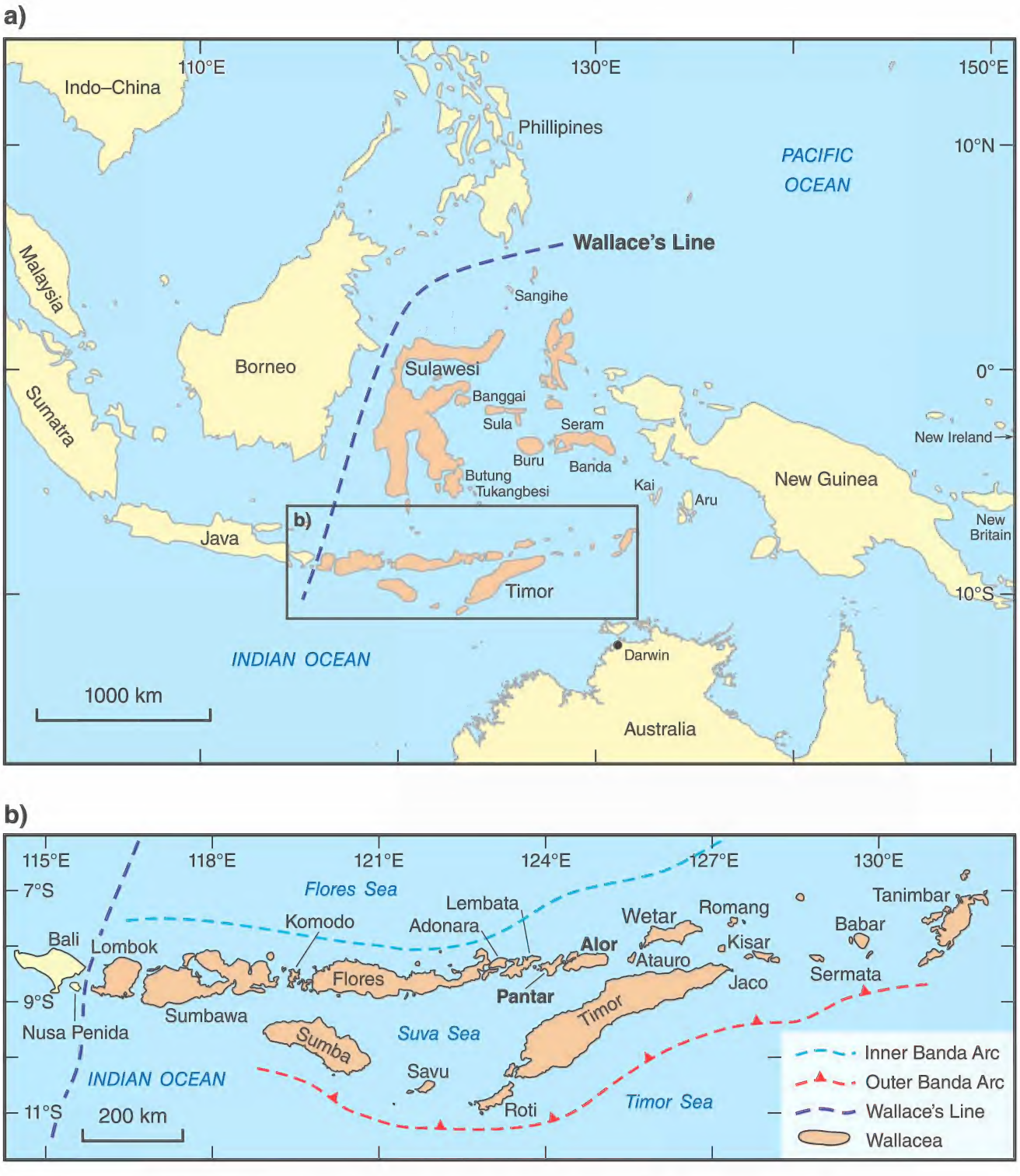

Figure 1. a) Wallacea and nearby regions; b) Lesser Sunda Islands showing Alor and Pantar Islands.

some endemic subspecies known from both Alor and Pantar.

Owls in the genus *Tyto* are one of the most secretive and hence poorly studied taxonomic groups in Wallacea. Within this group are several closely related species and subspecies including the 'Barn Owl' *Tyto alba* (Scopoli, 1769) complex, the Sulawesi Masked Owl *Tyto rosenbergii* (Schlegel, 1866), Minahassa Owl *Tyto inexspectata* (Schlegel, 1879), the Taliabu Owl *Tyto nigrobrunnea* Neumann, 1939, the Lesser Masked Owl *Tyto sororcula* (P.L. Sclater, 1883) and the Seram Masked Owl *Tyto almae* Jønsson *et al.*, 2013. The phylogeny and taxonomic status within the genus *Tyto* remains largely unresolved. Konig & Weick (2008) recognised 25 species within *Tyto*; however, many of these have yet to be subjected to molecular phylogenetic analysis, so their taxonomic and

systematic status is unclear. For example, we follow them in treating the Moluccan Masked Owl *Tyto sororcula* as a full species rather than as a subspecies of the Australian Masked Owl *Tyto novaehollandiae* (Stephens, 1826). The islands of eastern Indonesia, which harbour about 11 taxa and exhibit relatively high levels of endemism and speciation, are central to providing insights into the origin, colonisation and genetic differentiation within the genus (Fig. 2). A good example of this problematic taxonomy at the species and subspecies levels is the Common Barn Owl *Tyto alba* complex, which was long recognised as a single, nearly cosmopolitan species with 28 to 46 subspecies (del Hoyo & Collar 2014).

There is extensive geographic variation in plumage and body size across the vast range of the *Tyto alba* complex, and recent molecular studies have cast doubt on the validity of many subspecies while elevating others to species rank. Wink *et al.* (2008) identified 3 widely distributed species within this complex: the Common Barn Owl *T. alba*, in which they placed 10 subspecies (*T. a. alba*, *T. a. affinis*, *T. a. erlangeri*, *T. a. ernesti*, *T. a. gracilirostris*, *T. a. guttata*, *T. a. hypermetra*, *T. a. javanica*, *T. a. schmitzi* and *T. a. stertens*) from Africa, Europe and parts of south and South-East Asia; the Western or American Barn Owl *Tyto furcata*, which comprises 5 subspecies (*T. f. furcata*, *T. f. contempta*, *T. f. hellmayri*, *T. f. pratincola* and *T. f. tuidara*) from North, Central and South America; and the Eastern Barn Owl *Tyto delicatula*, which includes at least 4 subspecies (*T. d. delicatula*, *T. d. interposita*, *T. d. meeki* and *T. d. sumbaensis*) restricted to the easternmost part of South-East Asia, Australia, New Zealand, New Guinea and parts of Polynesia. In addition to these taxa, Konig & Weick (2008) considered 6 restricted-range island taxa to be separate monotypic species and mentioned that *Tyto alba sumbaensis* from Sumba in the eastern Lesser Sundas could also be considered a separate species, although they did not formalize this suggestion. Mikkola (2012) treated several subspecies of the Barn Owl (*T. alba*) *sensu lato* complex (including the West Indian taxa *glaucops*, *insularis* and *nigrescens*) as full species (although some with reservations).

Recent phylogenetic analyses (Aliabadian *et al.* 2016) confirmed that the *T. alba* complex contains at least 3 species, with the Old World and New World groups, *T. alba* and *T. furcata* respectively, showing a high degree of genetic divergence and best considered as seperate species. They also showed that *Tyto alba javanica* (from the Malay Peninsula and the Greater and Lesser Sundas), and *Tyto alba stertens* (of South-East Asia) are both more closely related to the *T. a. delicatula* group, and that the name *javanica* (Gmelin, 1788) has nomenclatural priority

Figure 2. Map showing speciation and subspeciation within the genus *Tyto* in eastern Indonesia (artwork adapted from del Hoyo & Collar 2014).

over *delicatula* (Gould, 1836). Therefore, *T. javanica* (including *delicatula* and *stertens*) is the correct name for the Eastern Barn Owl. Their study confirmed that *Tyto alba sumbaensis* (*sensu lato*) showed high genetic divergence from *T. j. delicatula* and might represent a distinct species, although they did not distinguish it as a full species. We follow this treatment, including the retention of *sumbaensis* as a subspecies of *T. javanica*.

A comprehensive molecular phylogeny of Barn Owls and relatives by Uva *et al.* (2018) confirmed that the Common Barn Owl, *Tyto alba*, may be divided into 3 main evolutionary units: the American Barn Owl, *T. furcata*; the Western Barn Owl, *T. alba*; and the Eastern Barn Owl, *T. javanica*. Noteworthy, however, in this study was the inclusion of the Sulawesi Masked Owl *Tyto rosenbergii* and the Minahassa Owl (Minahassa Masked Owl), *Tyto inexspectata*, within the Eastern Barn Owl *T. javanica.*

Tyto species within Wallacea

Based on del Hoyo & Collar (2014), Aliabadian *et al.* (2016), Uva *et al*. (2018) and Gill *et al*. (2022), we accept that the following *Tyto* species and subspecies occur in eastern Indonesia (Fig. 2).

EASTERN BARN OWL

Tyto javanica javanica (J. F. Gmelin, 1788) is present in Burma, south-west China, Thailand, Cambodia, Laos, South Vietnam, Malay Peninsula, Greater and Lesser Sundas (east to Flores). Christidis & Boles (2008) treated birds from southern Asia through Australia and the Pacific as *T. a. javanica.* Alternatively, Mees (2006) showed that birds from Australia are paler on their upper parts than those from Java, and that birds from Flores are similar to those from Java. They concluded that *T. a. delicatula* is a valid subspecies differing from *T. a. javanica* by its smaller size and paler colouration.

Tyto javanica delicatula (Gould, 1837) ranges across the eastern Lesser Sundas (Savu, Roti, Timor, Jaco and Wetar, Kisar and Tanimbar Islands), Australia and Pacific Ocean islands such as New Britain, New Ireland, Bougainville and Solomon Islands, New Caledonia, Loyalty Islands, and east to Fiji, Tonga and Samoa. Specimens in the Western Australian Museum from Savu and Roti are similar in size and colouration to birds from northern Australia.

Tyto javanica sumbaensis (Hartert, 1897) is confined to Sumba in the eastern Lesser Sundas. Few specimens of this subspecies are known and Mees (2006) considered the validity of *sumbaensis* required confirmation; however, a specimen in the Western Australian Museum has the very pale cinnamon-buff tail, marked only with 3 narrow dusky bars (Fig. 2). The tail is the main character of this subspecies and Wink *et al.* 2004 show the distinctiveness of this taxon. Although we retain *sumbaensis* as a subspecies of *javanica*, it may well deserve full specific status.

The form *T. alba everetti* Hartert, 1929 was described from birds collected from Savu. Hartert (1929) commented that in colour, they were inseparable from his *T. a. kuehni* specimens from Kisar, differing only in their slightly smaller size. In his review of the birds of Timor and Sumba, Mayr (1944) treated both *everetti* and *kuehni* as synonyms of *delicatula.* The single specimen A23508 from Savu in the Western Australian Museum is, however, most distinctive. It lacks any buff colouration whatsoever. The tail pattern best resembles that of *T. j. sumbaensis* but the ground colour is whitish, and there are some fine markings between the distinct tail bars. Based on the single specimen A23508, we choose to resurrect the taxon *T. j. everetti*, as this bird lacks buff pigmentation (Fig. 2). Although Hartert (1929) commented that the specimens he named *everetti* were indistinguishable from Timor birds (= *delicatula*), this is definitely not the case with our male specimen A23508. The form *T. a. kuehni* Hartert, 1929 from Kisar (specimens of which were borrowed from the American Museum of Natural History) could not be distinguished from specimens of *Tyto javanica delicatula* from Timor, as noted by Mayr (1944).

Birds collected from Kalao and Kalaotoa (between Sulawesi and Flores) have not been examined by us. Hartert (1929) suggested that they differed from Savu birds (*T. a. everetti*) in being more golden brownish above especially on the tail. They seem to resemble more closely the Indian subspecies *T. j. stertens.* Peters (1940) noted that these birds differ from others but had not (at the time of his writing) been assigned to any taxon. White & Bruce (1986) list them under *T. a. javanica*, but note that they are small, with a wingspan between 265 and 273 mm, and markedly red-brown on the dorsal surface, especially on the tail. It is of interest that these forms come from smaller islands between the *T. j. javanica* and the *T. j. delicatula* interface, as does our new subspecies from Alor and Pantar. To some degree this parallels the situation of *Ninox* owl species in that there are several taxa limited to islands between Sumba and the Moluccas.

SULAWESI MASKED OWL

Tyto rosenbergii (Schlegel, 1866) occurs on the Sangihe Islands, Sulawesi and Butung, and *T. r. pelengensis* Neumann, 1939 is tentatively identified from the Banggai Islands (Peleng).

MINAHASSA MASKED OWL

Tyto inexspectata (Schlegel, 1879), or the Minahassa Masked Owl, is confined to northern Sulawesi.

TALIABU MASKED OWL

Tyto javanica nigrobrunnea Neumann, 1939, is sometimes considered conspecific with *T. inexspectata*. It is found on Taliabu in the Sula Islands.

MOLUCCAN MASKED OWL

Tyto sororcula (P.L. Sclater, 1883), also known as the Lesser Masked Owl, is treated here as a full species, but was recently considered to be a subspecies of *T. novaehollandiae* (Stephens, 1826) by del Hoyo *et al*. (2014). The species includes *T. s. cayelii* (Hartert, 1900), from the south Moluccan island of Buru, and *T. s. sororcula*, from the Tanimbar Islands of Larat and Yamdena. Known only from 4 specimens, the nominate subspecies was collected on Tanimbar in 1882 and 1923 (Sclater 1883; Stresemann 1934), and *T. s. cayelii* is known only from 2 specimens from Buru Island collected in 1898 and 1921 (Hartert 1900; Siebers 1930).

Tyto sororcula almae Jønsson *et al.*, 2013, also known as the Seram Masked Owl, comes from Seram Island in the Moluccas. It is known only from a single specimen in the Museum Zoologicum Bogoriense and is sometimes considered a full species: *T. almae*.

EASTERN GRASS OWL

Tyto longimembris (Jerdon, 1839) is known from Sulawesi, Tukangbesi Islands, Flores, Sumba and northern Australia.

Background

Between 1987 and 2006, the Western Australian Museum and the Museum Zoologicum Bogoriense (MZB: Cibinong, Java, Indonesia) conducted 13 surveys of the terrestrial vertebrates on 29 islands of eastern Indonesia—from Bali east through the Lesser Sundas and southern Moluccas to the Aru Islands on the Sunda Shelf. The main purpose of these surveys was to record the distribution and examine the taxonomy of amphibians, birds, mammals and reptiles throughout the region. Extensive observations were made of the birds, and specimens were collected across this zone of complex speciation and taxonomy. Based on these, several island avifaunal checklists have been prepared and new taxa described (Johnstone 1994; Johnstone & Sudaryanti 1995; Johnstone & Jepson 1996; Johnstone *et al.* 1996; Johnstone & Darnell 1997a, 1997b; Johnstone & van Balen 2013; and Johnstone *et al.* 2014).

Recent taxonomic studies on other faunal groups including bats, rodents, skinks and snakes show that several species or subspecies are endemic to Nusa Tenggara (e.g. Auffenberg 1980; Kitchener *et al.* 1991, 1992; Aplin *et al.* 1993) and from these it is obvious that there have been many mammal, bird and reptile speciation events in this region. A good example is the Johnstone's Mastiff Bat *Otomops johnstonei*, Kitchener *et al.*, 1992, described from Alor (Kitchener *et al.* 1992), which is distinct from its nearest congeners on Java and in New Guinea. This is an example of a species that, although able to fly, has not extended its distribution beyond these islands. Also noteworthy was the description of a new subspecies of the montane Sunda Bush Warbler *Cettia vulcania kolichisi* from Alor (Johnstone & Darnell 1997a). Trainor (2005) mentions that a revision of the taxonomic status of some restricted-range species on Alor including the Lesser Shortwing *Brachypteryx leucophrys* and Yellow-breasted Warbler *Seicercus montis* is needed.

Surveys during April 1991 (by R. E. J.) on Alor were done near Kalabahi (8°14′S, 124°32′E) and Mali (8°08′S, 124°36′E) on its western end and near Apui in the central mountains (at 8°17′39″S, 124°43′17″E). On Pantar the surveys included the north-east at Batu (8°15′16″S, 124°17′59″E) and the north-western side at Kabir (8°15′30″S, 124°13′05″E).

On 20 April 1991, an adult female *Tyto* owl (Western Australian Museum A24588) was collected at Kabir on Pantar from a coconut palm in a small plantation backing a patch of dense low scrub and mangroves. It was listed in field notes as a *Tyto ?alba* buff morph. On 25 April 1991, another adult female *Tyto* owl from Apui on Alor Island (WAM A24508) came from a patch of rainforest at the edge of cultivation (kebun, gardens). This bird was collected along with a large pin-feathered chick (WAM A24243) from a large tree hollow. It was noted that this adult was another buff-cinnamon-coloured specimen similar to the bird from Pantar with a much darker mask and back, and heavily marked underparts, compared to typical *Tyto alba* specimens from other adjacent islands.

On 27 April 1991, a third adult *Tyto* owl, a male, was collected at Apui on Alor (WAM A24528) among gardens, trees and palms at the edge of the rainforest. This bird was noted as being dark on its upperparts, but with a white belly rather than a buff-cinnamon one as in the other specimens.

That both females were dark-coloured and heavily marked whilst the male was white and speckled black on its underparts, raises the question whether the plumage differences represented differing colour morphs or they were sexual variation. Because female birds in many of the '*Tyto alba*' complex are more intensely coloured than the males, we have concluded that this is an exceptionally extreme instance of sexual dimorphism. To our knowledge, no other taxon within the '*Tyto alba*' *sensu lato* complex exhibits such marked sexual diversity (Fig. 2).

METHODS

Morphometrics

We compared the 3 *Tyto* specimens collected on Pantar and Alor with *Tyto alba – Tyto javanica* specimens from Indonesia housed in the Western Australian Museum, Museum Zoologicum Bogoriense (MZB), the American Museum of Natural History (AMNH), and the Natural History Museum, Tring (NHMUK), as well as with other *Tyto* specimens including *T. novaehollandiae* from Western Australia.

We also compared our specimens with photos taken of the type specimen (MCZ 270559) of *Tyto rosenbergii pelengensis* from Peleng Island (Banggai Islands, central Sulawesi Province) in the Museum of Comparative Zoology, Harvard University, and with figures of *Tyto sororcula* and *Tyto almae* in Jønsson *et al.* (2013). These photographs demonstrate overall similarities, but also highlight some conspicuous plumage differences. Ridgway (1912) was used as a standard for colour terminology.

Molecular analyses

TAXONOMIC SAMPLING

Toe pad samples from the 4 Western Australian Museum *Tyto* specimens include 3 from Pantar and Alor and one from Sumba Island. Toe pads were also sampled from specimens from the American Natural History Museum, including 3 *Tyto javanica sumbaensis* from Sumba, 2 *Tyto javanica javanica* from Java, and one *Tyto javanica delicatula* from Kisar. Additionally, DNA sequences were downloaded from GenBank (see Appendix A).

MOLECULAR METHODS

DNA was extracted from toe pads using a dedicated cabinet workstation for historical specimens, cleaned with

10% bleach and ultraviolet light. A QIAGEN extraction kit was used but included the addition of 20 µL DTT (1M) in the protein denaturing step and a Qiaquick column in exchange for the DNeasy column. Library preparations were conducted by Kerensa McElroy, ANWC, CSIRO, Canberra and sequenced using standard depth paired-end sequencing at the Garvan Institute of Medical Research. Whole mitochondrial genomes were assembled iteratively using MITObim (Hahn *et al.* 2013) and the *Strix leptogrammica* mitochondrial genome (KC953095) as a reference. Three mitochondrial loci (*Cox1*, *Cytb* and *16s*) were extracted from the whole mtDNA genome for further analysis and comparison with DNA sequences available on GenBank. GenBank numbers are provided in Appendix A.

PHYLOGENETIC ANALYSIS

The 3 mitochondrial loci (*Cox1*, *Cytb* and *16s*) were concatenated and aligned with the same 3 mtDNA loci from representatives of *Phodilus badius*, *Tyto alba* and *Tyto furcata* from Aliabadian *et al.* (2016) (omitting some replicates where possible, particularly those missing data). The nuclear locus *Rag1* was also included from this dataset and *Cytb* and *Rag-1* were included from *Tyto castanops*, *Tyto longimembris* and *Tyto novaehollandiae* (Appendix A). Concatenated sequences were generated in Geneious version 10.2.3 (http://www.geneious.com, Kearse *et al.* 2012) and aligned using MAFFT Multiple Sequence Alignment and the FFT-NS-2 algorithm (Katoh & Standley 2013). Bayesian phylogenetic analyses were done using MRBAYES 3.2.6 (Huelsenbeck & Ronquist 2001); the GTR model on the dataset partitioned as follows: 16S; *Cox1* 1st + 2nd codons; *Cox1* 3rd; *Cytb* 1st + 2nd codons; *Cytb* 3rd; *Rag-1* 1st + 2nd codons; *Rag1* 3rd. Four chains were run for 1.5×10^{-7} generations and a subsampling frequency of 15,000. Burnin length was 3×10^{-6}. Convergence and effective sample sizes were assessed for all parameters using a tracer within Geneious version 10.2.3. (http://www.geneious.com; Kearse *et al.* 2012). A maximum likelihood tree with 10,000 bootstrap replicates was generated in RAxML 8.2.7 (Stamatakis 2014) using the same partitioning scheme as the Bayesian analysis and the GTR+gamma model.

TAXONOMY

Based mainly on plumage patterns and morphology, and to a lesser degree genetic divergence, the *Tyto* specimens from Pantar and Alor fall outside the variation seen in *T. j. javanica* and *T. j. delicatula* of the Lesser Sundas, *T. sororcula* of Buru and Tanimbar, *T. almae* of Seram, *T. j. rosenbergii* from Sulawesi and *T. novaehollandiae* from the Australo-Papuan region. Consequently, we describe them here as a new subspecies: *Tyto javanica fallens* **subsp. nov.**

Etymology

The specific epithet is from Latin *fallens* [deceiving], in allusion to it having been mistaken for the Common Barn Owl *Tyto alba* or the Eastern Barn Owl *Tyto javanica javanica.*

Holotype

The holotype is held at the Western Australian Museum, study skin WAM A24508, adult female; it was collected by R. E. J. at Apui, Alor Island, Indonesia, elevation approximately 1,000 m, 8°17′39″ S, 124°43′17″ E, on 25 April 1991. It was found with a pin-feathered chick in a large hollow 9.5 m up in the main trunk of a partly dead tree in a patch of rainforest backing a small coconut plantation.

The adult breeding cinnamon-coloured female (ovary 20 × 7 mm), has a total length of 360 mm, weight 475 g, wing length 285 mm, tail 114 mm, tarsus 74 mm, middle toe and claw 44 mm, bill entire (from base of skull) 40 mm, bill exposed (from feathering) 23 mm, bill width 17.7 mm, and bill depth 17.4 mm. Iris brown, orbital ring pinkish, bill bone or whitish, mouth flesh pink, legs grey, tarsus feathered almost to base of toes; sparse, stiff hair-like bristles on tops of toes, claws blackish brown.

Description

Upperparts

Variable, crown, nape, mantle, back, rump and wing coverts greyish brown or hair brown, the feathers tinged and variegated with greyish white and cinnamon buff and with a black or blackish sub-terminal or terminal shaft streak and a white spot at or near the tip. The spots finer on crown than on the back and wings but giving an overall finely spotted appearance. Primaries and secondaries mostly mottled cinnamon and brown, barred with fuscous or dark brown and inner webs broadly margined with white that increases in extent on secondaries. Outer edge of wing white to cinnamon buff spotted with fuscous. Tail mostly dark cinnamon mottled with fuscous or dark brown and with 5 fuscous bars (Fig. 3).

Facial disc

Dull greyish white, more whitish on chin and buffy brown to dusky grey tinge behind the eye (the feathers with pale greyish tips), with a blackish brown or rufous brown spot in front of the eye. Feathers of the thick facial ruff mostly white to dull cinnamon or cinnamon. The gular plumes whitish to cinnamon, the feathers with a broad blackish brown tip forming a distinct black fringe to lower section of the mask.

Underparts

Chin and centre of the throat mostly white. Sides of the neck cinnamon buff, the feathers with white bases and cinnamon tips marked with fuscous spots and bars. Breast and belly cinnamon buff heavily marked with fuscous brown spots, chevrons and vermiculations. Flanks and legs to toes dull to rich cinnamon buff, heavily marked with fuscous or dark brown spots, chevrons and vermiculations (Fig. 3). Undertail dull greyish white with dark grey bars.

PARATYPE WAM A24528

Western Australian Museum, study skin WAM A24528, adult white male, collected by R. E. J. at Apui, Alor Island, Indonesia on 27 April 1991. This specimen was collected in dense palms and gardens at the edge of rainforest.

Adult male (testes 10 × 5 mm) is 350 mm long, weight 340 g, wing length 291 mm, tail 118 mm, tarsus 77 mm,

Figure 3. Dorsal and ventral view of WAM A24508 female Holotype of *Tyto javanica fallens* from Alor Island.

middle toe and claw 46 mm, bill entire 37 mm, bill exposed 22.5 mm, bill width 16.2 mm and bill depth 16.4 mm. Iris brown, orbital ring pinkish, bill pinkish white, mouth flesh pink, legs pinkish grey, tarsus and claws as for holotype.

Upperparts

Variable, crown, nape, mantle, back, rump and wing coverts mouse grey (mostly pale brownish grey), the feathers finely variegated with greyish white, greyish brown, cinnamon buff and buff, and with a black or blackish subterminal shaft streak and a white or dull white spot at the tip (sometimes the white spot edged above and below with black). The spots finer on the crown than on the back and wings, and the cinnamon buff often more extensive on the wing coverts; overall giving a mottled appearance (Fig. 4). Outer edge of wing white, some feathers with a small black central streak at the tip.

Outer web of primaries and secondaries cinnamon buff, barred with dark brown, inner web more broadly margined with dull white that increases in extent on secondaries and with a white spot edged black at the tip. Tertiaries mostly greyish brown mottled with white and cinnamon buff.

Tail mostly cinnamon buff, mottled with greyish brown and dusky white and with 5 fuscous brown or dark brownish olive bars. The inner webs of all but central pair of feathers margined with white.

Facial disc

Dull white with a pale grey tinge on outer feathers and a dark blackish brown spot in the eye pit (front of the eye). Long bristle-like feathers at the base of the bill, mostly white with a rufous tinge.

Feathers of the thick facial ruff mostly white, tinged cinnamon buff, with a blackish shaft streak or Vshaped bar, a wavy subterminal bar and whitish tip. The gular

plumes whitish, all distinctly tipped with a narrow subterminal cinnamon buff bar and broad black tip forming a distinct black fringe to the lower section of the mask (Fig. 4).

Underparts

Breast, belly flanks and thighs white with greyish brown or fuscous spots, streaks and chevron marks that become larger on the belly and flanks (Fig. 4).

Underwing white except for blackish brown subterminal spots on lesser coverts, broad dull grey tips to outer greater coverts, and greyish brown bars and mottling on distal portion of the flight feathers. Undertail mostly dull white with greyish bars and mottling.

PARATYPE WAM A24588

Western Australian Museum, study skin WAM A24588, adult cinnamon-coloured female, collected by R.E. Johnstone at Kabir, Pantar Island on 20 April 1991. This specimen was collected from a coconut palm in a small plantation backing mangroves.

Adult female (ovary 15 × 5 mm), is 345 mm long, with a weight of 470 g, wing length 284 mm, tail 114 mm, tarsus 73 mm, middle toe and claw 39 mm, bill entire 38 mm, bill exposed 24 mm, bill width 18.4 mm, and depth 15.6 mm. Iris brown, orbital ring pink, bill white, mouth flesh pink, legs grey.

Upperparts

Crown, nape, mantle and back greyish brown or hair brown, tinged with cinnamon, the bases of the feathers cinnamon grading to brownish grey and with a black sub-terminal shaft streak and white tip. The wing coverts similar, but with richer cinnamon bases to feathers visible. Primaries and secondaries mostly cinnamon with well-spaced fuscous bars and mottling or stippling between the bars in the cinnamon zones. Tail feathers mostly dark cinnamon with 5 exposed fuscous or sepia

Figure 4. Dorsal and ventral view of WAM A24528 male Paratype of *Tyto javanica fallens* from Alor Island.

brown bars and mottling between the bars within the cinnamon zones (Fig. 5).

Facial disc

Mostly whitish inclining to grey or tinged with grey behind the eye, the feathers in front of the eye with chestnut-rufous bases, dull white distally and with pale grey tips. Feathers of the thick facial ruff mostly white, cinnamon buff and cinnamon, and the gular plumes with blackish tips forming a distinct black fringe to the lower section of the mask.

Underparts

Centre of the throat mostly white. Sides of the neck cinnamon buff, the feathers with white bases and cinnamon tips and with fuscous and sepia brown spots and chevrons. Breast and belly mostly dull white tinged with cinnamon buff, darker on the breast and grading slightly more whitish on the belly, the feathers with whitish bases grading to cinnamon buff distally and with extensive sepia brown and fuscous spots, bars and chevrons giving an overall heavily spotted appearance. Thighs and legs to toes rich cinnamon buff spotted and marked with sepia brown (Fig. 5). Undertail dull greyish white with dark grey bars.

Diagnosis

The head is large and round with a well-defined heart-shaped facial disc; the tail is moderately long; legs are long, as is typical of masked-owls in the genus *Tyto*. It is generally similar in size and colouration to *Tyto j. javanica*. It differs strikingly, however, from nominate *javanica* and for that matter all other Indonesian *Tyto* species in having 2 conspicuously different colour morphs—one cinnamon (females) and the other white (male), in being considerably darker on upperparts (in both morphs), more heavily marked on underparts (especially the cinnamon females), and in having a more well-defined facial disc. Overall the rich dorsal pattern, the facial disc outlined in black or blackish brown (in both phases)

Figure 5. Dorsal and ventral view of WAM A24588 female Paratype of *Tyto javanica fallens* from Pantar Island.

and the more heavily marked underparts (again in both phases) are the most significant differences between *fallens* and other members of the *T. alba* and *T. javanica* group making these unique characteristics.

RESULTS AND DISCUSSION

Variation among type specimens

The holotype and both paratypes were breeding adults. The holotype A24508 is a cinnamon female, as is paratype A24588, and the holotype was selected because it is a breeding adult and showing the distinctive colour characteristics of this sex. The 2 paratypes differ markedly, one being another cinnamon female and the other a more typical white adult male of *Tyto j. javanica*. Overall, paratype A24588 is more richly cinnamon than the holotype and has more extensive dark fuscous markings on underparts. The white male, paratype A24528, highlights the marked sexual variation–dimorphism in colour found in this subspecies. It has upperparts more mouse-grey rather than brownish grey with larger white terminal spots, the wings more greyish lacking cinnamon, and the throat, breast and belly are more pure white with fuscous spots and marks. While its general appearance is much like that of *Tyto j. javanica*, it differs in being considerably darker in dorsal coloration to typical *T. j. delicatula* specimens from the nearby islands of Savu, Sumba, Kisar (see Figs 6–8) and Timor, and it has a more boldly defined facial mask and a longer wing and tarsus. Being generally similar in size and colouration to *Tyto j. javanica* along with its geographical location, this initially led us to believe that it belonged within that subspecies.

Breeding information

Judging from these 3 specimens, breeding was in progress during the period from late March to early

Figure 6. Dorsal and ventral view of WAM A23508 *Tyto javanica delicatula* from Savu Island.

May. The female holotype was collected from a hollow with a pin-feathered chick and had an enlarged ovary and worn plumage. The male from Apui had enlarged testes measuring 10 × 5 mm. The female from Kabir also had an enlarged ovary measuring 15 × 5 mm and was in breeding condition.

Systematic relationships

Phenotypically, the closest relatives of *Tyto j. fallens* appear to be the historic *Tyto alba* complex (worldwide distribution), *Tyto j. rosenbergii* (of the Sulawesi region) and *Tyto novaehollandiae* (from the Australian region).

We have considered whether the new form might be a well-differentiated species or a geographic representative of the *Tyto alba–javanica* complex and, based on the recent genetic studies by Uva *et al.* (2018), thought that it is best treated as subspecifically distinct. The sub-species most resembles *T. j. javanica* in general morphology, size and partly in colouration. The 2 subspecies differ, however, in some important respects: *Tyto j. fallens* has 2 conspicuously different colour morphs, one white (male), and the other rich cinnamon buff with grey and white markings (female). Extreme sexual dimorphism is not known in the Asian *Tyto javanica* complex, including specimens typical of this subspecies, were collected on the Lesser Sunda islands of Savu (Fig. 6), Sumba (Fig. 7), Kisar (Fig. 8), Timor and Roti. Based mainly on morphology we treat *fallens* as a distinct subspecies.

Comparison with *T. javanica* populations within the region

Rensch (1931) placed the Barn Owls from Java, Lombok, Flores and Timor in the subspecies *javanica* and accepted the subspecies *sumbaensis* from Sumba, *everetti* from Savu, and *kuehni* from Kisar that were described by Hartert (1897, 1929). White & Bruce (1986) included birds from Lombok, Flores and Alor as *javanica,* birds from Savu, Timor and Kisar in *delicatula,* and noted that *javanica* is larger and darker than *delicatula.* We compared specimens

Figure 7. Dorsal and ventral view of WAM A22855 *Tyto javanica sumbaensis* from Sumba Island.

Figure 8. Dorsal and ventral view of AMNH 629341 *Tyto javanica 'kuehni'* from Kisar Island.

and photographs of birds from neighbouring islands Kisar and Timor (Figs 6–9); in size and colouration they matched typical *T. j. delicatula.*

A specimen from Kisar (*T. j. kuehni* AMNH 629341; Figs 8, 9) is close in colouration to birds from Timor and Roti as well as birds from northwestern Australia. Specimens in the Western Australian Museum from Sumba (*T. j. sumbaensis* A22855) and Savu (*T. j. everetti* A23508) are also similar to Timor birds but differ in that *sumbaensis* has a mainly pale buff tail and *everetti* has a greyish white tail (Fig. 2), although overall they match well with *T. j. delicatula* populations in the region. Mayr (1944) pointed out that Hartert's *everetti* from Savu and *kuehni* from Kisar are synonyms of *delicatula*. This is a little surprising considering our single specimen from Savu appears to differ significantly from the birds examined by Mayr in that it lacks any buff pigmentation and, from a plumage aspect, is most similar to the birds from Sumba (not Timor). Further observations are needed to determine the plumage characteristics of birds from Savu. The Kisar birds (= *T. a. kuehni* of Hartert) clearly resemble *delicatula* and we agree with Mayr's findings.

Throughout its distribution *T. javanica* shows little intra-island differentiation, which is expected from a vagile species with island populations that are effectively a single population. Potential must have existed recently for ready exchange of genes between populations throughout these geographically close islands.

The Alor and Pantar *T. j. fallens* specimens on the other hand are conspicuously different to both the nominate *T. j. javanica* and *T. j. delicatula* from neighbouring islands and differ mainly in having a much darker dorsal pattern, a darker tail and a darker, more distinct blackish facial disc (Figs 2 & 5). Additionally, the females exhibit patterning of dark chevron feather edges to the underparts, a feature somewhat similar to the *T. j. rosenbergii* forms but absent in most other *javanica* taxa. The male, however, has underparts close to those of other *T. javanica* taxa. Noteworthy is that its occurrence on 2 islands in a region that has given rise to endemic *Tyto* species, most of which are confined to one or only a few islands, highlights Wallacea as a region of speciation in this genus. It is therefore not surprising to find that the form of *Tyto* on Alor and Pantar is a distinct subspecies.

Molecular analyses

There were no premature stop codons found within *Cox1* and *Cytb* DNA sequences. The complete dataset consisted of 2,776 base pairs. There was a total of 229 polymorphic sites and 178 parsimony informative sites. For Bayesian

Figure 9. Dorsal and ventral views of A24528 *Tyto javanica fallens* and AMNH 629341 *Tyto javanica 'kuehni'*.

analyses, ESS for all parameters were above or close to 900. Multiple analyses in both RAxML and Bayesian analyses converged on identical tree topology of all lineages discussed here (Fig. 10).

Our analyses confirm that the *Tyto alba* complex is divided into 3 major lineages: *Tyto alba* (Africa, Europe), *Tyto furcata* (the Americas), and *Tyto javanica* (Australasia) (Aliabadian *et al.* 2016). These 3 lineages are well supported (all have Bayesian posteriors of 1.0; Maximum Likelihood, ML bootstrap support of 79, 80 and 96, respectively). Tree topology suggests *T. furcata* and *T. alba* are sister lineages (similar to the analyses of the concatenated dataset in Aliabadian *et al.* 2016) with high support (Bayesian posterior of 1.0, ML bootstrap of 80).

Within the *Tyto javanica* lineage, *T. j. javanica*, *T. j. delicatula* and *T. j. sumbaensis* all form monophyletic lineages with strong support (see Fig. 10). However, their relationships could not be resolved, which suggests either a lack of statistical power in our data or a period of recent and rapid evolution. Our specimens from Alor and

Table 1 Measurements of *T. javanica* subspecies.

***Tyto javanica* subspecies**	**Wing (mm)**	**Tail (mm)**	**Tarsus (mm)**	**Culmen from cere (mm)**
T. j. javanica 15 males	295–324 (308.1)	114–132 (121.5)	68–77 (71.6)	22–24 (23.1)
T. j. javanica 17 females	286–321 (305.4)	110–126 (119.5)	65–74 (70.1)	22–24 (23.5)
T. j. delicatula 15 males from Western Australia	275–290 (281)	101–117 (112.6)	61–70 (64.5)	20–34 (21.4)
T. j. delicatula 21 females from Western Australia	274–289 (281)	99–117 (112.5)	54–68 (62.5)	18–23 (21)
T. j. sumbaensis	274–287 (281)	114	66	23

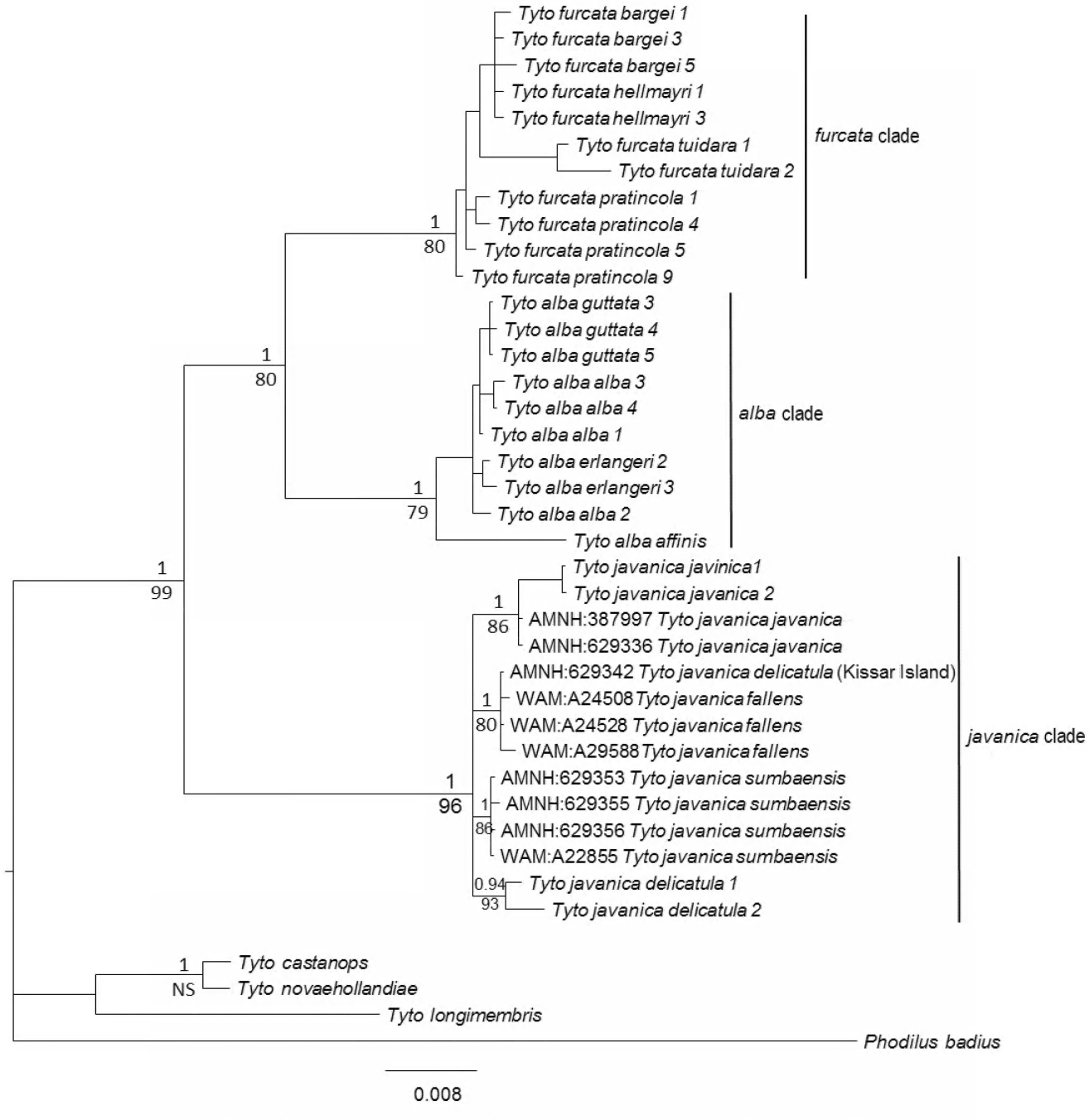

Figure 10. Phylogeny of *Tyto alba* complex represented by a Bayesian summary tree based on 2,776 base pairs of *16s*, *Cox1*, *Cytb*, and *Rag1*. Posterior probability values from Bayesian analyses are indicated on top of the branch and maximum likelihood bootstrap values from RAxML analyses are indicated below the branch.

Pantar form a fourth lineage within the *T. javanica* clade, but this lineage also includes a specimen of *T. j. delicatula* from Kisar (AMNH 629342), collected in 1901 and held at the American Museum of Natural History. Further whole mitochondrial genome analysis, not presented here, separates this specimen from *T. j. fallens*.

The morphology of the Kisar specimen (AMNH 629341) of *T. j. delicatula* was compared directly with *fallens*, and it is typical of *T. j. delicatula*. In light of the strong morphological evidence presented here suggesting *Tyto fallens* may well be a distinct subspecies, the molecular alignment of this specimen with *fallens* suggests either incomplete lineage sorting or a hybridisation event. Lineage sorting as part of the coalescent process is known to go through various stages before lineages become reciprocally monophyletic (Omland *et al*. 2006; Joseph & Omland 2009). Recent evolution of *T. j. fallens* is congruous with the *T. javanica* group being polyphyletic because of a period of rapid evolution. This understanding of population genetic processes, together with clear morphological differentiation, contributes to a multi-criteria approach

to species delimitation (de Queiroz 1998) and suggests that *fallens* represents a recently divergent subspecies within *javanica*. See also Uva *et al*. (2018) on the haplotype network of mitochondrial cytochrome b gene, in which shared haplotypes are common within the Australasian group.

Conservation

The Alor Barn Owl *Tyto javanica fallens* ssp. nov. is an endemic restricted to Alor and Pantar, both small islands in eastern Wallacea. It represents the first *Tyto* specimens recorded from these islands. Almost nothing is known about this owl's local distribution, relative abundance and ecology, and judging from currently limited knowledge, the taxon could be considered endangered. Further studies should be a priority to inform the conservation management of this subspecies.

ACKNOWLEDGEMENTS

We acknowledge the support provided by the Western Australian Museum in Perth, and the Museum Zoologicum Bogoriense in Cibinong, Java, Indonesia. We gratefully acknowledge Dr Kerensa McElroy (CSIRO) for library construction of historical DNA for next-generation sequencing and bioinformatics analyses to construct whole mitochondrial genome DNA sequences. We thank Jeremiah Trimble of the Museum of Comparative Zoology, Harvard University, for providing photographs and details of the type specimen of *Tyto rosenbergii pelengensis*. We also thank Paul Sweet of the American Museum of Natural History for the loan of study specimens. It is also a pleasure to thank Mr Nick Kolichis, whose grants to the Western Australian Museum defrayed the costs of R. E. Johnstone's field expedition to Alor and Pantar. We also thank Kim Sarti for his help with the preparation of this paper, Rob Fleming for his owl biogeographic artwork and Pamela Rasmussen for valuable comments on the manuscript.

REFERENCES

Aliabadian M, Alaei-Kakhki N, Mirshamsi O, Nijman V & Roulin A 2016. Phylogeny, biogeography, and diversification of barn owls (Aves: Strigiformes). *Biological Journal of the Linnean Society* **119**, 904–918.

Aplin K P, How R A & Boeadi 1993. A new species of the *Glaphromorphus isolepis* Species Group (Lacertilia: Scincidae) from Sumba Island, Indonesia. *Records of the Western Australian Museum* **16**, 235–242.

Auffenberg W 1980. The herpetofauna of Komodo, with notes on adjacent areas. *Bulletin of the Florida State Museum, Biological Sciences* **25**, 39–156.

Christidis L & Boles W E 2008. *Systematics and Taxonomy of Australian Birds*. CSIRO Publishing, Melbourne, 277 pp.

de Queiroz K 1998. The general lineage concept of species, species criteria, and the process of speciation: a conceptual unification and terminological recommendations. Pages 57–75 *in* D J Howard, & S H Berlocher, editors, *Endless Forms: Species and Speciation*, Oxford University Press, New York.

del Hoyo J & Collar N J 2014. *HBW and BirdLife International Illustrated Checklist of the Birds of the World. Volume 1: Non-passerines*. Lynx Edicions, Barcelona, 904 pp.

Diamond J M 1974. Colonisation of exploded volcanic islands by birds: the supertramp strategy. *Science* **184**, 803–805.

Gill F, Donsker D & Rasmussen P (Eds) 2022. IOC World Bird List (v 12.2).

Hahn C, Bachmann L & Chevreux B 2013. Reconstructing mitochondrial genomes directly from genomic next-generation sequencing reads—a baiting and iterative mapping approach. *Nucleic Acids Research* **41**, e129. doi: 10.1093/nar/gkt371

Hartert E 1897. On the birds collected by Mr Everett on the island of Savu. *Novitates Zoologicae* **4**, 263–273.

Hartert E 1900. The birds of Buru, being a list of collections made on that island by Messrs William Doherty and Dumas. *Novitates Zoologicae* **7**, 226–242.

Hartert E 1929. On the various forms of the genus *Tyto*. *Novitates Zoologicae* **35**, 93–104.

Holloway J D & Jardine N 1968. Two approaches to zoogeography: a study based on the distributions of butterflies, birds and bats in the Indo–Australian area. *Journal of the Proceedings of the Linnean Society,* London **179**, 153–188.

How R A & Kitchener D J 1997. Biogeography of Indonesian snakes. *Journal of Biogeography* **24**, 725–735.

Huelsenbeck J P & Ronquist F 2001. MRBAYES: Bayesian inference of phylogenetic trees. *Bioinformatics* **17**, 754–755.

Johnstone R E 1994. Observations of seabirds and shorebirds in Nusa Tenggara (Lesser Sundas) and Moluccas, Indonesia. *Western Australian Naturalist* **19**, 339–349.

Johnstone R E & Darnell J C 1997a. Description of a new subspecies of bush-warbler of the genus *Cettia* from Alor Island, Indonesia. *Western Australian Naturalist* **21**, 145–151.

Johnstone R E & Darnell J C 1997b. Description of a new subspecies of Boobook Owl *Ninox novaeseelandiae* (Gmelin) from Roti Island, Indonesia. *Western Australian Naturalist* **21**, 161–173.

Johnstone R E, Hidayat O, Darnell J C & Trainor C R 2014. The avifauna of Semau Island, Lesser Sundas, Indonesia: ecology, taxonomy and conservation. *Western Australian Naturalist* **29**, 162–222.

Johnstone R E & Jepson P 1996. The Birds of Roti Island, Nusa Tenggara, Indonesia. *Western Australian Naturalist* **21**, 23–35.

Johnstone R E, Jepson P, Butchart S H M, Lowen J C & Prawiradilaga D 1996. The birds of Sumbawa, Moyo and Sangeang Islands, Nusa Tenggara, Indonesia. *Records of the Western Australian Museum* **18**, 157–178

Johnstone R E & Sudaryanti 1995. The birds of Banda Neira, Moluccas, Indonesia. *Western Australian Naturalist* **20**, 15–19.

Johnstone R E & van Balen S (Bas) 2013. The birds of the Kai and Tayandu Islands, Maluku Region, Indonesia. *Western Australian Naturalist* **29**, 11–56.

Jønsson K A, Poulsen M K, Haryoko T, Reeve A H & Fabre P-H 2013. A new species of masked-owl (Aves: Strigiformes: Tytonidae) from Seram, Indonesia. *Zootaxa* **3635**, 51–61.

Joseph L & Omland K E 2009. Phylogeography: its development and impact in Australo-Papuan ornithology with special reference to paraphyly in Australian birds. *Emu* **109**, 1–23.

Katoh K & Standley D M 2013. MAFFT Multiple Sequence Alignment Software Version 7: improvements in performance and usability. *Molecular Biology and Evolution* **30**, 772–780.

Kearse M, Moir R, Wilson A, Stones-Havas S, Cheung M, Sturrock S, Buxton S, Cooper A, Markowitz S, Duran C, Thierer T, Ashton B, Mentjies P & Drummond A 2012. Geneious Basic: an integrated and extendable desktop software platform for the organization and analysis of sequence data. *Bioinformatics* **28**, 1647–1649.

Kitchener D J, How R A & Maharadatunkamsi 1991. A new species of *Nyctophilus* (Chiroptera: Vespertilionidae) from Lembata Island, Nusa Tenggara, Indonesia. *Records of the Western Australian Museum* **15**, 97–107.

Kitchener D J, How R A & Maryanto I 1992. A new species of *Otomops* (*Chiroptera; Molossidae*) from Alor I., Nusa Tenggara, Indonesia. *Records of the Western Australian Museum* **15**, 729–738.

Kitchener D J & Suyanto A 1996. Intraspecific morphological variation among island populations of small mammals in southern Indonesia. Pages 7–13 *in* D J Kitchener & A Suyanto, editors, *Proceedings of the First International Conference on Eastern Indonesian–Australian Vertebrate Fauna, Manado, Indonesia, November 22–26, 1994.* Lembaga Ilmu Pengetahuan Indonesia, Jakarta.

Konig C & Weick F 2008. *Owls of the World.* 2nd edition. Christopher Helm, London, 528 pp.

Mayr E 1944. The birds of Timor and Sumba. *Bulletin of the American Museum of Natural History* **83**, 123–194.

Mees G F 1973. Description of a new member of the *Monarcha trivirgata*-group from Flores, Lesser Sunda Islands (Aves, Monarchinae). *Zoologische Mededelingen* **46**, 179–181.

Mees G F 2006. The avifauna of Flores (Lesser Sunda Islands). *Zoologische Mededelingen* **80**, 1–261.

Mikkola H 2012. *Owls of the World – A Photographic Guide*. Christopher Helm, London, 512 pp.

Morley R J & Flenley J R 1987. Late Cainozoic vegetational and environmental changes in the Malay Archipelago. Pages 50–59 *in* T C Whitmore, editor, *Biogeographical Evolution of the Malay Archipelago.* Claredon Press, Oxford.

Olsen J, Wink M, Sauer-Gurth H & Trost S 2002. A new *Ninox* owl from Sumba, Indonesia. *Emu* **102**, 223–231.

Omland K E, Baker J M, & Peters J L 2006. Genetic signatures of intermediate divergence: population history of Old and New World Holarctic ravens (*Corvus corax*). *Molecular Ecology* **15**, 795–808.

Peters J L 1940. *Check-list of Birds of the World.* Volume 4. Harvard University Press.

Ridgway R 1912. *Color Standards and Color Nomenclature.* Author, Washington, DC.

Rensch B 1931. Die Vogelwelt von Lombok, Sumbawa und Flores. *Mitteilungen aus dem Zoologischen Museum in Berlin* **17** (4), 451–637.

Roy K, Valentine J W, Jablonski D & Kidwell S 1996. Scales of climatic variability and time averaging in Pleistocene biotas: implications for ecology and evolution. *Trends in Ecology & Evolution* **11**, 458–463.

Rozendaal F G 1987. Description of a new species of bush warbler of the genus *Cettia* Bonaparte, 1834 (Aves: Sylviidae) from Yamdena, Tanimbar Islands, Indonesia. *Zoologische Mededelingen* **61**, 177–202.

Sangster G & Rozendaal F G 2004. Systematics on Asian birds, 41. Territorial songs and species-level taxonomy of nightjars of the *Caprimulgus macrurus* complex, with the description of a new species. *Zoologische Verhandelingen Leiden* **350**, 7–45.

Sclater P L 1883. On birds collected in the Timor–Laut or Tenimber Group of islands by Mr Henry O. Forbes. *Proceedings of the Zoological Society of London*, 1883, 48–58.

Siebers H C 1930. Fauna Buruana. Aves. *Treubia* **7**, Suppl., 165–303.

Simpson G G 1977. Too many lines: the limits of the Oriental and Australian zoogeographic regions. *Proceedings of the American Philosophical Society* **121**, 107–120.

Stamatakis A 2014. RAxML Version 8: a tool for phylogenetic analysis and post-analysis of large phylogenies. *Bioinformatics* **30**, 1312–1313.

Stresemann E 1934. Über Vögel, gesammelt von Dr F. Kopstein auf den Süd-Molukken und Tenimber 1922–1924. *Zoologische Mededelingen* **17**, 15–19.

Trainor C R 2005. Species richness, habitat use and conservation of birds of Alor Island, Lesser Sundas, Indonesia. *Emu* **105**, 127–135.

Vane-Wright R I 1991. Transcending the Wallace line: do the western edges of the Australian Region and the Australian Plate coincide? *Australian Systematic Botany* **4**, 183–197.

Veevers J J 1991. Phanerozoic Australia in the changing configuration of proto-Pangea through Gondwanaland and Pangea to the present dispersed continents. *Australian Systematic Botany* **4**, 1–11.

Uva V, Päckert M, Cibois A, Fumagalli L & Roulin A 2018. Comprehensive molecular phylogeny of barn owls and relatives (Family: Tytonidae), and their six major Pleistocene radiations. *Molecular Phylogenetics and Evolution* **125**, 127–137.

Wallace A R 1876. The geographical distribution of animals; with a study of the relations of living and extinct faunas as elucidating the past changes of the Earth's surface, Volume 2. Macmillan and Co., London.

White C M N & Bruce M D 1986. *The Birds of Wallacea (Sulawesi, the Moluccas & Lesser Sunda Islands, Indonesia). An Annotated Checklist*. Checklist 7, British Ornithologists' Union, London, 524 pp.

Wink M, Sauer-Gürth H & Fuchs M 2004. Phylogenetic relationships in owls based on nucleotide sequences of mitochondrial and nuclear marker genes. Pages 517–526 *in* R D Chancellor & B-U Meyburg, editors, *Raptors Worldwide*. World Working Group on Birds of Prey, Berlin.

Wink M, Heidrich P, Sauer-Gürth H, Elsayed A A & Gonzalez J 2008. Molecular phylogeny and systematic of owls (Strigiformes). Pages 42–63 *in* C König & F Weick, editors, *Owls of the World*. Christopher Helm, London.

Wink M, Elsayed A A, Sauer-Gürth H & Gonzalez J 2009. Molecular phylogeny of owls (Strigiformes) inferred from DNA sequences of the mitochondrial cytochrome b and the nuclear RAG-1 gene. *Ardea* **97**, 581–591.

APPENDIX A

Specimens of the Barn Owl *Tyto alba* complex: collection and GenBank accession numbers for the 4 genes sampled from the Aliabadian *et al.* (2016) study and 3 genes in the current study.

Taxon		GenBank accession numbers				Collection no.	Locality	Reference
	(*sensu lato*)	Cytb	Cox1	16s	Rag-1			
Tyto alba guttata 3		KX440453	KF432220	KX440413	KX440475	ZMA58962	Netherlands	Aliabadian *et al.* (2016)
Tyto alba guttata 4		KX440454	KF432219	KX440414	KX440476	ZMA58963	Netherlands	
Tyto alba guttata 5		KX440455	KF432218	KX440415	KX440477	ZMA58964	Netherlands	
Tyto alba alba 1		KX440449	KF432226	KX440409	KX440471	NHMC80.4.108.8	Greece	
Tyto alba alba 2		KX440450	KF432223	KX440410	KX440472	NHMC80.4.108.9	Greece	
Tyto alba alba 3		KX440451	KF432225	KX440411	KX440473	NHMC80.4.108.7	Greece	
Tyto alba alba 4		KX440452	KF432224	KX440412	KX440474	NHMC80.4.108.6	Greece	
Tyto alba affinis		–	–	KX440425	–	ZMA19883	Ethiopia	
Tyto javanica javanica 1	*Tyto alba javanica* 1	KX440459	KX440429	KX440419	–	ZMA334	Indonesia	
Tyto javanica javanica 2	*Tyto alba javanica* 2	KX440460	KX440430	KX440420	–	ZMA335	Indonesia	
Tyto alba erlangeri 2		KX440447	KF432227	KX440407	KX440469	MFUM800002	Iran	
Tyto alba erlangeri 3		KX440448	KX440428	KX440408	KX440470	MFUM800003	Iran	
Tyto furcata bargei 1	*Tyto alba bargei* 1	KX440432	KX440426	KX440394	–	ZMA55930	Netherlands Antilles	
Tyto furcata bargei 3	*Tyto alba bargei* 3	KX440434	FJ465379	FJ465285	–	ZMA55941	Netherlands Antilles	
Tyto furcata bargei 5	*Tyto alba bargei* 5	KX440436	KF432207	KX440395	–	ZMA58966	Netherlands Antilles	
Tyto furcata hellmayri 1	*Tyto alba hellmayri* 1	KX440437	FJ465375	FJ465281	–	ZMA55945	Netherlands Antilles	
Tyto furcata hellmayri 3	*Tyto alba hellmayri* 3	KX440438	FJ465377	FJ465283	–	ZMA58259	Netherlands Antilles	
Tyto furcata pratincola 1	*Tyto alba pratincola* 1	KX440439	KF432212	KX440396	KX440461	LSUMZ16306	USA	
Tyto furcata pratincola 4	*Tyto alba pratincola* 4	KX440441	KF432210	KX440399	KX440463	LSUMZ20485	USA	
Tyto furcata pratincola 5	*Tyto alba pratincola* 5	KX440442	KF432215	KX440400	KX440464	LSUMZ49512	USA	
Tyto furcata pratincola 9	*Tyto alba pratincola* 9	KX440445	KF432211	KX440404	KX440467	LSUMZ21784	USA	
Tyto javanica delicatula 1	*Tyto alba delicatula* 1	–	KX440431	KX440421	–	ZMA21.978	Australia	
Tyto javanica delicatula 2	*Tyto alba delicatula* 2	–	–	KX440422	–	ZMA21.979	Australia	
Tyto furcata tuidara 1	*Tyto alba tuidara* 1	–	–	KX440423	–	ZMA22.100	Argentina	
Tyto furcata tuidara 2	*Tyto alba tuidara* 2	–	–	KX440424	–	ZMA22.101	Argentina	
Tyto javanica fallens		TBA	TBA	TBA	–	WAM:A24508	Apui, Alor Is, Indonesia	this paper
Tyto javanica fallens		TBA	TBA	TBA	–	WAM:A24528	Apui, Alor Is, Indonesia	
Tyto javanica fallens		TBA	TBA	TBA	–	WAM:A29588	Pantar Is, Indonesia	
Tyto javanica javanica	*Tyto alba javanica*	TBA	TBA	TBA	–	AMNH:629336	Java - Cheribon	
Tyto javanica delicatula	*Tyto alba delicatula*	TBA	TBA	TBA	–	AMNH:629342	South-west Kissar Is	
Tyto javanica javanica	*Tyto alba javanica*	TBA	TBA	TBA	–	AMNH:387997	Java - Buitenzorg	
Tyto javanica sumbaensis	*Tyto alba sumbaensis*	TBA	TBA	TBA	–	WAM:A22855	Sumba - Waitabula Forest Reserve	
Tyto javanica sumbaensis	*Tyto alba sumbaensis*	TBA	TBA	TBA	–	AMNH:629353	Sumba - Waingapo	
Tyto javanica sumbaensis	*Tyto alba sumbaensis*	TBA	TBA	TBA	–	AMNH:629355	West Sumba	
Tyto javanica sumbaensis	*Tyto alba sumbaensis*	TBA	TBA	TBA	–	AMNH:629356	Sumba - Waingopo	
Tyto castanops		EU349007	–	–	EU348954	IPMB 20995		Wink *et al.* (2009)
Tyto longimembris		EU349008	–	–	EU348955	IPMB 9579		
Tyto novaehollandiae		EU349009	–	–	EU348956	IPMB 20990		
Phodilus badius		KF961183	KF961183	KF961183	–	IPMB		Mahmood *et al.* (2014)